Studies of the design, use, and characteristics of methacrylic acid-based polymer gel dosimeters

By

Heather Marie Whitney

Dissertation

Submitted to the Faculty of the

Graduate School of Vanderbilt University

in partial fulfillment of the requirements

for the degree of

DOCTOR OF PHILOSOPHY

in

Physics

May, 2009

Nashville, Tennessee

Approved:

Professor John C. Gore

Professor Malcolm J. Avison

Professor Daniel F. Gochberg

Professor Richard F. Haglund

Professor Todd E. Peterson

DEDICATION

In memory of John L. Barker, Jr. (1923-2008)
loving grandfather

and

for my husband, Joshua
my best friend and my love

ACKNOWLEDGEMENTS

There is one author on this dissertation, but there are many people who contributed to its completion. Professor John Gore, as my advisor, directed the project and offered helpful insight into research problems. I am grateful to him for the opportunity of training in the fascinating field of magnetic resonance imaging. Professor Dan Gochberg met with me regularly to discuss the details of problem-solving for the work, and I am appreciative for our regular meetings.

I am grateful to Kenneth Nichols at Tri-Cities Christian School and Professors Pat Flannagan, Ray Bloomer, and Dan Cross at King College, who encouraged me to pursue work in the sciences and offered excellent instruction as well as their friendship. Professor Royal Albridge at Vanderbilt played a key role in my pursuit of graduate admission to Vanderbilt, through his leadership in the Vanderbilt Research Experiences for Undergraduates program in the physics department, and Professor Alan Bradshaw directed my first foray into scientific research.

I am fortunate to have performed my graduate work in the Institute of Imaging Science, not only because of the tremendous facilities but also for the excellent faculty and staff there. Jeff Luci, Jim Joers, and Richard Baheza all significantly assisted me with experiment design and deployment. Nancy Hagans was helpful with the many administrative tasks associated with graduate school.

In the Department of Radiation Oncology, Professors Charles Coffey and George Ding assisted with the irradiation of the samples used in this project, and I appreciate their time and effort in this.

My family and friends have been sources of support throughout my years in graduate school, and I thank them wholeheartedly. My parents in particular have been enthusiastic cheerleaders and always had encouraging words. I am grateful to them for providing opportunities when they were able and cheering me on when opportunities were up to me. I have enjoyed the camaraderie of my student colleagues and wish them well as they finish their work and continue on to life's next projects and adventures. A special note of thanks goes to my friends who opened their homes to me during the year of graduate school when I was resident in Knoxville, as they allowed me to crash on sofas and futons so that I could spend multiple days at a time at Vanderbilt.

Finally, my husband Joshua, who at the same time is also pursuing a Ph.D. in physics, has been a practical, patient, and loving support, doing everything from advising on programming methods, to keeping me company during lonely hours of scanning on weekends, to encouraging me to keep going no matter what. I hope I can repay him with the same support as he finishes his own work, and I look forward to life with him outside of graduate school.

TABLE OF CONTENTS

LIST OF TABLES

LIST OF FIGURES

CHAPTER I

INTRODUCTION

Principles from both classical and quantum physics are used to describe spin systems of protons and nuclear magnetic resonance (NMR). Since the relatively few years since its discovery, researchers have used NMR techniques for quantitative and qualitative studies of a variety of materials. The extension of NMR into magnetic resonance imaging (MRI) has afforded the opportunity to map distributions of NMR phenomena in two and three dimensions. To date, ^{1}H (usually as a component of water molecules) is the most widely studied isotope. Its presence as the major component of aqueous, tissue-equivalent polymer gels for radiation dosimetry lends to the usefulness of NMR and MRI studies to characterize the dose response of appropriate polymer gels to radiation.

1. Nuclear magnetic resonance

Hydrogen atoms have a single proton in their nucleus, which possesses spin (also called angular momentum). The spin (often denoted *I*) behaves as a small electric current loop, which generates a weak magnetic field according to Ampere's Law. These nuclei are thus magnetic dipoles, and nuclear magnetic resonance experiments measure the net behavior of a collection of dipoles in a given sample. In a magnetic field these spins have (2I + 1) energy levels, which are equally separated by ΔE, where

$$\Delta E = \frac{\mu B_0}{I} \qquad \textbf{Eq. 1}$$

where μ is the nuclear magnetic moment, and B_0 is the applied magnetic field (in Tesla). For example, for spin ½ there are two possible states: +½ (aligned with the magnetic field) or -½ (aligned against). The frequency of radiation that induces a transition between adjacent levels is

$$\nu_0 = \frac{\Delta E}{h} = \frac{\gamma B_0}{2\pi} \qquad \textbf{Eq. 2}$$

or

$$\omega = \gamma B_0 \qquad \textbf{Eq. 3}$$

where ν_0 and ω are the Larmor resonant frequency of precession (Hz and rad/sec, respectively) and γ is the gyromagnetic ratio. The gyromagnetic ratio depends on the element under consideration, and is equal to 42.5 MHz/Tesla for hydrogen. The ratio is proportional to the magnitude of the magnetic moment μ and is inversely proportional to the spin, in the relation

$$\gamma = \frac{2\pi\mu}{Ih}. \qquad \textbf{Eq. 4}$$

A torque is produced when a magnetic moment μ is placed in a magnetic field, and is expressed as a vector product

$$\bar{\tau} = \frac{d\bar{I}}{dt} = \bar{\mu} \times \bar{B}. \qquad \textbf{Eq. 5}$$

When the magnetic moment is static, the torque causes the magnetic moment to line up with the magnetic field. However, if the magnetic moment has angular momentum, a Larmor precession occurs. The magnetic moment precesses at the related Larmor frequency around the direction of the magnetic field rather than lie in alignment with the magnetic field. The effect of torque is as follows:

$$\tau = \frac{\Delta I}{\Delta t} = \frac{I \sin\theta \Delta\varphi}{\Delta t} = \left|\mu B \sin\theta\right| = \frac{ge}{2m_p} IB \sin\theta \qquad \textbf{Eq. 6}$$

where *I* is the angular momentum of the spin, θ is the angle between the magnetic moment and the z axis, φ is the angle through which the moment has rotated around the z axis, *g* is the electron spin factor (approximately 2), *e* is the charge of the electron, and m_p is the mass of the proton. The Larmor frequency is defined as

$$\omega_{Larmor} = \frac{d\varphi}{dt} = \frac{ge}{2m_p} B = \gamma B . \qquad \textbf{Eq. 7}$$

Elements other than hydrogen can be investigated using NMR, but as the ability to detect NMR signals depends both on the gyromagnetic ratio and the natural abundance of the nuclei, hydrogen is the most often studied in biological MRI. Ratios are given below (see Table 1) for several elements, along with their percent abundance, sensitivities, and frequency at 11.7T.

Table 1: The Properties of NMR-Active Nuclei (Mirau, 2005)

Isotope	Abundance (%)	Spin	γ x 10^{-8} *SI units*	Sensitivity *Relative to protons*	Frequency (MHz) At 11.7T
^{1}H	99.98	½	2.6752	1.0	500.0
^{19}F	100	½	2.5167	0.83	470.2
^{29}Si	4.7	½	-0.5316	0.078	99.3
^{31}P	100.0	½	1.0829	0.066	202.3
^{13}C	1.1	½	0.6726	0.0159	125.6
^{2}H	0.015	1	0.4107	0.00964	76.7
^{15}N	0.365	½	-0.2711	0.001	50.6

When no magnetic field is present in a sample, the dipoles are randomly distributed. But when a magnetic field is applied a slightly greater number of dipoles will align along the field, according to the Boltzmann distribution. The population difference is given as

$$\frac{N^+}{N^-} = e^{\frac{2\mu B}{kT}} \qquad \textbf{Eq. 8}$$

where N^+ is the population in the upper energy state (parallel to the field), N^- is the population in the lower energy state (anti-parallel), k is the Boltzmann constant, and T is the temperature of the system (measured with the Kelvin scale). The population difference tends to be very small, on the order of $1/10^5$. However, a net effect is indeed present and is called the nuclear magnetization (M). Nuclear magnetic resonance experiments perturb the dipoles from their equilibrium, and information is gained about the spin system by monitoring their relaxation back to equilibrium.

The difference in populations in alignment with or against the magnetic field, and thus the nuclear magnetization, increases linearly with magnetic field strength. Resonance occurs when the required energy of transition is applied to a

sample at a frequency proportional to the energy difference (ΔE = hv, where *h* is Planck's constant, and v is the frequency of precession). By this means the magnetization (and spin populations) can be changed, e.g., it can be inverted.

After such a disturbance by a radiofrequency (rf) pulse of energy, the system will begin to recover. The recovery of the component of magnetization along the axis of the field is called spin-lattice relaxation. This relaxation occurs when excited nuclei return to their original lower energy level. The recovery is characterized by the spin-lattice or longitudinal relaxation time, denoted as T1. In simple systems it follows an exponential behavior over a given course of time.

After a 90-degree rf pulse the residual longitudinal relaxation is expressed as

$$M_z(t) = M_0\left(1 - e^{\frac{-t}{T_1}}\right) \qquad \textbf{Eq. 9}$$

where M_z is the longitudinal magnetization after a time *t* in a material with a relaxation constant T1.

After a period of 3T1, 95% of the magnetization is re-established. Full recovery is usually considered to be achieved after a period of 5T1. Longitudinal relaxation is an indicator of physical characteristics of tissues, as a long T1 indicates an inability to release energy to the lattice. The inverse of the T1 value, R1, is the longitudinal relaxation rate and is also used as a way to report the longitudinal relaxation characteristics of a substance. T1 relaxation is also dependent on field strength; the rate usually decreases as field strength increases.

Ninety degree rf pulses equalize the spins so that they are distributed equally between two starting energy levels. Their net longitudinal magnetization (in the z-direction) is then zero, but a coherent transverse magnetization can be realized in the x-y plane. These spins create a magnetic flux which can be detected via a coil wrapped around the sample, according to Faraday's law. The received signal is maximized the instant after the ninety-degree pulse has been turned on and decays over time as the magnetization relaxes into its preferred longitudinal state.

Its behavior is also often exponential and is characterized via T2, the spin-spin or transverse relaxation time. Spin-spin interactions arise when spins are in close proximity and modify the local field experienced by neighboring nuclei. Individual spins precess at different frequencies due to these slight changes in the local magnetic field. Dephasing, or the loss of phase coherence from intrinsic spin-spin interactions, is measured by the relaxation time T2. Inhomogeneities from external fields also affect the relaxation dephasing. The transverse magnetization is described by the equation

$$M_{xy} = M_0 e^{-\frac{t}{T_2}} \qquad \textbf{Eq. 10}$$

where M_{xy} is the transverse magnetization. The inverse of the transverse relaxation time, R2, is the transverse relaxation rate.

Inhomogeneities in B_0 can cause more rapid loss of phase coherence than spin-spin interactions alone, and this higher rate of decay occurs in time characterized by $T2^*$. In general, it is always true that $T_2^* \leq T_2 \leq T_1$.

Relaxation times are sensitive to the macromolecular composition of tissues and the way water interacts with protein surfaces, and are affected by the rates and amplitudes of fluctuations of magnetic fields due to atomic motions.

In 1946 Felix Bloch described relaxation processes mathematically (Bloch, 1946). With the assumptions that I = ½ and that the direction of the static field is along the *z* axis, the magnetization precesses around the *z* axis. For a magnetic moment,

$$\frac{d\overline{\mu}}{dt} = \gamma \frac{d\overline{p}}{dt} = \gamma \overline{\mu} \times \overline{H} \,. \qquad \textbf{Eq. 11}$$

M is the vector sum of all the magnetic moments; macroscopic magnetization is then

$$\frac{d\overline{M}}{dt} = \gamma \overline{M} \times \overline{H} \,. \qquad \textbf{Eq. 12}$$

At equilibrium the vector components of the magnetization can be set forth as

$$\frac{dM_z}{dt} = 0$$

$$\frac{dM_x}{dt} = \gamma M_y \cdot B_0 = \omega_0 M_y \qquad \textbf{Eq. 13}$$

$$\frac{dM_y}{dt} = -\gamma M_x \cdot B_0 = -\omega_0 M_x$$

When a B_1 field (in the form of an rf pulse) is applied along the *x* or *y* axis, the effect can be described as the tipping of magnetic vectors by a magnetic field and gives

$$\begin{aligned}\frac{dM_x}{dt} &= \gamma\left[M_y B_0 - M_z (B_1)_y\right] \\ \frac{dM_y}{dt} &= -\gamma\left[M_x B_0 + M_z (B_1)_x\right] \\ \frac{dMz}{dt} &= \gamma\left[M_x B_1 - M_y (B_1)_x\right]\end{aligned} \qquad \textbf{Eq. 14}$$

where $(B_1)_x$ and $(B_1)_y$ are the components of B_1 along the *x* and *y* axes, and are given by

$$\begin{aligned}(B_1)_x &= B_1 \cos(\omega t) \\ (B_1)_y &= -B_1 \sin(\omega t).\end{aligned} \qquad \textbf{Eq. 15}$$

Relaxation of the spin system occurs for all three axes and is given by

$$\begin{aligned}\frac{dM_z}{dt} &= \frac{M_z - M_0}{T_1} \\ \frac{dM_x}{dt} &= \frac{M_x}{T_2} \\ \frac{dM_y}{dt} &= \frac{M_y}{T_2}\end{aligned} \qquad \textbf{Eq. 16}$$

where M_0 is the equilibrium magnetization, T1 is the spin-lattice relaxation time, and T2 is the spin-spin relaxation time.

The Bloch equations are formed by combining the steady state and relaxation equations, as follows:

$$\frac{dM_x}{dt} = \gamma\left[M_y B_0 - M_z B_1 \sin(\omega t)\right] - \frac{M_x}{T_2}$$
$$\frac{dM_y}{dt} = \gamma\left[M_z B_1 \cos(\omega t) - M_x B_0\right] - \frac{M_y}{T_2} \qquad \textbf{Eq. 17}$$
$$\frac{dM_z}{dt} = -\gamma\left[M_x B_1 \sin(\omega t) + M_y B_1 \cos(\omega t)\right] - \frac{M_z - M_0}{T_1}$$

Early NMR experiments detected signals by sweeping the magnetic field and monitoring a change in the absorption of rf energy. Modern experiments are much more efficient and sample the NMR signals with pulsed rf energy while keeping the magnetic field constant. The length, frequency, and phase of the pulse as well as the strength of the B_1 field determine the effect the pulses have on the magnetization. Rotation of the magnetization by the B_1 field is called the tip angle θ and is given by

$$\theta = \gamma B_1 t_p \qquad \textbf{Eq. 18}$$

where t_p is the pulse length.

Relaxation of magnetization may be caused by a combination of mechanisms, inter- or intramolecular, but may be dominated by one efficient process for a given system (Farrar and Becker, 1971). The local magnetic field experienced by a nucleus will fluctuate over time because of interactions; the average time of these interactions is the correlation time τ_c. It is dependent upon temperature, viscosity, and mobility. The Fourier transform (see below) of this time course data is the power spectral density, J(ω) (see Figure 1).

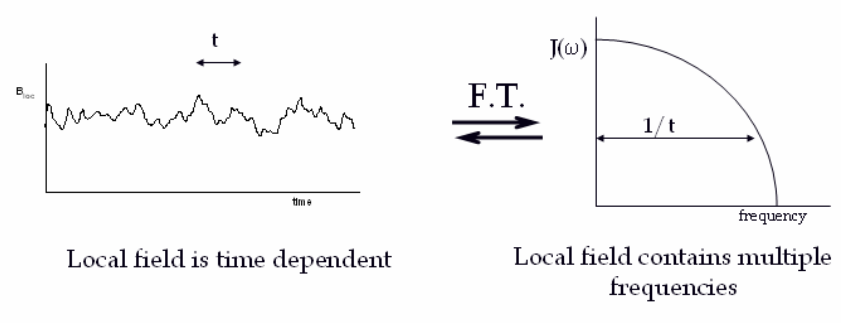

Figure 1: Relationship between time of correlation and spectral density.

More specifically, the correlation function K(τ) and the spectral density function are related by

$$J(\omega) = \int_{-\infty}^{+\infty} K(\tau) \exp(i\omega\tau) d\tau \,. \qquad \textbf{Eq. 19}$$

Relaxation times are minimized when the value of τ_c is most appropriate: this condition is present when the largest Fourier components of the molecular motion are at the resonant frequency. If τ_c is short, the molecular motions are distributed over a very wide frequency range and are not especially effective at any specific field. If τ_c is long, the intensity of lower frequencies increased (see Figure 2).

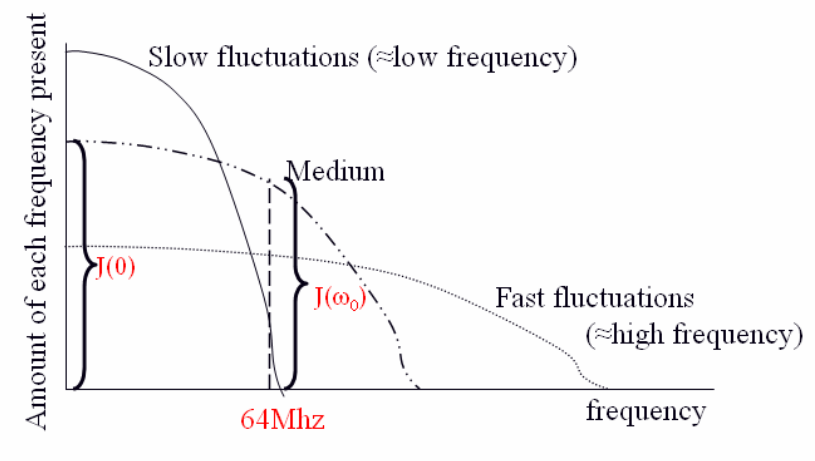

Figure 2: Spectral density versus frequency for water.

Spectral density functions relate reorientation molecular motions to relaxation rates. Thus

$$J_0(\omega) = \frac{24}{15r^6}\frac{\tau_c^2}{1+\omega^2\tau_c^2}$$
$$J_1(\omega) = \frac{4}{15r^6}\frac{\tau_c^2}{1+\omega^2\tau_c^2} \qquad \textbf{Eq. 20}$$
$$J_2(\omega) = \frac{16}{15r^6}\frac{\tau_c^2}{1+\omega^2\tau_c^2}$$

where *r* is the distance between molecules. For spin-1/2 nuclei, effects from dipole-dipole interactions usually dominate relaxation. The phenomenon arises from the direct through-space interaction between nuclei, and the energy of dipolar-dipolar interactions depends on the distance between the two nuclei as given by

$$E_{DD} \propto \frac{\bar{\mu}_1 \cdot \bar{\mu}_2}{r^3} \qquad \textbf{Eq. 21}$$

where *r* is the distance between the two dipoles. Specifically, the relaxation rates due to the interactions are given by

$$R_1 = \frac{3}{2}\gamma^4\hbar^2 I(I+1)\{J_1(\omega) + J_2(2\omega)\}$$
$$R_2 = \gamma^4\hbar^2 I(I+1)\{\frac{3}{8}J_0(0) + \frac{15}{4}J_1(\omega) + \frac{3}{8}J_2(2\omega)\} \quad \textbf{Eq. 22}$$

where *I* is the spin. Intramolecular dipole interactions are involved in rotational motion, and the rotational component of the dipole-dipole interactions is given by

$$R_{1-rot} = \frac{2}{5}\gamma^4\hbar^2 I(I+1) \Big/ r^6 \left[\frac{\tau_c}{1+\omega^2\tau_c^2} + \frac{4\tau_c}{1+4\omega^2\tau_c^2}\right]$$
$$R_{2-rot} = \frac{1}{5}\gamma^4\hbar^2 I(I+1) \Big/ r^6 \left[3\tau_c + \frac{5\tau_c}{1+\omega^2\tau_c^2} + \frac{2\tau_c}{1+4\omega^2\tau_c^2}\right]. \quad \textbf{Eq. 23}$$

When $\omega_0\tau_c << 1$, the system is nonviscous and the relaxation rates become equal:

$$R_1 = R_2 = \frac{2\gamma^4\hbar^2 I(I+1)}{r^6}\tau_c . \quad \textbf{Eq. 24}$$

Intermolecular relaxation is made up primarily of translation motions, and the longitudinal relaxation rate is as follows:

$$R_{1-transl} = \frac{3}{2}\frac{\gamma^4\hbar^2 I(I+1)}{r^6}\{J_1(\omega) + J_2(\omega)\} . \quad \textbf{Eq. 25}$$

Chemical shift anisotropy depends on the strength of the magnetic field, which may be adjusted by the chemical shift. Circulating electrons induce a small

magnetic field at the nucleus, which opposes the static magnetic field. The effective field is generally less than the primary field by a fraction σ called the shielding factor:

$$B_{effective} = B_0(1-\sigma)\,. \qquad \textbf{Eq. 26}$$

This shielding can affect the relaxation time, in the given relation:

$$R_1 = \frac{1}{15}\gamma^2 B_0^2(\sigma_{//} - \sigma_{\perp})^2 \frac{2\tau_c}{1+\omega^2\tau_c^2}$$
$$R_2 = \frac{1}{90}\gamma^2 B_0^2(\sigma_{//} - \sigma_{\perp})^2\left(\frac{6\tau_c}{1+\omega^2\tau_c^2} + 8\tau_c\right) \qquad \textbf{Eq. 27}$$

where $\sigma_{//}$ and $\sigma_{\perp}$ are the shielding parallel and perpendicular to the static magnetic field. For non-viscuous liquids,

$$R_1 = \frac{2}{15}\gamma^2 B_0^2(\sigma_{//} - \sigma_{\perp})^2\tau_c$$
$$R_2 = \frac{7}{45}\gamma^2 B_0^2(\sigma_{//} - \sigma_{\perp})^2\tau_c. \qquad \textbf{Eq. 28}$$

Spin-rotation is the direct interaction of nuclear moments with the magnetic field, and is usually only applicable to interactions of gas molecules.

For spins greater than ½, quadrupole coupling is a factor in relaxation, but this is out of the scope of this work and will not be discussed.

The general relationship between the timescale of fluctuations in the magnetic field due to interactions and the relaxation times can be summarized in the graph below (Figure 3).

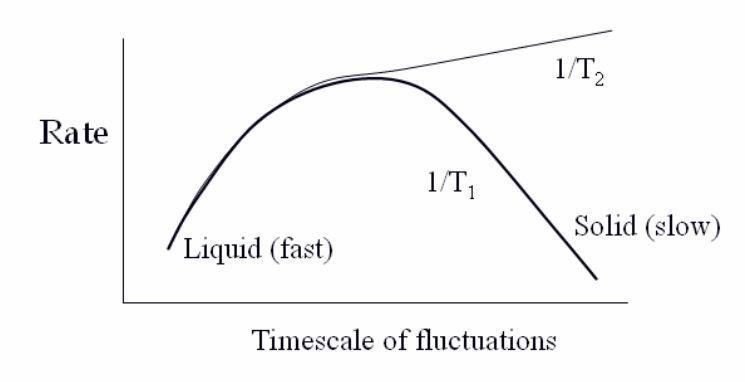

Figure 3: Rate of relaxation versus time scale of fluctuations.

2. Magnetic resonance imaging

Magnetic resonance imaging (MRI) uses gradient magnetic fields, ones that change over space, in addition to the main field B_o to associate spatial information with NMR signals. In the presence of a first gradient, called the slice selective or z-gradient, the field varies across space, so the NMR frequency necessary for resonance also varies across space. A selective excitation rf pulse is simultaneously applied to a sample and designed to affect only those spins in the slice of interest. After this pulse (90 degrees), these spins then lie in the x-y plane, while the rest of the sample remains unaffected. Signal is induced in a receiving coil. Immediately after the initial excitation a second gradient (called the frequency encoding gradient) (e.g., in the x-direction) may be applied. At this point, the precessional frequencies of the spins are directly related to their position across the sample, according to the gradient magnetic field. The resulting signal is a mixture of all signals received from the slice of interest and is recorded in the presence of the read-out gradient by a computer and analyzed by Fourier analysis into individual frequencies. If a third (e.g., y-gradient) is pulsed

on before data acquisition, the signal phase is dependent upon position in the y-direction and by acquiring many such data, the 2-D distribution can be calculated. This process is used to acquire data for multi-slice 2D imaging. For true three-dimensional imaging, phase encoding is used in 2 directions, instead of slice selection. The two-dimensional imaging equation is given by

$$s(k_x, k_y) = \int dx \int dy \rho(x, y) e^{-i2\pi(k_x x + k_y y)} \quad \textbf{Eq. 29}$$

where *k* is the spatial frequency in a given dimension (x or y in Eq. 29) and *ρ(x,y)* is the physical density of the object. The term “k space” describes the spatial frequency content of the image and is given by

$$k_n(t) = \frac{\gamma}{2\pi} \int_t G_n(t) dt \quad \textbf{Eq. 30}$$

where *n* is the dimension in which the gradient is applied and $G_n(t)$ is the gradient, which is given by

$$G_n \equiv \frac{\partial B_n}{\partial n}. \quad \textbf{Eq. 31}$$

The two-dimensional signal equation can be easily extended to three dimensions for volume imaging.

The image is created via the inverse Fourier transform. For a 2D image orthogonal to the z axis, the signal is given by

$$\rho(x, y) = \int dk_x s(k_x, k_y) e^{i2\pi(k_x x + k_y y)} = \int dz \rho(x, y, z). \quad \textbf{Eq. 32}$$

The intensity of the NMR signal depends upon both hydrogen density (or the density of the element of interest) and the relaxation times of the sample. Radiologists take advantage of the fact that relaxation times vary a great deal between types of soft tissue, enabling physicians to noninvasively detect structures of interest.

3. Polymer Gel Dosimetry

Dosimetry gels are tissue-equivalent systems made up of water, gelatin, and either ferrous ions or monomers which react upon irradiation. The dosimeters are made according to a given formulation, irradiated with radiation of choice; dose response is then evaluated via different imaging modalities such as computed tomography, ultrasound, or magnetic resonance imaging. Gel dosimeters are unique from other dosimetry methods in that they provide a three-dimensional, integrating measure of dose with high spatial resolution.

3.1 History of Dosimetry Gels

Fricke Dosimeters

Fricke gels measure radiation dose from the oxidation of ferrous ions to ferric, initiated by free radicals produced by radiolysis of water, following the equation

$$H\bullet + O_2 \rightarrow HO_2\bullet . \qquad \textbf{Eq. 33}$$

The process was first described in the early 20th century (Fricke and Morse, 1927). The conversion of ferrous to ferric ions is as follows:

$$
\begin{aligned}
&Fe^{2+} + OH\bullet \rightarrow Fe^{3+} + OH^{-} \\
&Fe^{2+} + HO_2\bullet \rightarrow Fe^{3+} + HO_2^{-} \\
&HO_2^{-} + H_3O^{+} \rightarrow H_2O_2 + H_2O \\
&Fe^{2+} + H_2O_2 \rightarrow Fe^{3+} + OH^{-} + OH\bullet .
\end{aligned}
\qquad \textbf{Eq. 34}
$$

The change in ferric ion concentration is thus related to the radiation dose (energy per unit mass) by

$$
\Delta\left[Fe^{3+}\right] = \frac{D \cdot G\left(Fe^{3+}\right) 10 \rho}{N_A \cdot e} \qquad \textbf{Eq. 35}
$$

where *D* is the dose, *G(Fe^{3+})* is the chemical yield of Fe^{3+} (in ions produced per 100 eV), ρ is the density in kg liter^{-1}, N_A is Avogadro's number, and *e* is the number of Joules per electron volt.

In the early days of MRI, Gore et al. proposed to implement the Fricke solution in a gelatin matrix, thereby localizing the 3-dimensional spatial irradiation fields (Gore et al., 1984). A typical Fricke gel is made up of distilled or de-ionized water, ferrous ion (usually from ferrous ammonium sulphate), sulphuric acid (to lower pH), air or oxygen, and gel (which may be gelatin or agarose). The preparation technique is simpler compared to most polymer based dosimeters, which are discussed later. For a large range of energies used in radiation therapy, Fricke gels may be closer to water equivalence than PAG gels (see below).

The dose response of Fricke gels may be characterized using optical spectrophotometry scanning techniques, utilizing the optical property of the ferric ion, which strongly absorbs wavelengths of ultraviolet light at 224 and 304 nm

(Fricke and Morse, 1927). The dose response of the irradiated ferrous sulphate solution is then

$$D = \frac{N_A \cdot e}{\rho \cdot \ell \cdot G\left(Fe^{3+}\right)} \frac{OD(D) - OD(0)}{\varepsilon_m} \qquad \textbf{Eq. 36}$$

where *l* is the optical path length, *OD(D)* and *OD(0)* are the optical densities at 304 nm of the irradiated and unirradiated dosimeter, respectively, and ε_m is the molar extinction coefficient for Fe^{3+} (approximately 2200 $M^{-1}cm^{-1}$ at 25˚C) (Fricke and Hart, 1955). Ferric ions also produce a strong paramagnetic enhancement of NMR relaxation rates, particularly R1, and are more effective at reducing T1 than ferrous ions. The NMR dose response of Fricke is analogous to the spectrophotometric equation above and is given by

$$D = \frac{N_A e}{10 \rho G\left(Fe^{3+}\right)} \frac{R_1(D) - R_1(0)}{r_{eff}^{3+} - r^{2+}} \qquad \textbf{Eq. 37}$$

where R1(0) is the relaxation rate of the unirradiated dosimeter and r^{3+} and r^{2+} are the relaxivities for the ferrous and ferric ions, respectively. The subscript "*eff*" is added because the ferric ion hydration is affected by complexing with the gelatin. Thus maps of R1 can be used to portray spatial distribution of ferric ions after irradiation.

It was later shown that diffusion causes significant blurring of radiation fields soon after irradiation in Fricke dosimeters (Schulz et al., 1990) and that an rf field applied to the gels is attenuated because of their high electrical conductivity. Still, the technique is in limited use due to its relative ease of preparation and tissue equivalence.

Polymer Gel Dosimeters

Polymer gel dosimetry is based upon the concept of recording the effects of free radicals (generated primarily from the radiolysis of water) initiating polymerization of monomers. Their use takes advantage of two phenomena: 1 – radiation-induced polymerization and cross-linking, and 2 – a change in water proton relaxation in the presence of a macromolecular substance, in this case a polymer. The monomers are placed in a solution (usually of water and gelatin) which preserves the spatial distribution of the polymers that are formed upon exposure to radiation.

For absolute measurements of dose distributions, calibration tubes must be made in conjunction with the actual gel dosimeter. This may be accomplished by filling a number of test tubes with dosimetry gel from the same batch as the larger dosimeter, and irradiating them to known doses. Figure 4 shows a collection of calibration tubes prepared in conjunction with a larger dosimeter, irradiated to 33 Gy.

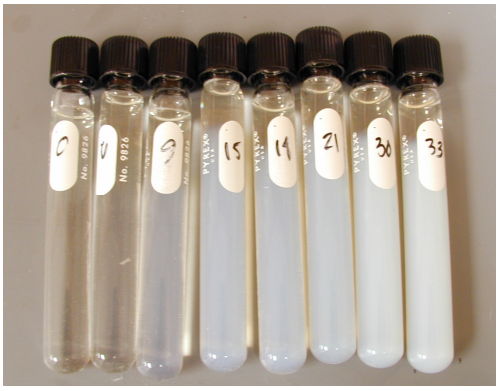

Figure 4: Calibration tubes irradiated to different doses.

The larger gel is imaged simultaneously with the calibration tubes (see Figure 5). The dose-dependent factor (such as R2 for magnetic resonance measurements) is plotted versus dose, creating a means of mapping measured R2 values in the larger dosimeter to dose.

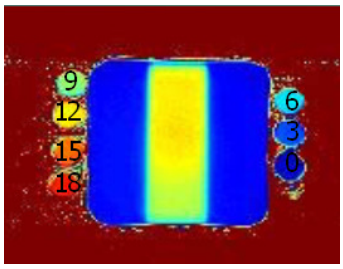

Figure 5: R2-image of larger dosimeter irradiated to 10 Gy with accompanying calibration dosimeters.

3.2 Formulations

An initial attempt to formulate a dosimeter without the inhibitions of Fricke dosimeters resulted in the BANANA gel (Maryanski et al., 1993). These gels were made up of N,N'-methylene-bisacrylamide cross-linker (2.5% or 4% by weight), acrylamide monomer (2.5% or 4%), agarose gel, and distilled water, produced in a nitrogen environment. Sulphuric acid was dissolved in the solution as well in order to obtain a specific pH (3, in this case).

A later system was BANG gels, which are comprised of N,N'-methylene-bisacrylamide cross-linker, acrylamide monomer, gelatin, in varying amounts depending upon a desired recipe (3%, 3%, 5% respectively for the first formulation), and distilled water, and which are prepared in an oxygen-free environment of nitrogen. Production involves deoxygenating water by bubbling humidified nitrogen through it for at least one hour, adding gelatin, and allowing it to bloom. The flask is then protected from light, the monomers added, and the

solution magnetically stirred. Care must be taken to remove all oxygen from the production environment. After the mixture is mixed thoroughly, it may be poured into the desired vessel.

Gelatin was chosen for the gelling matrix of BANG gels because its R2 is nearly an order of magnitude lower than agarose gels, which had been used in the earlier versions of polymer gels. Additionally, the spatial progression of gelation is more uniform in gelatin, and gelatin is more transparent than agarose.

BANG-2 was later introduced and was comprised of 3% bis, 3% acrylic acid, 1% sodium hydroxide, 5% gelatin, and 88% water, all percentages by weight (Maryanski et al., 1996a). It has been shown to have decreasing sensitivity with increasing photon or electron energy, and no dependence upon dose rate (Novotny et al., 2001).

PAG (polyacrylamide gel) is a more general term for this class of polymer gels, which may have different proportions of acrylamide and bis. Work has been performed to model the behavior of the radiation-induced polymerization of the gel using kinematic equations (Fuxman et al., 2003).

Previous formulations of polymer gel dosimeters were dependent upon a hypoxic environment during their preparation and throughout use. Fong *et al* (Fong et al., 2001) developed a formulation (termed MAGIC) that could be prepared in normal atmospheric conditions. The authors used previous studies that indicated a reaction in which a bivalent metal may complex with ascorbic acid and molecular oxygen, and allows an electron to transfer through the complex to an external species. Free radicals are thus generated which can be

used to initiate polymerization. The following solution (for 1 kg of dosimeter) was found to be the most sensitive to radiation:

Table 2: Components for MAGIC gel formulation

Component	Amount (g)
Gelatin (type A, 300 bloom)	80
Methacrylic acid	90
Ascorbic acid	0.352
$CuSO_4 \cdot 5H_2O$	0.02
Hydroquinone	2.0
Distilled water	828

The dosimeter has been shown to have close equivalence to water for radiation therapy purposes (Venning et al., 2005). The dosimeter was later optimized for measurement of R2 for doses of 0 – 20 Gy and this formulation was termed MAGIC-2 (Luci et al., 2007); this work is described in Chapter II.

Other variations on the MAGIC theme include MAGAS (methacrylic acid gelatin gel with abscorbic acid) and MAGAT (methacrylic acid gelatin and tetrakis phosphonium chloride) formulations. These formulations have different properties but rely on the same fundamental mechanisms for recording dose.

3.3 Methods of Measurements

Optical Computed Tomography

Optical computed tomography can be used to measure the change in optical density of polymer gels as a function of dose. Planar images of the dosimeter are constructed from a series of line integrals obtained from projections taken from different directions, read with a detector system. This technique was first applied

to polymer gels in the mid-1990s (Gore et al., 1996, Maryanski et al., 1996b) and continued by other authors (McJury et al., 2000, Oldham et al., 2003, Gambarini et al., 2004). The optical density changes after irradiation mainly because the polymer particles formed scatter visible light.

Ultrasound

Ultrasound, a non-invasive diagnostic technique that is mostly used to identify structures in the human body based on how they reflect sound waves, has been used to characterize dose distributions in polymer gel dosimeters. Investigators have shown that the ultrasonic speed of propagation and attenuation in a gel varies with absorbed dose (Mather et al., 2002, Mather and Baldock, 2003). However, spatial resolution and ability to quantify dose are not adequate for practical applications.

X-ray Computed Tomography

Dose distributions may also be measured using x-ray computed tomography techniques. To prevent further polymerization from the radiation exposure in CT, PAG gels are left open to atmosphere beginning at least one day after irradiation, until evaluation (Hilts et al., 2000). Dose response as measured by CT is determined by Hounsfield units versus dose (Trapp et al., 2001, Hilts et al., 2005), which reflect changes in gel density.

Magnetic Resonance Imaging

Magnetic resonance imaging techniques are by far the most widely used to study dose distributions in polymer gels. The procedure was first introduced as a method to measure dose distributions in Fricke gels (Gore et al., 1984) and was

later used for both PAG and MAGIC formulations (Maryanski et al., 1993, Maryanski et al., 1996a, Fong et al., 2001). Typically, simple CPMG spin-echo sequences are used, because T2 changes are the most apparent effect of radiation and sequences are widely available on clinical MRI scanners.

3.4 Gel production and processes

Dose Response

To relate polymer gel response to dose, measurements of R2 versus dose are most commonly used, although some studies have measured R1, diffusivity constants, MT rates, or Hounsfield units, for example. When irradiated, monomers polymerize and the NMR properties of water in the gels are changed, particularly T2. The change in this time can be related to dose. Method of preparation can affect the dose response, as R2 has been shown to be determined by the temperature to which the gelatin solution is heated in order to obtain a sol (De Deene et al., 2000).

Dose uncertainty and resolution

Measurements of T2 have inherent uncertainties due to many factors. These have been analyzed previously (Baldock et al., 2001). It has been shown that noise in a T2 map derived from MRI data is the largest contributor to the uncertainty in dose estimates (Baldock et al., 1999). The standard uncertainty of the dose is given, using the propagation of errors, as

$$u_c^2(D) = \left[\frac{\partial D}{\partial T_2}\right]^2 \left[u^2(T_2)\right]. \qquad \textbf{Eq. 38}$$

We can define dose resolution D^{p}_{Δ} as the minimal separation between two absorbed doses, distinguished with the level of confidence *p* (Baldock et al., 2001).

3.5 Uses

The goal for the clinical use of polymer gel dosimeters is to utilize them as three-dimensional, integrating dosimeters in situations where traditional dosimeters, such as film or diodes, do not suffice, such as the complex fields produced by intensity modulated radiation therapies (IMRT) or stereotactic surgery. Gels have also been developed as test objects for both radiotherapy and diagnostic physics uses, such as contrast-detail test patterns for MRI quality assurance (Gore et al., 1997).

Polymer gel dosimeters have been used to calculate percent depth dose curves and dose profiles (Haraldsson et al., 2000) and to validate IMRT (Gustavsson et al., 2003). Gels have also been used to demonstrate irradiation fields from brachytherapy (Fragoso et al., 2004) and for verification of dynamic radiation therapy techniques with respiratory gating (Ceberg et al., 2008).

Comparison to Present Techniques

Gels have been shown to agree well with film (Berg et al., 2001, Berg et al., 2004). Under ideal scanning conditions, it is possible to achieve voxel resolution down to 0.04 mm^3, determined via studies of the modulation transfer function. Spatial resolution can be better than 280 μm, depending on scanning equipment. (Berg et al., 2004)

Problems with Gel

Previous studies have shown that gel dosimeters have potential for use in both radiation therapy and diagnostic physics applications, but several authors have pointed out observations of post-irradiation events that indicate the need for closer study and improvement in gels. For example, edge enhancement at the boundary of radiation fields has been seen in PAG (Fuxman et al., 2005) and in BANG (Maryanski et al., 1994). Some sensitivity decrease with increasing energy of irradiation beam has been observed in BANG (Novotny et al., 2001). Others have reported apparent dose differences for dosimeters irradiated in fractionation schemes for methacrylic acid-based gels (Karlsson et al., 2007).

4. Thesis overview

While much work has previously been done to demonstrate the use of gels in radiation therapy dose verification and to describe important experimental considerations for their use, there is a need to move beyond anecdotal demonstrations and into more specific investigations into the underlying mechanisms of the dosimeter. Most formulations of gels have been implemented for measurements of specific dose responses, but it would be helpful to optimize a polymer gel for dose response in terms of a particular NMR parameter. Additionally, methods of measurement of dose response other than the widely used transverse relaxation rate could be more robust in the face of imaging errors that may be present but not obvious to those implementing the dosimeter. Finally, understanding the precise mechanisms of relaxation is an important area

of research because the knowledge gained could be used to formulate more sensitive versions of the dosimeters.

This work seeks to address several issues regarding methacrylic acid-based polymer gels. The second chapter describes a revised formulation, called MAGIC-2, which optimizes the dosimeter for measurements of R2. The bulk of this chapter comes from the article “Optimization of MAGIC gel formulation for three-dimensional radiation therapy dosimetry” which was published as a note in the journal *Physics in Medicine and Biology* in 2007 (Luci et al., 2007).

The third chapter details comprehensive measurements of the NMR properties of the revised MAGIC gel formulation at high field strengths. The dosimeter responses for R2 and R1 are measured, along with quantitative magnetization transfer parameters. The work in the chapter is one of the first to directly compare magnetization transfer rates measured with two different measurement schemes, selective inversion recovery and pulsed magnetization transfer, in order to develop a model of the dose response.

The fourth chapter describes an alternative method to measure dose response for polymer gel dosimetry. In particular, it investigates how the measurement of magnetization transfer can be used to quantify dose and how the dose response changes in the face of inhomogeneities in the B_1 field, as compared to changes in the transverse relaxation rate measurement. We introduce a new magnetization transfer parameter, called the magnetization transfer proportion. This work was published in 2008 as a full paper entitled “Magnetization transfer proportion: a simplified measure of dose response for

polymer gel dosimetry" in the journal *Physics in Medicine and Biology* (Whitney et al., 2008).

Finally, the fifth chapter attempts to describe the relaxation mechanisms responsible for the dose response of the methacrylic acid-based polymer dosimeter. The polymer gel dosimeter is deconstructed into its parts and samples of pure monomer/polymer and gelatin are investigated. The role of chemical exchange in transverse relaxation is evaluated in order to understand how the role of chemical exchange changes as higher dose is applied to the gel and more polymerization occurs. A model relating R2 dose response to fast exchange processes in the gels is presented.

References

Baldock, C., Lepage, M., Back, S.A.J., Murry, P.J., Jayasekera, P.M., Porter, D. & Kron, T. (2001) Dose resolution in radiotherapy polymer gel dosimetry: Effect of echo spacing in mri pulse sequence. *Phys. Med. Biol.,* 46**,** 449-460.

Baldock, C., Murry, P. & Kron, T. (1999) Uncertainty analysis in polymer gel dosimetry. *Phys. Med. Biol.,* 44**,** N243-N246.

Berg, A., Ertl, A. & Moser, E. (2001) High resolution polymer gel dosimetry by parameter selective mr-microimaging on a whole body scanner at 3 t. *Med. Phys.,* 28**,** 833-843.

Berg, A., Pernkopf, M., Waldhausl, C., Schmidt, W. & Moser, E. (2004) High resolution mr based polymer dosimetry versus film densitometry: A systematic study based on the modulation transfer function approach. *Phys. Med. Biol.,* 49**,** 4087-4108.

Bloch, F. (1946) Nuclear induction. *Phys. Rev.,* 70**,** 460-474.

Ceberg, S., Karlsson, A., Gustavsson, H., Wittgren, L. & Back, S.A.J. (2008) Verification of dynamic radiotherapy: The potential for 3d dosimetry under respiratory-like motion using polymer gel. *Phys. Med. Biol.,* 53**,** N387-N396.

De Deene, Y., Hanselaer, P., De Wagter, C., Achten, E. & De Neve, W. (2000) An investigation of the chemical stability of a monomer/polymer gel dosimeter. *Phys. Med. Biol.,* 45**,** 859-878.

Farrar, T.C. & Becker, E.D. (1971) *Pulse and fourier transform nmr: Introduction to theory and methods,* New York, Academic Press.

Fong, P.M., Keil, D.C., Does, M.D. & Gore, J.C. (2001) Polymer gels for magnetic resonance imaging of radiation dose distributions at normal room atmosphere. *Phys. Med. Biol.,* 46**,** 3105-3113.

Fragoso, M., Love, P.A., Verhaegen, F., Nalder, C., Bidmead, A.M., Leach, M. & Webb, S. (2004) The dose distribution of low dose rate cs-137 in intracavitary brachytherapy: Comparison of monte carlo simulation, treatment planning calculation and polymer gel measurement. *Phys. Med. Biol.,* 49**,** 5459-5474.

Fricke, H. & Hart, E. (1955) Chemical dosimetry. IN ATTIX, F. H. & ROESCH, W. C. (Eds.) *Radiation dosimetry.* New York, Academic Press.

Fricke, H. & Morse, S. (1927) The chemical action of roentgen rays on dilute ferrosulphate solutions as a measure of dose. *Am. J. Roent. Radium Ther. Nucl. Med,* 18**,** 430-2.

Fuxman, A.M., Mcauley, K.B. & Schreiner, L.J. (2003) Modeling of free-radical crosslinking copolymerization of acrylamide and n,n '-methylenebis(acrylamide) for radiation dosimetry. *Macromolecular Theory and Simulations,* 12**,** 647-662.

Fuxman, A.M., Mcauley, K.B. & Schreiner, L.J. (2005) Modelling of polyacrylamide gel dosimeters with spatially non-uniform radiation dose distributions. *Chemical Engineering Science,* 60**,** 1277-1293.

Gambarini, G., Birattari, C., Mariani, M., Marchesini, R., Pirola, L., Prestini, P., Sella, M. & Tomatis, S. (2004) Study of light transmittance from layers of fricke-xylenol-orange-gel dosimeters. *Nucl Instrum Meth B,* 213**,** 321-324.

Gore, J.C., Kang, Y.S. & Schulz, R.J. (1984) Measurement of radiation-dose distributions by nuclear magnetic-resonance (nmr) imaging. *Phys. Med. Biol.,* 29**,** 1189-1197.

Gore, J.C., Maryanski, M.J. & Schulz, R.J. (1997) Test objects for mri quality assurance based on polymer gels. *Med. Phys.,* 24**,** 1405-1408.

Gore, J.C., Ranade, M., Maryanski, M.J. & Schulz, R.J. (1996) Radiation dose distributions in three dimensions from tomographic optical density scanning of polymer gels: 1. Development of an optical scanner. *Phys. Med. Biol.,* 41**,** 2695-2704.

Gustavsson, H., Karlsson, A., Back, S.A.J., Olsson, L.E., Haraldsson, P., Engstrom, P. & Nystrom, H. (2003) Magic-type polymer gel for three-dimensional dosimetry: Intensity-modulated radiation therapy verification. *Med. Phys.,* 30**,** 1264-1271.

Haraldsson, P., Back, S.A.J., Magnusson, P. & Olsson, L.E. (2000) Dose response characteristics and basic dose distribution data for a polymerization-based dosemeter gel evaluated using mr. *Brit J Radiol,* 73**,** 58-65.

Hilts, M., Audet, C., Duzenli, C. & Jirasek, A. (2000) Polymer gel dosimetry using x-ray computed tomography: A feasibility study. *Phys. Med. Biol.,* 45**,** 2559-2571.

Hilts, M., Jirasek, A. & Duzenli, C. (2005) Technical considerations for implementation of x-ray ct polymer gel dosimetry. *Phys. Med. Biol.,* 50**,** 1727-1745.

Karlsson, A., Gustavsson, H., Mansson, S., Mcauley, K.B. & Back, S.A.J. (2007) Dose integration characteristics in normoxic polymer gel dosimetry investigated using sequential beam irradiation. *Phys. Med. Biol.,* 52**,** 4697-4706.

Luci, J.J., Whitney, H.M. & Gore, J.C. (2007) Optimization of magic gel formulation for three-dimensional radiation therapy dosimetry. *Phys. Med. Biol.,* 52**,** N241.

Maryanski, M.J., Gore, J.C., Kennan, R.P. & Schulz, R.J. (1993) Nmr relaxation enhancement in gels polymerized and cross-linked by ionizing radiation: A new approach to 3d dosimetry by mri. *Magn. Reson. Imag.,* 11**,** 253-258.

Maryanski, M.J., Ibbott, G.S., Eastman, P., Schulz, R.J. & Gore, J.C. (1996a) Radiation therapy dosimetry using magnetic resonance imaging of polymer gels. *Med. Phys.,* 23**,** 699-705.

Maryanski, M.J., Schulz, R.J., Ibbott, G., Gatenby, J.C., Xie, J., Horton, D. & Gore, J.C. (1994) Magnetic resonance imaging of radiation dose distributions using a polymer-gel dosimeter. *Phys. Med. Biol.,* 39**,** 1437-1455.

Maryanski, M.J., Zastavker, Y.Z. & Gore, J.C. (1996b) Radiation dose distributions in three dimensions from tomographic optical density scanning of polymer gels .2. Optical properties of the bang polymer gel. *Physics in Medicine and Biology,* 41**,** 2705-2717.

Mather, M. & Baldock, C. (2003) Ultrasound tomography imaging of radiation dose distributions in polymer gel dosimeters: Preliminary study. *Med. Phys.,* 30**,** 2140-2148.

Mather, M.L., De Deene, Y., Whittaker, A.K., Simon, G.P., Rutgers, R. & Baldock, C. (2002) Investigation of ultrasonic properties of pag and magic polymer gel dosimeters. *Phys. Med. Biol.,* 47**,** 4397-4409.

Mcjury, M., Oldham, M., Cosgrove, V.P., Murphy, P.S., Doran, S., Leach, M.O. & Webb, S. (2000) Radiation dosimetry using polymer gels: Methods and applications. *Brit J Radiol,* 73**,** 919-929.

Mirau, P.A. (2005) *A practical guide to understanding the nmr of polymers,* Hoboken, New Jersey, John Wiley & Sons, Inc.

Novotny, J., Spevacek, V., Dvorak, P. & Cechak, T. (2001) Energy and dose rate dependence of bang-2 polymer-gel dosimeter. *Med. Phys.,* 28**,** 2379-2386.

Oldham, M., Siewerdsen, J.H., Kumar, S., Wong, J. & Jaffray, D.A. (2003) Optical-ct gel-dosimetry i: Basic investigations. *Med. Phys.,* 30**,** 623-634.

Schulz, R.J., Deguzman, A.F., Nguyen, D.B. & Gore, J.C. (1990) Dose-response curves for fricke-infused agarose gels as obtained by nuclear-magnetic-resonance. *Phys. Med. Biol.,* 35**,** 1611-1622.

Trapp, J.V., Aring, S., Baumick, J., Lepage, M., Michael, G. & Baldock, C. (2001) An experimental study of the dose response of polymer gel dosimeters imaged with x-ray computed tomography. *Phys. Med. Biol.,* 46**,** 2939.

Venning, A.J., Nitschke, K.N., Keall, P.J. & Baldock, C. (2005) Radiological properties of normoxic polymer gel dosimeters. *Med. Phys.,* 32**,** 1047-1053.

Whitney, H.M., Gochberg, D.F. & Gore, J.C. (2008) Magnetization transfer proportion: A simplified measure of dose response for polymer gel dosimetry. *Phys. Med. Biol.,* 53**,** 7107-7124.

CHAPTER II

OPTIMIZATION OF MAGIC GEL FORMULATION FOR THREE-DIMENSIONAL RADIATION THERAPY DOSIMETRY

1. Introduction

Polymer gel dosimeters are comprised of an aqueous matrix (usually gelatin) in which one or more monomers are dispersed. When exposed to ionizing radiation, polymerization is initiated by radicals that result from radiolysis. Several bulk properties (e.g. the nuclear magnetic resonance transverse relaxation rate R_2 and optical density) are sensitive to the molecular weight of the resultant polymer, and measurements of these can be used to determine the absorbed dose. Employing large containers of the gelatin mixture, it is possible to produce a 3D dose map using magnetic resonance imaging or optical scanning that may be used to validate radiation therapy planning or for quality assurance.

The first polymer gel dosimeters (BANG©, or non-commercially, PAG) were based on the monomers acrylamide and bisacrylamide (Maryanski et al., 1993, Baldock et al., 1998). Although effective, these dosimeters required hypoxic conditions in order to prevent molecular oxygen quenching of the short-lived initiating radicals. This prerequisite dictated that inert atmosphere glove boxes be used in their preparation, and that container materials be limited to oxygen-impermeable plastics and glass. Since most clinical radiation physicists had neither the equipment nor the technical resources to prepare oxygen sensitive formulations, the use of these gels was hampered.

Previously Fong et al. (Fong et al., 2001) introduced a formulation that permitted gel dosimeters to be prepared under normal atmospheric conditions. The new type of dosimeter was termed Methacrylic and Ascorbic acid in Gelatin Initiated by Copper, or MAGIC, and is less toxic than acrylamide-based dosimeters. The polyacrylamide gel dosimeter formulation was later adapted for preparation in regular atmospheric conditions through the addition of antioxidants such as tetrakis (hydroxymethyl) phosphonium chloride (Venning et al., 2005a, De Deene et al., 2006a). A summary of the different combinations of formulae can be found elsewhere (Senden et al., 2006).

A recent study (De Deene et al., 2006a) has compared the PAG, nPAG (a normoxic PAG), and MAGIC gel formulations for properties such as tissue equivalence, dose sensitivity, spatial integrity, temperature sensitivity, and energy and dose-rate dependence. The authors found that the methacrylic acid-based gel was superior in terms of dose sensitivity and stability over time while nPAG performed better in other areas. However, the differences in normoxic gel dosimeters are due to different chemical reaction schemes and both types deserve more in-depth study. The utility of MAGIC dosimeters depends heavily on the ability to measure accurately a significant response to polymerization of some localized property. The precise dependence of the dose response on the composition of the gels has not been described in detail. We present here studies designed to investigate the influences of different components with the aim of optimizing the performance of MAGIC polymer gel dosimeters for practical applications.

2. Methods

2.1 Gel preparation

The formulation of polymer gels studied here contains the same basic ingredients as the previous formulation: gelatin (300 bloom, Aldrich: Milwaukee, WI), ascorbic acid (Mallinckrodt; Paris, KY), $CuSO_4 \bullet 5H_2O$ (Aldrich: Milwaukee, WI), methacrylic acid (Sigma; St. Louis, MO), and HPLC grade distilled water. We omit hydroquinone as it is already present in the methacrylic acid, added by the manufacturer.

Gels for all experiments were prepared in the following manner: a flask containing the water was placed in an equilibrated water bath at 48 C. The gelatin, ascorbic acid solution (AA), and copper sulfate solution (Cu^{2+}) were all added and the solution stirred with a magnetic bar for two minutes. Methacrylic acid (MAA) was then added and the solution stirred for an additional ninety seconds. The gel was immediately poured into glass test tubes, sealed with screw-cap tops, and centrifuged at 15.4g for 15 seconds plus ramp time. The gels were taken out of the centrifuge and placed in a refrigerator for storage overnight, approximately eighteen hours.

The effects of variations of the gelatin, monomer and copper concentrations were investigated, as described below.

2.2 Gel irradiation

In each experiment, one gel dosimeter for each concentration variation was reserved unirradiated, and one was irradiated. Samples to be irradiated were

placed in a room temperature water bath for approximately two hours to equilibrate temperature, and irradiated to 20 Gy using a Therapax orthovoltage X-ray unit with dose rate of 1.844 Gy/min, 180 kVp, and 17 mA.

2.3 Relaxation measurements

The measurements of relaxation times were performed on a standard clinical MRI scanner. The ultimate goal of gel dosimetry is to provide high resolution maps of radiation doses for practical applications. To that end, the main criterion used in the development of the MR imaging protocol was that the method should be reasonable for the widest range of clinical MR scanners. Hardware and software limitations of the three most popular MR scanner vendors were taken into consideration, and the protocol tailored to suit all of them. Thus, other approaches may provide more accurate data for specific purposes and choice of equipment.

The echo train length was the most notable limitation. For some scanners, the maximum number of echoes in a multi-echo (CPMG-type) spin-echo is four. Theoretically, it is possible to calculate T2 from the signal measured at two echo times, but the accuracy and reproducibility suffer if stringent T2-dependent criteria are not met. Since a gel dosimeter in a practical application will undoubtedly have regions of greatly-differing T2 values, it is necessary to sample a range of TE values.

The limitation of four echoes was dictated by the scanner software, so the echo times become the most important parameter to optimize. Linear echo

spacing is also a limitation in practice, so an echo spacing of 30ms was chosen, yielding echo times of 30, 60, 90, and 120ms. These echo times ensure that an appropriate range of T2 values was adequately measured. For example, if a minimum echo spacing of 15 ms were selected, the high dose range would be more optimally sampled while the low dose range would not be adequately sampled, and vice versa for echoes longer than 30 ms.

To optimize the signal-to-noise ratio, a TR of at least 5 times the longest T1 is necessary. For MAGIC gel dosimeters we have found T1 to be in the range of approximately 0.9-1.2 s, and chose TR to be 7 or 8 seconds, detailed below. The matrix size was chosen to produce the resolution necessary for most dosimetry applications.

Twenty-four hours following irradiation, samples were placed in a custom-made holder, immersed in mineral oil, and imaged with a GE Signa 3T MRI system with a multi-echo spin echo pulse sequence with the following parameters: TR = 8s (7s for the optimization of monomer concentration), TE = 30ms, 4 echoes, slice thickness = 10mm, 256×128 matrix, 140 × 140 mm field-of-view, and bandwidth = 15.64 kHz. T2 images were calculated by performing a least-squares fit to a single exponential for each pixel of the transaxial echo images. R2 values were taken as the inverse of the average T2 value of a circular region of interest for each sample. Dose sensitivity ($s^{-1}Gy^{-1}$) was calculated as the slope of the linear portion of the R2-dose response between 0 and 20 Gy. Dose resolution (Gy) was calculated using a previously published

method (Baldock et al., 2001) for 95% confidence. It is desirable to maximize dose sensitivity while also optimizing dose resolution.

3. Results

3.1 Gelatin concentration

In order to determine the optimum concentration of gelatin in the MAGIC gels over a useful dose range, the experiment above was performed, with the concentration of gelatin being varied while all other formulation components were kept constant. The dose sensitivity and dose resolution values are displayed in Figure 6.

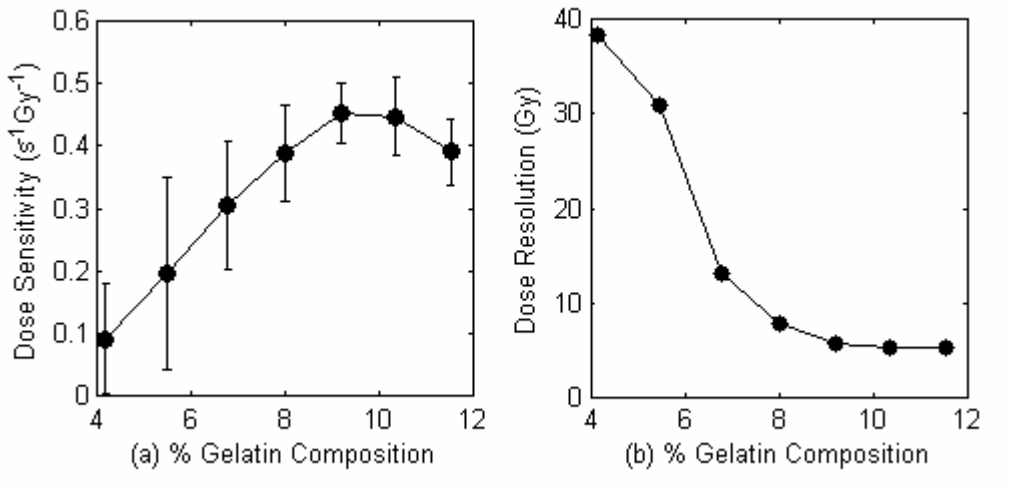

Figure 6: Dose sensitivity (a) and resolution (b) versus percent gelatin composition. A concentration of 9% is chosen as optimal.

A concentration of 9% was chosen as optimal, because neither the dose sensitivity nor the dose resolution improves past this point. These results are slightly different than those found in a recent report (De Deene et al., 2006a),

where the authors found no significant change in dose sensitivity for gelatin compositions above 8% in methacrylic-acid based gels.

3.2 Monomer concentration

In order to determine the optimum monomer concentration of the MAGIC gels over a useful dose range, seven sets of gels were prepared identically, each with a different concentration of methacrylic acid. The dose sensitivity and dose resolution values are displayed below in Figure 7.

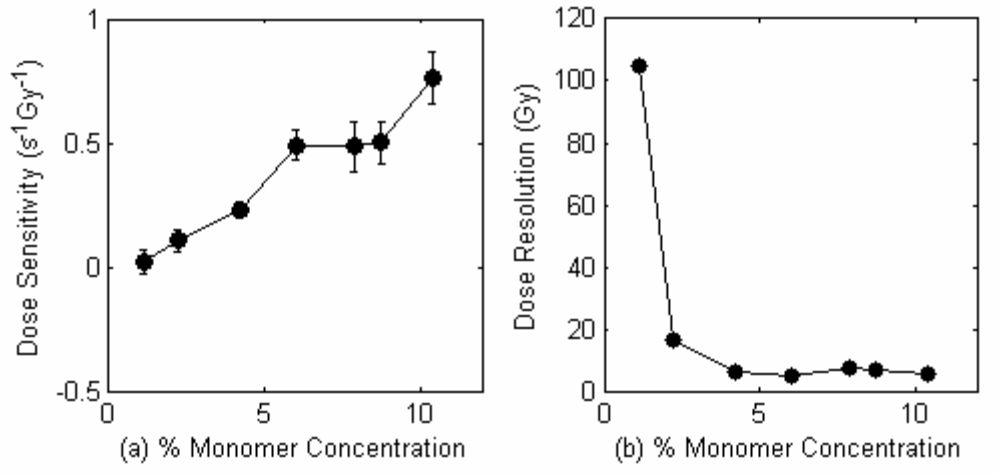

Figure 7: Dose sensitivity (a) and resolution (b) versus monomer concentration. A concentration of 4% is chosen as optimal.

The optimal concentration of methacrylic acid is chosen to be 4%. While the dose sensitivity is higher for greater concentrations, the uncertainty of dose sensitivity also increases and the dose resolution is relatively unchanged. Lower dose sensitivity is useful for a wider range of doses. Additionally, as previously reported (Fong et al., 2001), increasing the amount of methacrylic acid increases the intercept or background of the response curve, reducing the slope-to-

intercept ratio (another determinant of how well small changes in dose may be detected). Note however, that larger dose sensitivities can be obtained at higher percent monomer, and such a response may be desirable under circumstances in which the dose resolution and dynamic range are less important.

Figure 8 provides further explanation for the choice of 4% monomer concentration. Greater concentrations of monomer shorten the T2 of the unirradiated gel. The range of T2 values for a 4% gel is approximately 70 and 50 ms for doses of 0 and 20 Gy, respectively, which matches the choice of TE values on clinical scanners well.

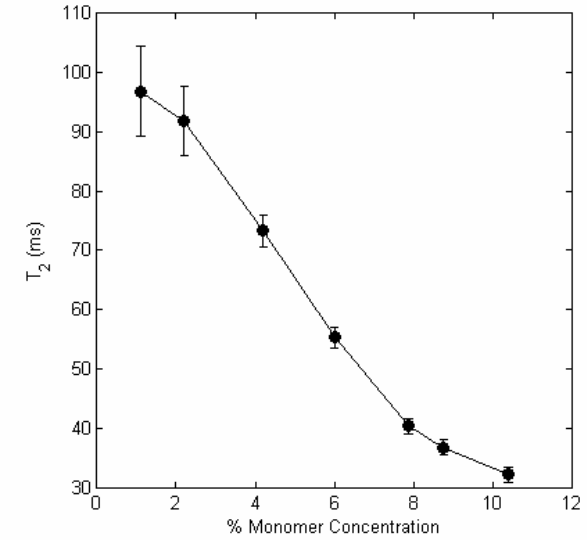

Figure 8: T_2 of unirradiated gels versus concentration for optimization of monomer.

3.3 Cu^{2+} concentration

The above experiment was repeated, with the concentration of copper being varied. Nine sets of gels were prepared identically, each with a different

concentration of copper sulfate. The dose sensitivity and dose resolution values are displayed in Figure 9.

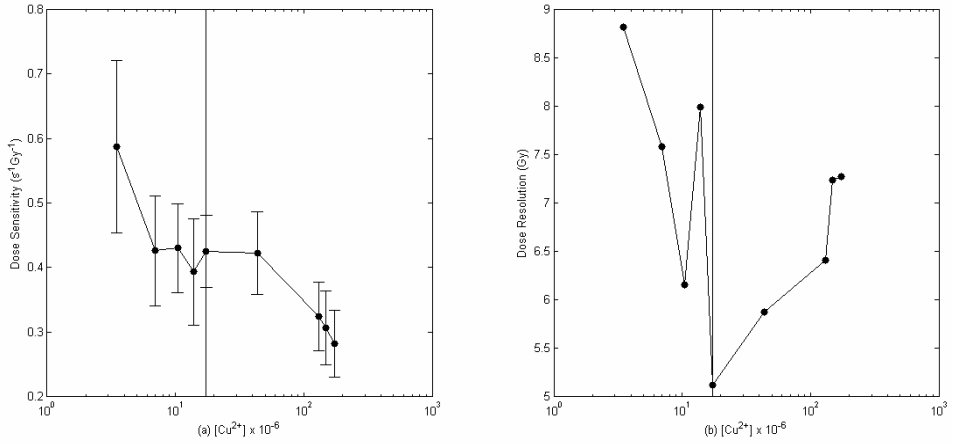

Figure 9: Dose sensitivity (a) and resolution (b) versus [Cu^{2+}]. The vertical line in both plots indicates the chosen concentration of 17.38×10^{-6} M. Note the semilog plot.

The optimum concentration of Cu^{2+} was determined to be 17.38×10^{-6} M, beyond which the dose sensitivity and resolution deteriorate as [Cu] increases. It is interesting to note from our data that the optimal dose sensitivity does not arise when the concentration of copper is maximal, when (presumably) the level of oxygen is minimized.

When compared to the original MAGIC gel formulation, this new formulation, which we call "MAGIC-2," has a 22% higher (0.503 versus 0.413 $s^{-1}Gy^{-1}$) dose sensitivity than the original, as shown in Figure 10.

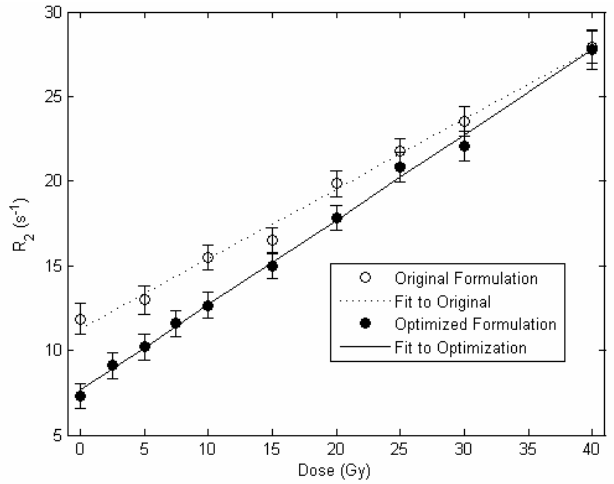

Figure 10: Comparison of dose response for original and optimized formulations, measured at 3T.

3.4 Density measurements and tissue equivalence

To determine the density of the unirradiated formulation, the dosimeter was manufactured and poured into a flask of known mass and volume. Weight fractions and the effective atomic number were calculated to determine the formulation's comparison to human muscle tissue and water. These values are given in Table 3

Table 3: Comparison of elemental composition, electron densities (mass density ρ and relative electron density ρ_e^w), and average atomic numbers for various normoxic gel dosimeter formulations, human muscle tissue, and water (weight fractions denoted as w_k).

Material	w_H	w_C	w_N	w_O	w_S	$w_{Cu(ii)}$	ρ (g cm^{-3})	ρ_e^w	Z_{eff}[a]
MAGIC-2 (this work)	0.1066	0.0604	0.0129	0.8202	7.732×10^{-7}	1.532×10^{-6}	1.017	1.015	7.12
MAGIC (Fong et al., 2001)	0.1062	0.0751	0.0139	0.8021	2.58×10^{-6}	5.08×10^{-6}	1.060	1.055	7.07
nPAG[b] (De Deene et al., 2006a)	0.1073	0.0625	0.0218	0.8080	0.0002	-	1.035	1.033	7.11
PAGAT[c] (Venning et al., 2005a)	0.1059	0.0681	0.0242	0.8008	-	-	1.026	1.027	7.10
Muscle	0.1020	0.1230	0.0350	0.7298	-	-	1.030	1.014	6.92
Water	0.1111	-	-	0.8889	-	-	1.000	1.000	7.22

[a] Calculated as $Z = \sum_k w_k Z_k$

[b] $w_P = 0.0003$

[c] $w_P = 0.0002$, $w_{Cl} = 0.0002$

4. Discussion

4.1 Comparison with other normoxic polymer gel dosimeters.

As mentioned previously, several authors have reported the dose response characteristics of other normoxic polymer gel dosimeters. Table 4 summarizes the dose response characteristics of these various formulations, including the optimized MAGIC formulation.

Table 4: Dose response characteristics for various normoxic polymer gel formulations. Values are quoted as published except where noted.

Formulation	Dose sensitivity ($s^{-1}Gy^{-1}$)	Intercept	Calculated slope-intercept ratio	Field strength of measurement (T)	Linear region
MAGIC-2	0.503	7.653	0.066	3	0-20 Gy
MAGIC	0.413	11.290	0.037	3	0-30Gy
†nPAG	0.19*	0.9*	0.211	1.5	
PAGAT	0.183	1*	0.183	1.5	0-7 Gy

* From inspection

† Dose sensitivity and intercept estimated in the dose range of 0-10Gy

In comparison to other normoxic formulations, the MAGIC-type gels both have significantly higher dose sensitivities, while acrylamide-based formulations have the advantage of lower intercepts, indicative of less pre-irradiation polymerization.

4.2 General discussion

The new formulation performs better as a dosimeter than the original MAGIC gel formulation. Although we report the results of varying only one ingredient at a time, in practice we have also explored other combinations and have not found better dose responses.

These results indicate a clear benefit to using a higher gelatin composition than that originally reported. Although the dose resolution does not decrease by a substantial amount after approximately 8% composition, the dose response continues to increase beyond that level. Using a higher concentration of gelatin appears to improve the dose response, presumably because the gel facilitates grafting or propagation of the polymerization.

There does not seem to be an appreciable benefit to using greater than 4% monomer concentration. Although the dose sensitivity is higher, the uncertainty of dose measurements may also be higher, and the overall dose resolution is about the same.

The slope-to-intercept ratio of the dose-response of polymer gels is another index for quantifying dose-response and comparing different formulations. The

new formulation has a ratio of 0.066, compared to the original formulation's ratio of 0.037, an increase of 78%.

Finally, dose resolutions for the original MAGIC gel formulation and MAGIC-2 were calculated. Over a range of 40Gy, the original formulation has dose resolution of 6.4 Gy while the MAGIC-2 formulation has dose resolution of 5.1 Gy for the parameters discussed above, an improvement of 20%.

5. Conclusion

By comparing the effects of different compositions, we have optimized the formulation for making MAGIC gel dosimeters, producing a dosimeter with greater dose sensitivity while maintaining the desirable qualities of less toxicity, normoxic manufacture, and tissue equivalence. In addition, we anticipate that studies of the effects of different compositions will help to better understand the mechanisms of the response of polymer gel dosimeters.

References

Baldock C, Burford R P, Billingham N, Wagner G S, Patval S, Badawi R D and Keevil S F (1998) Experimental procedure for the manufacture and calibration of polyacrylamide gel (PAG) for magnetic resonance imaging (MRI) radiation dosimetry. *Phys. Med. Biol.* 43**,** 695-702.

Baldock C, Lepage M, Back S a J, Murry P J, Jayasekera P M, Porter D and Kron T (2001) Dose resolution in radiotherapy polymer gel dosimetry: effect of echo spacing in MRI pulse sequence. *Phys. Med. Biol.* 46**,** 449-460.

De Deene Y, Vergote K, Claeys C and De Wagter C (2006) The fundamental radiation properties of normoxic polymer gel dosimeters: a comparison between a methacrylic acid based gel and acrylamide based gels. *Phys. Med. Biol.* 51**,** 653-673.

Fong P M, Keil D C, Does M D and Gore J C (2001) Polymer gels for magnetic resonance imaging of radiation dose distributions at normal room atmosphere. *Phys. Med. Biol.* 46**,** 3105-3113.

Maryanski M J, Gore J C, Kennan R P and Schulz R J (1993) NMR relaxation enhancement in gels polymerized and cross-linked by ionizing radiation: A new approach to 3D dosimetry by MRI. *Magn. Res. Imaging* 11**,** 253-258.

Senden R J, De Jean P, Mcauley K B and Schreiner L J (2006) Polymer gel dosimeters with reduced toxicity: a preliminary investigation of the NMR and optical dose-response using different monomers. *Phys. Med. Biol.* 51**,** 3301-3314.

Venning a J, Hill B, Brindha S, Healy B J and Baldock C (2005) Investigation of the PAGAT polymer gel dosimeter using magnetic resonance imaging. *Phys. Med. Biol.* 50**,** 3875-3888.

CHAPTER III

COMPREHENSIVE RELAXOMETRY AND MAGNETIZATION TRANSFER MEASUREMENTS FOR MAGIC-2 POLYMER GEL DOSIMETERS AT HIGH FIELD STRENGTH

1. Introduction

The dose response of polymer gels has been quantified with several different techniques. These include ultrasound, computed tomography, optical, and MRI methods, as discussed in the introduction. By far most studies have reported dose response in terms of parameters acquired through MRI, usually at field strengths of 1.5 T and below. However, higher field MRI should in principle afford higher signal-to-noise (SNR) data for more precise dose measurements, though the advantages of higher fields will depend on how dose response mechanisms vary with field too. Additionally, quantitative magnetization transfer parameters have not been reported for the newer MAGIC-2 gel formulation. The purpose of this work is to characterize the dose response of the methacrylic acid-based polymer gel dosimeter MAGIC-2 for several NMR parameters at high field strength. Relaxometry parameters to be investigated will include the longitudinal relaxation rate (R1), the transverse relaxation rate (R2), and the rates that define magnetization transfer.

2. Theory

2.1 Longitudinal and transverse relaxation

A brief overview of longitudinal and transverse relaxation is given in the introduction to this work.

2.2 Magnetization transfer

Magnetization transfer is a feature of how polymer gels change their NMR relaxation properties upon irradiation. In a simple model, the proton pools can be visualized as compartments of free water and other protons which exchange magnetization when probed with an off-resonance rf irradiation pulse. This exchange may occur through dipolar interactions between the pools or via chemical exchange of labile protons. A macromolecular pool of protons should have a T2 value much shorter than a free water pool, which dominates the MR signal. But the presence of the macromolecular pool and some specifics of the exchange between the pools can be observed by saturating the macromolecule pool and observing the change in the overall MR signal. Macromolecular protons are selectively saturated in MT sequences, taking advantage of the broad line width of the macromolecular protons versus the narrow line width of the water protons. Transfer of magnetization is observed as a decrease in the water signal. In clinical settings, magnetization transfer contrast (MTC) pulse sequences are designed to saturate the macromolecular pool and observe the change in the overall water signal. Certain tissues exhibit specific MTC behaviors which are of interest to medical professionals (Wolff and Balaban, 1989, Harrison et al., 1995,

Mehta et al., 1995, Quesson et al., 1997, Dresselaers et al., 2002, Steens et al., 2004, Stanisz et al., 2005).

A simple model of magnetization transfer incorporates the water and macromolecular pools as two separate compartments. Pool A represents the water spins, the number of which are normalized to 1 by convention ($M_{0A} = 1$). Macromolecular spins are located in pool B, the number of which is much less than that in pool A, and the relative fraction is given by M_{0B}. The unshaded portions of the compartments in Figure 11 indicate spins that are in the longitudinal orientation, while saturated spins are represented by the lower shaded portion. R_A and R_B are the longitudinal relaxation rates of pools A and B respectively, and *R* is the exchange rate between pools A and B. The rate of transfer from A to B is RM_{0B}. The rate from B to A is *R*, to conserve compartment sizes.

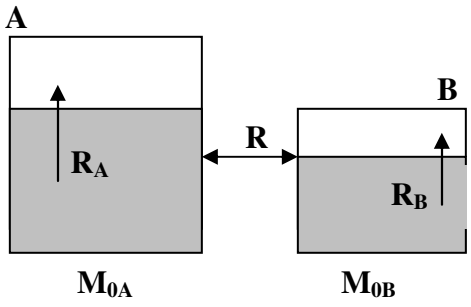

Figure 11: Two-pool model of magnetization transfer.

There are currently three methods in use to measure MT. The first measures the apparent relaxation of the magnetization while selectively saturating the immobile pool for a time long in comparison with the exchange

times and produces a first-order rate constant for exchange (Forsen and Hoffman, 1963). It requires the assumption of complete saturation of the immobile pool and no direct saturation of the mobile pool. The method has been applied to alter MR image contrast (Wolff and Balaban, 1989). Its more general practical validity has been called into question (Henkelman et al., 1993).

The second method measures the ratio of proton magnetization with and without varying amplitudes and frequencies of off-resonance saturation via steady-state techniques (Henkelman et al., 1993). The technique utilizes the two-pool model and avoids the usual assumptions that the macromolecular proton pool is completely saturated and that the water pool is unaffected. A Gaussian lineshape is most often used for the macromolecular proton pool, although Lorentzian and Super-Lorentzian lineshapes have been used in other similar studies (Morrison and Henkelman, 1995, Morrison et al., 1995, Stanisz et al., 2005).

For this coupled system, the Bloch equations can be modified to give quantification of several parameters of the system. Assuming the system is in steady state, it can be determined that

$$M_z^a = \frac{R_b\left[\frac{RM_0^b}{R_a}\right] + R_{rfb} + R_b + R}{\left[\frac{RM_0^b}{R_a}\right]\left(R_b + R_{rfb}\right) + \left(1 + \left(\frac{\omega_1}{2\pi\Delta}\right)^2\left[\frac{1}{R_a T_{2a}}\right]\right)\left(R_{rfb} + R_b + R\right)} \qquad \textbf{Eq. 39}$$

where M_z^a is the relative magnetization determined in the experiment, R_{rfb} is the rate of loss of longitudinal magnetization due to the off-resonance irradiation, ω_1

is the strength of the off-resonance pulse, and Δ is the frequency of the offset pulse, relative to an on-resonance pulse. R_{rfb} for specific lineshapes is as follows.

Lorentzian: $$R_{rfb} = \omega_1^2 T_{2b} \frac{1}{1+(2\pi\Delta T_{2b})^2}$$ **Eq. 40**

Gaussian: $$R_{rfb} = \omega_1^2 \sqrt{\frac{\pi}{2}} T_{2b} e^{-\frac{(2\pi\Delta T_{2b})^q}{2}}$$ **Eq. 41**

Super-Lorentzian: $$R_{rfb} = \omega_1^2 \pi \int_0^{\frac{\pi}{2}} d\theta \sin\theta \sqrt{\frac{2}{\pi}} \frac{T_{2b}}{\left|3\cos^2\theta - 1\right|} e^{-2\left[\frac{2\pi\Delta T_{2b}}{\left|3\cos^2\theta - 1\right|}\right]^2}$$ **Eq. 42**

These lineshapes may be summarized more elegantly as

$$R_{rfb} = \omega_1^2 \pi g(2\pi\Delta)$$ **Eq. 43**

where g(2πΔ) is the absorption lineshape for the spins, Δ is in Hz and ω_1 is in rad/sec.

A separate experiment is needed for the measurement of R_a. Because the usual measurement of the longitudinal relaxation rate through inversion recovery methods does not avoid the interference of the macromolecular pool, a correction should be made using the equation

$$R_a \approx \frac{R_a^{obs}}{1 + \frac{M_o^b}{R_a}\left(R_b - R_a^{obs}\right)}$$ **Eq. 44**

assuming that $R >> \left(R_b - R_a^{obs}\right)$. R_a^{obs} is the observed longitudinal relaxation rate for a typical inversion recovery experiment.

The reduced equation can be fitted to experimental results of normalized magnetization versus offset frequency, and five model parameters (R_b, $T2_b$, R, RM_0^b/R_a, and $1/R_aT2_a$) can be uniquely determined. M_0^b can be found by dividing and multiplying a parameter map for the fourth model parameter listed above by R and R_a, respectively.

Variations on this second method use pulsed approximations of the steady-state MT pulse to measure magnetization transfer. One model (Ramani et al., 2002) approximates the continuous wave power equivalent (CWPE) of the MT pulse as

$$\omega_{1,cwpe} = \sqrt{\frac{\int_0^{\tau} \omega_1^2(t)dt}{TR}}, \qquad \textbf{Eq. 45}$$

where TR is the pulse repetition period of the MT sequence. The expression for the equivalent power can be simplified as

$$\omega_{1,cwpe} = \sqrt{\frac{p_2}{\tau_{sat} TR'}} \frac{\theta_{sat}\pi}{p_1 180} \qquad \textbf{Eq. 46}$$

where θ_{sat} is the flip angle of the MT saturation pulse, τ_{sat} is the duration of the MT saturation pulse, *TR* is the pulse repetition period, p_1 is the area of the pulse relative to a rectangular pulse of the same amplitude and duration, and p_2 is the area under the square of the pulse B_1 value, relative to a rectangular pulse of the same amplitude and duration (Tozer et al., 2003, Tofts et al., 2005). The data is fitted to the same analytical equation as Eq. 39. This experiment will be referred to as CWPE in this work.

All of the methods of this type result in measurements of magnetization with and without saturation. In addition to the specific magnetization transfer

rates and measures of pool sizes, ratios of these values can be used as a more qualitative measure of magnetization transfer. One such measurement is the magnetization transfer ratio, which is calculated as

$$MTR = \frac{M_0 - M_s}{M_0} \quad \textbf{Eq. 47}$$

where M_0 is the magnetization of the unsaturated image of the sample and M_s is the magnetization of the image after an off-resonance saturation rf pulse is applied. Another measurement is the magnetization transfer proportion (MTP), which is given as (Whitney et al., 2008)

$$MTP = \frac{M_0 - M_s}{M_s} \quad \textbf{Eq. 48}$$

Chapter IV of this work will investigate the use of the MTP in polymer gel dosimetry.

The third method uses a single pulse sequence and transient methods to measure the recovery of the longitudinal magnetization after disturbance of either proton (Edzes and Samulski, 1977, Edzes and Samulski, 1978). The selective inversion recovery method can be used to measure residual magnetization after selectively saturating the immobile pool for a time long in comparison to exchange times (Gochberg et al., 2003, Gochberg and Gore, 2003).The magnetization recovers in a biexponential fashion according to the relationship

$$\frac{M_f(t)}{M_{f\infty}} = b_f^+ \exp\left(-R_1^+ t\right) + b_f^- \exp\left(-R_1^- t\right) + 1 \quad \textbf{Eq. 49}$$

where

$$2R_1^{\pm} = R_{1f} + R_{1m} + k_{fm} + k_{mf} \pm \sqrt{\left(R_{1f} + R_{1m} + k_{fm} + k_{mf}\right)^2 + 4k_{fm}k_{mf}} \quad \textbf{Eq. 50}$$

$$b_f^{\pm} = \pm \frac{\left[\frac{M_f(0)}{M_{f\infty}} - 1\right]\left(R_{1f} - R_1^{\pm}\right) + \left[\frac{M_f(0)}{M_{f\infty}} - \frac{M_m(0)}{M_m}\right] k_{fm}}{R_1^+ - R_1^-}. \quad \textbf{Eq. 51}$$

In these equations, *f* and *m* refer to the free solvent and macromolecular pools, respectively. R_1^- and R_1^+ are the slow and fast recovery rates, respectively, which have amplitudes b_f^- and b_f^+. R_{1f} and R_{1m} are the longitudinal relaxation rates of the free and macromolecular pools when there is no magnetization transfer between them. The equilibrium values of the magnetization are given by $M_{f\infty}$ and $M_{m\infty}$. The MT rates k_{mf} and k_{fm} are the "fast" and "slow" MT rates, respectively. Advantages of this method over the previously mentioned steady-state method are quick acquisition and less energy deposition to the sample. This method can yield information on parameters such as the ratio of the forward and reverse magnetization transfer rates and pool sizes. One disadvantage is that it does not allow for direction estimation of the transverse relaxation rate of the macromolecular pool. This selective inversion recovery experiment will be referred to as SIR in this work.

Transient methods have an advantage over steady-state methods in that they do not require long saturations (which may heat the sample), the time required for measurements is significantly less, no assumptions need be made about the lineshape, and no assumptions are needed regarding a fitting technique. However, steady-state measurements and their variants yield a more complete characterization of the MT system.

2.3 Measurement of dose response in gels

The transverse relaxation rate, R2, has been the most often-quoted dose response parameter for methacrylic acid-type dosimetry gels (Fong et al., 2001, Luci et al., 2007). A previous study measured magnetization transfer parameters for the original MAGIC gel formulation using the selective inversion recovery method (Gochberg et al., 2003). The steady-state magnetization transfer method (Henkelman et al., 1993) has been used to quantify MT behavior in polyacrylamide polymer (PAG) gels (Kennan et al., 1996). The authors in this study showed that the system favored a Gaussian lineshape.

3. Materials and Methods

3.1 Sample preparation, irradiation, and imaging

Polymer gel dosimeters, of the MAGIC-2 formulation, were produced using methods previously described in Chapter II. The dosimeters were poured into Pyrex test tubes, capped, and refrigerated for 24 hours. Before irradiation, the samples were brought to room temperature. The samples were immersed in a water bath and irradiated with 6MV photons with a dose rate of 2.84 Gy/min in parallel-opposed fashion, in increments of 1 Gy. Dosimeters were removed from the water bath in increments of 2 Gy, resulting in dosimeters at dose levels of 2 through 20Gy. One dosimeter was left unirradiated. Samples were stored at room temperature and protected from light for 24 hours to allow any post-irradiation polymerization processes to complete. After this time, samples were refrigerated and then brought again to room temperature before imaging.

Within three weeks following irradiation, samples were imaged at 4.7 and 9.4T using 31-cm and 21-cm bore Varian Inova (Varian Inc., Palo Alto, CA, USA) spectrometers respectively using a 63mm quadrature coil. The slice thickness was 4mm.

3.2 Transverse relaxation measurements

Transverse relaxation imaging was performed using an imaging variant of the CPMG sequence. All samples were imaged simultaneously. The field of view was 80 mm^2 and the imaging matrix was 64 by 64 pixels. The TE was 15ms, and the TR 15s; 32 echoes were recorded. The transverse relaxation rate was calculated on a pixel-by-pixel basis using a non-linear least squares fit of the data to an exponential decay model. Mean and standard deviations of reported values were measured for each dosimeter with regions of interest two pixels in radius, taken from parameter maps.

3.3 Magnetization transfer measurements

Magnetization transfer measurements for SIR analysis were performed using an inversion recovery-prepared fast spin echo sequence (Gochberg and Gore, 2007). There were sixteen echoes in the echo train. The delay before the inversion pulse was fixed for all measurements at 2.5 seconds, and the TE 25 ms. The inversion pulse was 1 ms in duration. Inversion times were a set of 24 logarithmically spaced time points between 2.9 and 150 ms, as well as 5 points at 0.3, 1, 2, 6, and 10 seconds. Dosimeters were imaged individually; the imaging

matrix was 64 by 64 pixels, and the field of view 40 mm^2. Unlike in Gochberg and Gore (2007), the data were fitted directly on a pixel by pixel basis to the model in Eq. 49, Eq. 50, and Eq. 51, avoiding the need for any assumptions of the exchange rates (Li et al., 2009). (We still assume a T2 between 10 us and 20 us and an R_1 of 1 Hz for the macromolecular pool.) This method is referred to as "SIR-exact" in this work. The data were also analyzed using a previously-published method, called "SIR-approx" in this work, which makes assumptions about the relative sizes of rates (Gochberg and Gore, 2007). Mean and standard deviations of reported values were measured for each dosimeter with regions of interest three pixels in radius, taken from parameter maps.

Magnetization transfer measurements for CWPE analysis were made using a spoiled gradient echo sequence with Gaussian-shaped magnetization transfer pre-pulse. The imaging matrix was 64 by 64 pixels and the field of view 100mm^2. The TR was 40 ms and the TE 4 ms. All samples were imaged simultaneously. Dummy scans were used so that the samples were pulsed for 20 seconds before actual data were acquired, in order to ensure that the magnetization was at steady-state. The pulse was applied for 30 values off resonance from water, logarithmically spaced between 10 and 200,000 Hz. Four acquisitions were averaged, resulting in a total acquisition time of 5 minutes, 27 seconds for each power that was used. The flip angles were nominally 200, 350, and 500 degrees for the 10 ms Gaussian pulse. The continuous wave power equivalent can be calculated for each power, using Eq. 46, and values are given in Table 5.

Table 5: Continuous wave power equivalent values

Nominal flip angle (degrees)	τ_{sat} (ms)	ω_{1cwpe} (rad/sec)
200	10	225
350	10	394
500	10	563

For the hardware used in these experiments, $p_1 = 0.4263$ and $p_2 = 0.3025$ in Eq. 46.

A B_1 map was also created for the CWPE analysis by acquiring gradient echo images at two different flip angles (60 and 120 degrees). The TR was 12 seconds and TE was 4 ms. The B_1 map was calculated by the double angle method (Insko and Bolinger, 1993) and used to scale the power of the MT pulse used in the CWPE experiment on a pixel-by-pixel basis.

The longitudinal relaxation rate is also needed via a separate experiment for this type of analysis, and the data were acquired via a fast spin echo inversion recovery experiment similar to that described above. The experiment was performed with an imaging matrix of 128 by 128 pixels, the field of view was $100mm^2$, and the echo spacing was 8.5 ms. Images were resized to 64 by 64 pixels so that the measurements of the longitudinal relaxation rate could be used pixel-by-pixel for the CWPE magnetization transfer analysis.

Data from each MT acquisition at each power were normalized to the data acquired at 200 kHz off resonance. Data acquired at offset frequencies of approximately 1200 Hz to 200 kHz off resonance for a given pixel were fitted to the model in Eq. 39. R_b was fixed at 1 Hz, as the model has been shown to be relatively insensitive to its value (Henkelman et al., 1993) and others have

commented that the CWPE method is more accurately performed on offset frequencies above 1000 Hz (Portnoy and Stanisz, 2007). A Gaussian lineshape was assumed. Mean and standard deviations of reported values were measured with regions of interest two pixels in radius, taken from parameter maps.

4. Results

4.1 Goodness-of-fit

To understand the following results for the magnetization transfer parameters, it is first important to know how well the data were fitted to the above models. Example fits of a single pixel for the CWPE model are shown in Figure 12.

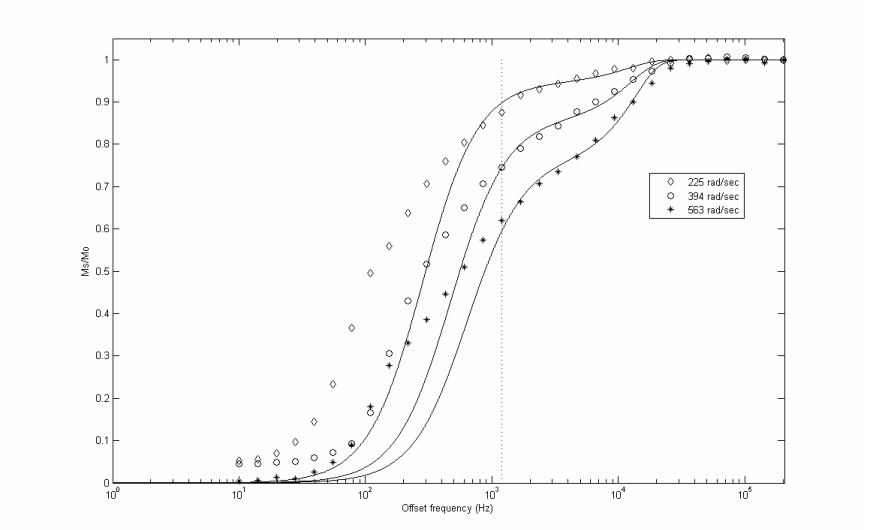

Figure 12: Example data and fit for a single pixel in the CWPE experiment. The vertical dotted line indicates the cutoff frequency below which data were not evaluated for the fit.

An example fit for the SIR experiment is given in Figure 13 and Figure 14.

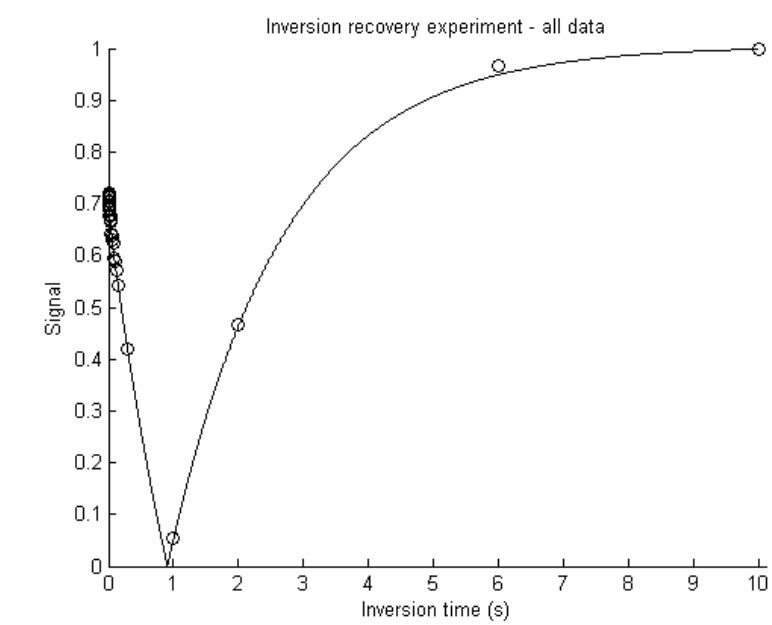

Figure 13: Example data and fit for a single pixel in the SIR experiment.

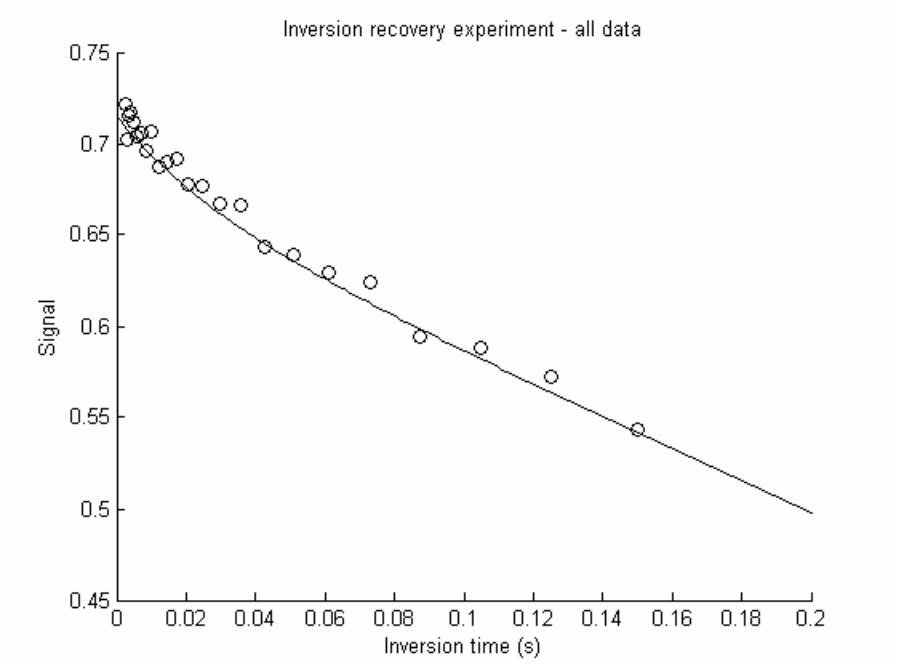

Figure 14: Example data and fit for a single pixel in the SIR experiment. The data presented here is the same as given in Figure 13, for a subset of the inversion times. The sample was a polymer gel dosimeter at 20Gy.

The statistic χ^2 can be used as a measure of the goodness-of-fit. According to Pearson's chi-square test, a fit to data can be assessed using the equation

$$\chi^2 = \sum_{i=1}^{n} \frac{(O_i - E_i)^2}{\sigma^2}$$ **Eq. 52**

where O_i is the observed frequency from the data, E_i is the expected frequency from the fit, n is the number of possible outcomes of each measurement (i.e., the number of measurements), and σ^2 is the variance of the measurement.

Because the measurements were not repeated for every offset frequency or inversion time, an estimation of the variance of the data was performed by repeating the CWPE experiment six times at two offset frequencies (3321 and 200,000 Hz) and the SIR experiment six times at two inversion times (0.013 and 10 seconds). The variance in each pixel of the CWPE was used to measure χ^2 at each pixel used in the region of interest for each dose level measurement, according to Eq. 52.

The χ^2 value achieved for each pixel can be assessed for goodness-of-fit by comparing its value against the expected χ^2 value for certain probabilities of measurement. The expected χ^2 value depends upon the degrees of freedom a measurement has, which is defined as the difference between the number of data points are used in the fit and the number of parameters the fit determines. For the experiments in this work, χ^2 for 2.5% tail probabilities are given in Table 6. These values were calculated using available functions in Matlab.

Table 6: Expected χ^2 values for the measurements

Measurement type	Degrees of freedom	χ^2 lower bound	χ^2 higher bound
SIR	24	12	39
CWPE	44	28	64

The SIR measurements were performed on each gel separately, which complicates the assessment of χ^2. The variance of the 8Gy dosimeter was used to estimate the variance for all dosimeters, and the χ^2 analysis performed. These results are given in Table 7 as the mean and standard deviation χ^2value for the pixels in the regions of interest for each sample at the different dose levels.

Table 7: Chi-squared for goodness-of-fit measure

Dose (Gy)	SIR - exact	SIR - approx.	CWPE
0	184 ± 65	196 ± 98	351 ± 385
2	12 ± 11	12 ± 10	234 ± 138
4	250 ± 287	229 ± 298	595 ± 467
6	294 ± 251	211 ± 185	414 ± 184
8	249 ± 307	264 ± 261	305 ± 193
10	85 ± 99	85 ± 99	857 ± 769
12	213 ± 294	213 ± 294	404 ± 193
14	95 ± 112	95 ± 112	459 ± 240
16	28 ± 47	28 ± 47	544 ± 268
18	21 ± 38	21 ± 38	346 ± 216
20	95 ± 127	94 ± 127	701 ± 646

It can be seen that the SIR method better fitted the data for that experiment than did the off-resonance CWPE experiment. This understanding of the goodness-of-fit should be considered when evaluating the quantitative MT parameter measurements below.

4.2 Longitudinal relaxation rate/magnetization transfer slow rate measurements

The longitudinal relaxation rate measurement at 4.7T was taken from the analysis of the selective inversion recovery data. Figure 15 displays the results for the same data set analyzed with both the exact and approximate SIR solution. The results vary slightly. Dose sensitivity, given as the slope of the dose response, is approximately 0.005 $s^{-1}Gy^{-1}$. The data between 2 and 20 Gy were fitted to a linear model using a least-squares method, and the best-fit line is also displayed in Figure 15. R^2, the coefficient of determination, is a useful measure of how well a model represents data. For these data points, R^2 is 0.9293 and 0.9296 for the exact and approximation methods, respectively, indicating that the data within this dose range is well-fitted by a linear model. Linear equations for the data are R_1 = 0.4611 + 0.0050* dose (Hz) and R_1 = 0.4709 + 0.0051*dose (Hz) for the exact and approximate methods respectively.

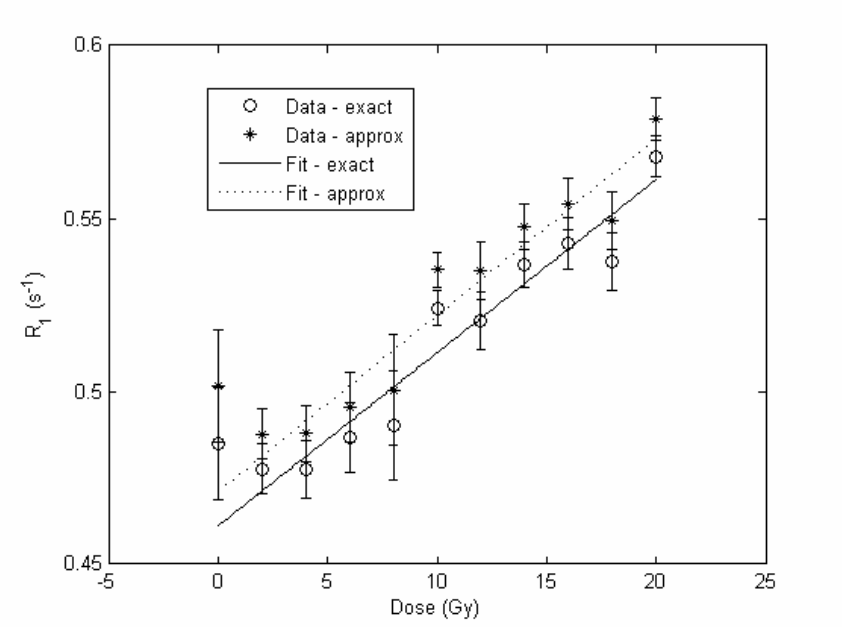

Figure 15: Longitudinal relaxation measurement at 4.7T.

4.3 Transverse relaxation measurements

Transverse relaxation measurements are shown in Figure 16, along with the best-fit line of a linear model. Dose sensitivity increases with field strength. R^2 is 0.9613 for the measurement at 4.7T and 0.9798 for the measurement at 9.4T for the dose range of 0 to 14 Gy. R2 at 4.7T can be modeled by the linear equation R2 = 3.6216 + 1.1078 * dose (Hz), and R2 at 9.4T by the linear equation R2 = 5.6482 + 1.3826 * dose (Hz).

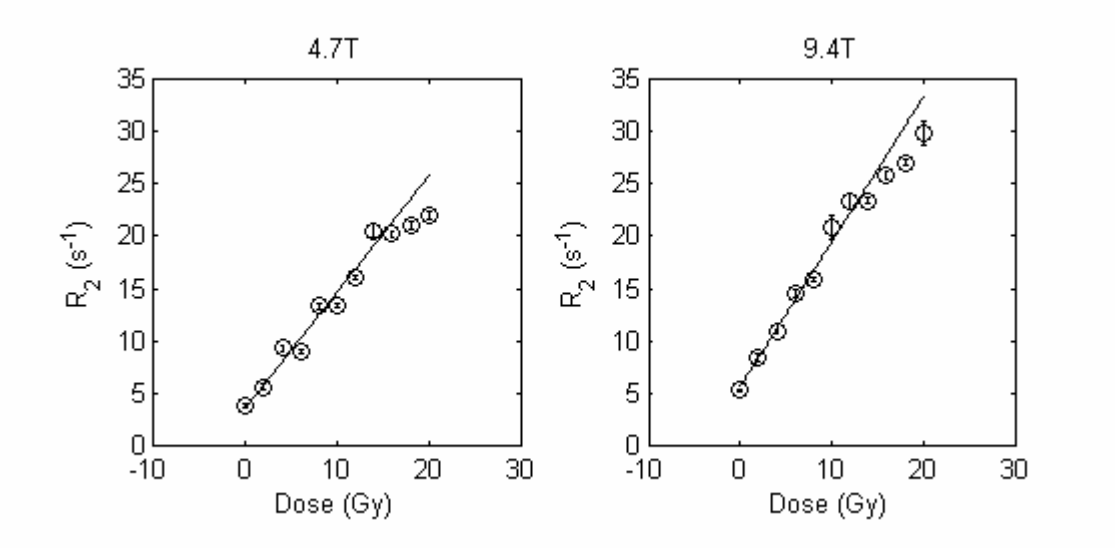

Figure 16: Transverse relaxation rate measurements at 4.7T and 9.4T

4.4 Magnetization transfer measurements

While both transient and steady-state measurements can make quantitative assessments of the same magnetization transfer parameters, these two methods have not yet been compared for polymer gel dosimeters. An initial study analyzed measurements of the fast MT rate using steady state measurements of the original MAGIC gel formulation and comparing them to those measured via

the selective inversion recovery method (Whitney et al., 2006). In this work, the full range of MT parameters is compared.

The two approaches to magnetization transfer analysis, steady-state and transient, have been developed using varying nomenclature to describe the same rates. To clarify, this work will refer to the parameters using the names in the first column of Table 8.

Table 8: Names of magnetization transfer parameters

Parameter name	SIR (Gochberg and Gore, 2007)	CWPE (Tozer et al., 2003)
Slow rate	R_1^-	R_{1obs}
Fast rate	k_{mf}	R
Slow MT rate	k_{fm}	RM_b^0
Poolsize	p_m/p_f	M_b^0

The tables below give the mean and standard deviation of the measurement of the magnetization transfer parameters for a given method (SIR or CWPE), measured at 4.7T. The results for the slow rate are given in Figure 15 and are redundant with the longitudinal relaxation rate.

SIR results for the fast rate are shown in Figure 17. The results are very similar for both analysis methods, and R^2 is 0.9352 and 0.8928 for the exact and approximate methods, respectively. Linear equations for the data are fast rate = 7.2603 + 2.9541*dose (Hz) and fast rate = 10.4164 + 2.6154*dose (Hz) for the exact and approximate methods respectively.

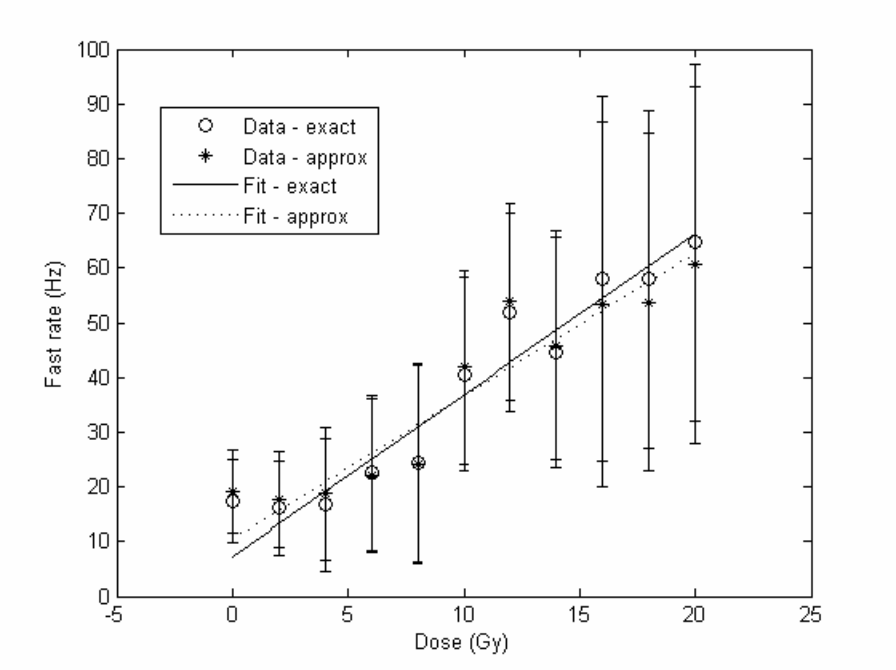

Figure 17: Fast magnetization transfer rate results at 4.7T

Table 9 lists detailed data for the measurement of the fast rate. As can be seen, the results for the CWPE method are very different than the SIR results and show no clear linear increase with dose. R^2 for the CWPE results fitted to a linear model is 0.2381, and the fast rate = 13.3906 + 0.4483*dose (Hz).

Table 9: Fast rate (Hz)

Dose (Gy)	SIR - exact			SIR - approx.			CWPE		
0	17.4141	±	7.5610	19.2497	±	7.1590	8.2813	±	1.8764
2	16.0868	±	8.7035	17.7528	±	8.5891	17.9307	±	9.5044
4	16.7835	±	12.1332	18.8187	±	11.8034	12.4192	±	2.7188
6	22.5392	±	14.0601	22.0705	±	10.6030	14.6542	±	5.0936
8	24.3783	±	18.1188	24.0978	±	14.4039	18.8280	±	8.2327
10	40.6159	±	17.6836	41.8469	±	15.9565	10.4403	±	2.3035
12	51.9113	±	18.0571	53.8206	±	17.4116	25.5920	±	10.9174
14	44.5648	±	20.9404	45.8749	±	19.9247	19.3105	±	5.4394
16	58.0674	±	33.3337	53.2872	±	19.6614	16.4588	±	3.9407
18	57.9264	±	30.8908	53.7038	±	19.2168	28.8175	±	20.0060
20	64.6827	±	32.5716	60.5863	±	17.5329	18.7671	±	5.7034

SIR results for the slow magnetization transfer rate are shown in Figure 18. There is some evidence of variance between the approximate method and the exact method. R^2 is 0.8507 and 0.7890 for the exact and approximate methods, respectively. Linear equations for the data are slow MT rate = 0.0065 + 0.0906* dose (Hz) and slow MT rate = 0.0856+ 0.1127*dose (Hz) for the exact and approximate methods respectively.

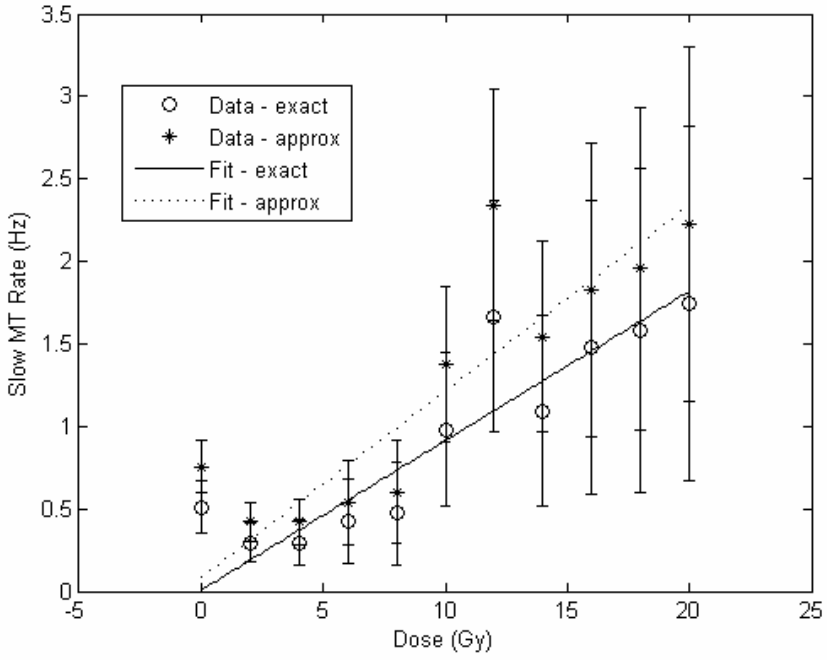

Figure 18: Slow magnetization transfer rate results at 4.7T.

Table 10 lists detailed data for the measurement of the slow magnetization transfer rate. Again, the results for the CWPE method are very different than the SIR results and show no clear linear increase with dose. R^2 for the CWPE results fitted to a linear model is 0.6937, and the fast rate = 0.3000 + 0.0368*dose (Hz).

Table 10: Slow MT Rate (Hz)

Dose (Gy)	SIR - exact			SIR - approx.			CWPE		
0	0.5077	±	0.1577	0.7563	±	0.2318	0.1803	±	0.0230
2	0.2958	±	0.1167	0.4215	±	0.1667	0.4001	±	0.1599
4	0.2940	±	0.1374	0.4204	±	0.1873	0.4020	±	0.0582
6	0.4233	±	0.2540	0.5405	±	0.2471	0.4680	±	0.1243
8	0.4711	±	0.3101	0.6024	±	0.3379	0.6333	±	0.2240
10	0.9824	±	0.4690	1.3753	±	0.5686	0.5105	±	0.0833
12	1.6671	±	0.6992	2.3403	±	0.9344	1.0501	±	0.3845
14	1.0939	±	0.5812	1.5442	±	0.7261	0.8389	±	0.1912
16	1.4757	±	0.8914	1.8287	±	0.6671	0.6873	±	0.1280
18	1.5825	±	0.9804	1.9548	±	0.7741	1.1094	±	0.5926
20	1.7484	±	1.0751	2.2228	±	0.7111	0.9490	±	0.2416

SIR results for the pool size ratio are shown in Figure 19. The results suggest a trend of increase in pool size as dose is increased, but the growth is not clear. Both SIR analysis methods show a change in pool size, although the absolute value of the results differ. R^2 is 0.4856 and 0.6131 for the exact and approximate methods, respectively. Linear equations for the data are pool size = 0.0198 + 0.0004* dose and pool size = 0.0227+ 0.0008*dose for the exact and approximate methods respectively.

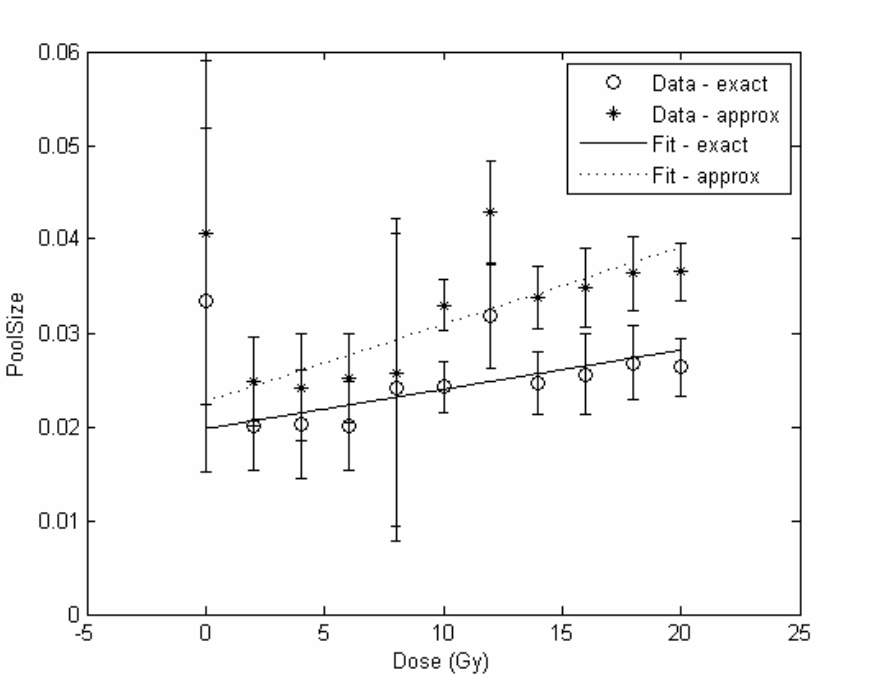

Figure 19: Pool size ratio results at 4.7T.

Table 11 lists the detailed data for pool size ratio measurements. The results for the CWPE method differ by an entire order of magnitude. R^2 for the CWPE results fitted to a linear model is 0.7202, and the fast rate = 0.1378 + 0.03217*dose (Hz).

Table 11: Pool size ratio

Dose (Gy)	SIR - exact	SIR - approx.	CWPE
0	0.0335 ± 0.0183	0.0407 ± 0.0062	0.0909 ± 0.0113
2	0.0201 ± 0.0047	0.0249 ± 0.0050	0.1980 ± 0.0807
4	0.0203 ± 0.0058	0.0242 ± 0.0056	0.1984 ± 0.0292
6	0.0201 ± 0.0048	0.0252 ± 0.0048	0.2381 ± 0.0640
8	0.0242 ± 0.0164	0.0258 ± 0.0045	0.3386 ± 0.1196
10	0.0243 ± 0.0027	0.0329 ± 0.0033	0.2646 ± 0.0441
12	0.0318 ± 0.0055	0.0429 ± 0.0070	0.5586 ± 0.2024
14	0.0246 ± 0.0033	0.0338 ± 0.0041	0.4652 ± 0.1082
16	0.0256 ± 0.0042	0.0349 ± 0.0056	0.3648 ± 0.0674
18	0.0268 ± 0.0040	0.0363 ± 0.0049	0.6112 ± 0.3191
20	0.0263 ± 0.0031	0.0365 ± 0.0039	0.5271 ± 0.1339

The measurement of the transverse relaxation time of the macromolecular pool is unique for the off-resonance method, and is reported here for the first time for any methacrylic acid-based dosimeter. The results for this measurement are shown in Figure 20. Similar to the measurement of this time in other materials that exhibit MT, the time is on the order of tens of microseconds and decreases as the size of the macromolecular pool increases. R2 shows a nearly linear increase.

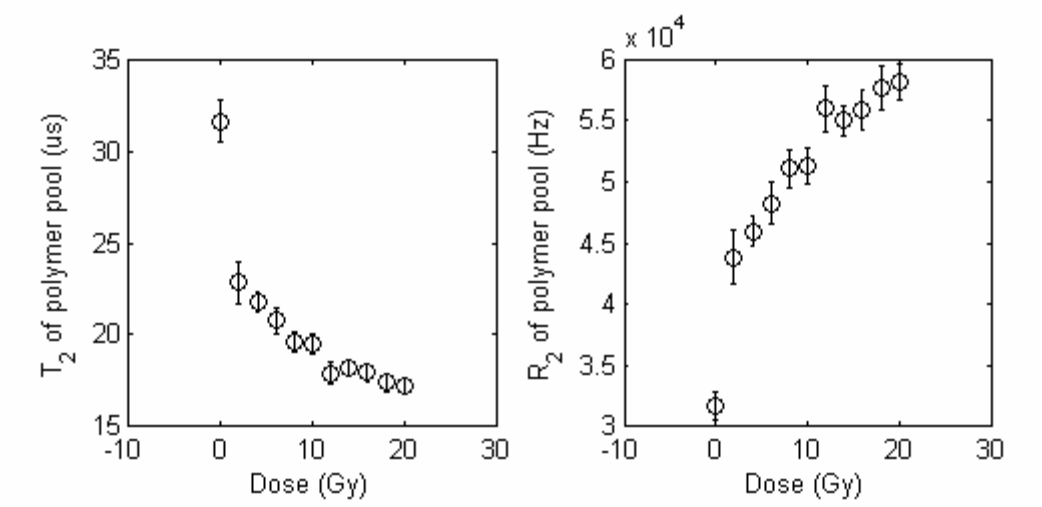

Figure 20: Transverse relaxation time and rate of the macromolecular pool at 4.7T

5. Discussion

The purpose of this work was to measure basic relaxometry parameters for the MAGIC-2 gel dosimeter at high field strengths. The following discussion compares the parameters to those previously published for the MAGIC dosimeter, as well as the MAGIC-2 dosimeter at lower field strengths.

5.1 Longitudinal relaxation rate

As compared to the MAGIC gel dosimeter (Gochberg et al., 2003), the MAGIC-2 dosimeter has a much lower magnitude of R_1 values (on the order of 0.5 Hz, compared to approximately 0.9Hz for the MAGIC dosimeter), as well as a lower dose response (0.005 compared to 0.0125 $s^{-1}Gy^{-1}$ for the MAGIC dosimeter). Because an increase in R_1 (and a decrease in T1) is seen in materials where dipolar cross-relaxation works as a relaxation mechanism, and dose response for R_1 is relatively flat, this suggests that dipolar cross-relaxation is not important for relaxation in polymer gel dosimeters at high fields.

5.2 Transverse relaxation rate

The dose response found at 4.7T and 9.4T was much greater than that at 3T (approximately 0.503 $s^{-1}Gy^{-1}$) (Luci et al., 2007), as seen in Table 12. Increased dose sensitivity is expected to be an advantage for polymer gel dosimetry as higher field strengths become available for more widespread use. Such an increase in R2 (and decrease in T2) is expected as increasing field strength increases the chemical shift between species undergoing chemical exchange (Zhong et al., 1989).

Table 12: Dose response for the MAGIC-2 dosimeter at different field strengths.

Field strength (T)	Dose response ($s^{-1}Gy^{-1}$)
3	0.503
4.7	1.108
9.4	1.383

The increase in the overall observed transverse relaxation rate with dose is likely related to the increase in the fast MT rate, as seen in Figure 17. This correlation will be investigated further in Chapter V.

5.3 Magnetization transfer rates

The selective inversion recovery analysis, both the exact and the approximation methods, assumed that T2 of the macromolecular pool is between 10 and 20 us. Numerical calculations give that the saturation of the macromolecular pool is around 0.83 +/- 0.07 for a 1 ms inversion pulse for this range of T2 values (Gochberg and Gore, 2007). As shown in Figure 20, the CWPE experiment suggests that T2 of the macromolecular pool is greater than 20 us for the MAGIC-2 dosimeter in the range of 0 to 6 Gy. To estimate the effect this difference had on the analysis, the SIR analysis was repeated for the 0Gy dosimeter. Numerical simulations showed that between 20 and 35 us, S_m has a value of 0.7127 +/- 0.0385, and 0.7127 was used as the fraction of saturation of the macromolecular pool in the SIR analysis. The same pixels used in the results reported above were used to measure the mean and standard deviation of the magnetization transfer parameters. Table 13 displays the results.

Table 13: Comparison of measured magnetization transfer parameters at 0Gy with different values for S_m.

Exact Method	Sm = 0.83			Sm = 0.7127		
Slow Rate	0.4847	±	0.0163	0.4832	±	0.0173
Fast Rate	17.4141	±	7.5610	17.3708	±	7.5497
Slow MT Rate	0.5077	±	0.1577	0.5526	±	0.1703
Pool Size	0.0335	±	0.0183	0.0367	±	0.0209

Approximation Method	Sm = 0.83			Sm = 0.7127		
Slow Rate	0.5017	±	0.0068	0.5017	±	0.0068
Fast Rate	19.2497	±	7.1590	19.2497	±	7.1590
Slow MT Rate	0.7563	±	0.2318	0.7896	±	0.2416
Pool Size	0.0407	±	0.0062	0.0424	±	0.0064

The slow and fast rates are virtually unchanged by the change in S_m. The slow MT rate and pool size measurements do vary, but these variances are well within the standard deviation of the measurements.

Others (Portnoy and Stanisz, 2007) have commented that alternative methods of approximated pulse magnetization transfer (Sled and Pike, 2000) are somewhat more accurate than the CWPE method used in our work. However, this method requires the calculation of the saturation fraction of the solvent pool for every potential T2 value of the free pool, offset frequency, and MT power, which can be time-intensive to calculate. Such calculations would be even longer if a separate calculation for B_1 map-adjusted MT powers were done on a pixel-by-pixel basis. For this reason, this study implemented the CWPE method, which is easier to correct for B_1 inhomogeneities.

In comparing magnetization transfer measurements between polymer gel formulations, it is important to note differences in composition. These are given in Table 14.

Table 14: Methacrylic acid-based polymer gel composition

Component	MAGIC	MAGIC-2
Water (w/w)	83%	87%
Gelatin (w/w)	8%	9%
Methacrylic Acid (w/w)	9%	4%
Cu^{2+} (M)	8×10^{-5}	17.38×10^{-6}
Ascorbic Acid (M)	2×10^{-3}	6×10^{-4}

Note that the primary difference between the two formulations is in the percentage of weight that is methacrylic acid: the MAGIC formulation is 9% w/w, while MAGIC-2 is 4% w/w. It is reasonable to expect that the MAGIC-2 dosimeter will exhibit less magnetization transfer, in the form of lower rates of magnetization transfer and smaller macromolecular pool sizes, than the MAGIC dosimeter.

Such differences are indeed seen when the results above are compared to those in the literature for the MAGIC dosimeter (Gochberg et al., 2003). For the 0-20Gy dose range, the magnetization transfer parameters are between approximately 0.8-1.1 Hz for the slow rate, 55-100 Hz for the fast rate, 2-6Hz for the slow MT rate, and 0.03-0.06 for the pool size in the MAGIC dosimeter. While the trend of increases in magnetization transfer rates and pool size remains with the MAGIC-2 dosimeter, the rate of increase is less, indicating that the strength of MT is not as much in that system.

It is interesting to compare the pool sizes calculated for each dosimeter to that which can be calculated directly from the formulation. For the MAGIC dosimeter (9% w/w MAA), the macromolecule pool fraction approximated as the number of exchangeable protons from the monomer is 0.0113. For the MAGIC-2

dosimeter (4% w/w MAA), it is 0.0046. This approximately 40% reduction in the pool size when the amount of MAA is decreased 44% is similar to the difference in pool size measured from magnetization transfer analysis for the two formulations. A previous study (Gochberg et al., 2003) showed an increase of poolsize from 0.03 to 0.06 for a dose range of 0-20Gy for the MAGIC gel formulation, and here we report an increase from approximately 0.02 to 0.03 for MAGIC-2. However, theoretically the size of the macromolecular pool should not change as polymerization occurs; there should still be the same number of exchangeable carboxyl protons available to participate in chemical exchange with the solvent water. Perhaps an additional component of the polymer dosimeter, such as the gelatin or the monomer grafted to it, also facilitates magnetization transfer and its contribution is seen in the measurement of the effective magnetization transfer rates and pool sizes. Additionally, it could be that as the polymer grows dipolar cross relaxation contribution could increasingly contribute to magnetization transfer, causing the apparent poolsize to increase.

The CWPE method appears to overestimate the size of the macromolecular pool by an order of magnitude. Given that the MAGIC-2 system has less monomer to begin with than the MAGIC dosimeter, it is reasonable to expect that pool sizes would be smaller than those achieved in the MAGIC dosimeter for a given dose level. Therefore, it is highly unlikely that poolsizes in the range of 20% were achieved in the dosimeters.

It is possible that the lesser quality of analysis via the CWPE model indicates a weakness in that method in a system that does not exhibit large

amounts of magnetization transfer. One work (Portnoy and Stanisz, 2007) has compared the CWPE model to an exact solution of pulsed magnetization transfer and found that the CWPE model determined the parameters of solid pool fraction and transverse relaxation with reasonable accuracy. However, the authors expressed caution for using the model to estimate the fast MT rate, as well as the solvent transverse relaxation rate which the model can also estimate.

6. Conclusions

Various relaxometry measurements of the MAGIC-2 dosimeter have been established at higher field strengths by this work. As expected, the dosimeter exhibits higher dose response for the measurement of R2 as field strength increases. The longitudinal rate remains less responsive. Quantitative MT measurements were performed using two different methods. The MAGIC-2 dosimeter exhibits MT rates that are less in magnitude and rate of change with dose than the MAGIC dosimeter. It is suggested that an additional component of the polymer gels, perhaps connected to the presence of gelatin, contributes to the magnetization transfer process.

References

Dresselaers, T., Bergans, N., Van Heckle, P. & Vanstapel, F. (2002) Proton magnetization transfer effect in rat liver lactate. *Magn. Reson. Med.,* 47**,** 880-887.

Edzes, H.T. & Samulski, E.T. (1977) Cross relaxation and spin diffusion in proton NMR of hydrated collagen. *Nature,* 265**,** 521-523.

Edzes, H.T. & Samulski, E.T. (1978) Measurement of cross-relaxation effects in proton NMR spin-lattice relaxation of water in biological-systems - hydrated collagen and muscle. *J. Magn. Reson.,* 31**,** 207-229.

Fong, P.M., Keil, D.C., Does, M.D. & Gore, J.C. (2001) Polymer gels for magnetic resonance imaging of radiation dose distributions at normal room atmosphere. *Phys. Med. Biol.,* 46**,** 3105-3113.

Forsen, S. & Hoffman, R.A. (1963) Study of moderately rapid chemical exchange reactions by means of nuclear magnetic double resonance. *J. Chem. Phys.,* 39**,** 2892-2901.

Gochberg, D.F., Fong, P.M. & Gore, J.C. (2003) A quantitative study of magnetization transfer in MAGIC gels. *Phys. Med. Biol.,* 48**,** N277-N282.

Gochberg, D.F. & Gore, J.C. (2003) Quantitative imaging of magnetization transfer using an inversion recovery sequence. *Magn. Reson. Med.,* 49**,** 501-505.

Gochberg, D.F. & Gore, J.C. (2007) Quantitative magnetization transfer imaging via selective inversion recovery with short repetition times. *Magn. Reson. Med.,* 57**,** 437-441.

Harrison, R., Bronskill, M.J. & Henkelman, R.M. (1995) Magnetization-Transfer and T-2 relaxation components in tissue. *Magn. Reson. Med.,* 33**,** 490-496.

Henkelman, R.M., Huang, X.M., Xiang, Q.S., Stanisz, G.J., Swanson, S.D. & Bronskill, M.J. (1993) Quantitative interpretation of magnetization-transfer. *Magn. Reson. Med.,* 29**,** 759-766.

Insko, E.K. & Bolinger, L. (1993) Mapping of the Radiofrequency Field. *J. Magn. Res. Ser. A,* 103**,** 82-85.

Kennan, R.P., Richardson, K.A., Zhong, J.H., Maryanski, M.J. & Gore, J.C. (1996) The effects of cross-link density and chemical exchange on magnetization transfer in polyacrylamide gels. *J. Magn. Res. Ser. B,* 110**,** 267-277.

Li, K., Zu, Z., Xu, J., Gore, J.C., Whitney, H.M. & Gochberg, D.F. (2009) Optimization of quantitative magnetization transfer imaging using a selective inversion recovery pulse. *Proceedings of the International Society of Magnetic Resonance in Medicine (submitted)*.

Luci, J.J., Whitney, H.M. & Gore, J.C. (2007) Optimization of MAGIC gel formulation for three-dimensional radiation therapy dosimetry. *Phys. Med. Biol.,* 52**,** N241.

Mehta, R.C., Pike, G.B. & Enzmann, D.R. (1995) Magnetization transfer MR of the normal adult brain. *Am. J. Neuroradiology,* 16.

Morrison, C. & Henkelman, R.M. (1995) A Model for magnetization-transfer in tissues. *Magn. Reson. Med.,* 33**,** 475-482.

Morrison, C., Stanisz, G.J. & Henkelman, R.M. (1995) Modeling magnetization transfer for biological-like systems using a semi-solid pool with a super-Lorentzian lineshape and dipolar reservoir. *J. Magn. Res. Ser. B,* 108**,** 103-113.

Portnoy, S. & Stanisz, G.J. (2007) Modeling pulsed magnetization transfer. *Magn. Reson. Med.,* 58**,** 144-155.

Quesson, B., Thiaudiere, E., Delalande, C., Dousset, V., Chateil, J.F. & Canioni, P. (1997) Magnetization transfer imaging in vivo of the rat brain at 4.7 T:

Interpretation using a binary spin-bath model with a superLorentzian lineshape. *Magn. Reson. Med.,* 38**,** 974-980.

Ramani, A., Dalton, C., Miller, D.H., Tofts, P.S. & Barker, G.J. (2002) Precise estimate of fundamental in-vivo MT parameters in human brain in clinically feasible times. *Magn. Reson. Imag.,* 20**,** 721-731.

Sled, J.G. & Pike, G.B. (2000) Quantitative interpretation of magnetization transfer in spoiled gradient echo MRI sequences. *J. Magn. Reson.,* 145**,** 24-36.

Stanisz, G.J., Odrobina, E.E., Pun, J., Escaravage, M., Graham, S.J., Bronskill, M.J. & Henkelman, R.M. (2005) T-1, T-2 relaxation and magnetization transfer in tissue at 3T. *Magn. Reson. Med.,* 54**,** 507-512.

Steens, S.C.A., Admiraal-Behloul, F., Bosma, G.P.T., Steup-Beekman, G.M., Olofsen, H., Le Cessie, S., Huizinga, T.W.J. & Van Buchem, M.A. (2004) Selective gray matter damage in neuropsychiatric lupus - A magnetization transfer imaging study. *Arthritis and Rheumatism,* 50**,** 2877-2881.

Tofts, P.S., Cercignani, M., Tozer, D.J., Ramani, A. & Barker, G.J. (2005) Quantitative magnetization transfer mapping of bound protons in multiple sclerosis (vol 50, pg 83, 2003). *Magn. Reson. Med.,* 53**,** 492-493.

Tozer, D., Ramani, A., Barker, G.J., Davies, G.R., Miller, D.H. & Tofts, P.S. (2003) Quantitative magnetization transfer mapping of bound protons in multiple sclerosis. *Magn. Reson. Med.,* 50**,** 83-91.

Whitney, H.M., Gochberg, D.F. & Gore, J.C. (2006) Magnetization transfer in polymer gel dosimeters. *J. of Phys.: Conf. Ser.,* 56**,** 253-255.

Whitney, H.M., Gochberg, D.F. & Gore, J.C. (2008) Magnetization transfer proportion: a simplified measure of dose response for polymer gel dosimetry. *Phys. Med. Biol.,* 53**,** 7107-7124.

Wolff, S.D. & Balaban, R.S. (1989) Magnetization transfer contrast (MTC) and tissue water proton relaxation in vivo. *Magn. Reson. Med.,* 10**,** 135-144.

Zhong, J.H., Gore, J.C. & Armitage, I.M. (1989) Relative contributions of chemical-exchange and oher relaxation mechanisms in protein solutions and tissues. *Magn. Reson. Med.,* 11**,** 295-308.

CHAPTER IV

MAGNETIZATION TRANSFER PROPORTION: A SIMPLIFIED MEASURE OF DOSE RESPONSE FOR POLYMER GEL DOSIMETRY

1. Introduction

Most polymer gel dose response has been measured by the transverse relaxation rate, R2. Alternative imaging metrics have also been investigated, including magnetization transfer (MT) imaging (Lepage et al., 2002). MT imaging is sensitive to the exchange of magnetization between proton pools in a sample that results from chemical exchange or through-space dipolar interactions (Wolff and Balaban, 1989, Henkelman et al., 1993). In a simple model that may be appropriate for polymer gels, two distinct proton populations are considered to be coupled together. One pool corresponds to the mobile solvent protons, and a second pool corresponds to hydrogen nuclei that are relatively immobile, associated with the polymer in some way, and have different relaxation times or different resonant frequencies because of chemical shift effects. The integrated signal from both pools is measured after the application of an appropriate saturating RF pulse at a frequency that is off-resonance to the free water. The magnetization transfer ratio (MTR) has often been used as an index of the degree of magnetization transfer. It is defined as

$$MTR = \frac{M_0 - M_{sat}}{M_0} \qquad \textbf{Eq. 53}$$

where M_0 is the signal of the sample acquired without off-resonance saturation and M_{sat} is the signal acquired with saturation. Gel dosimetry measurements of magnetization transfer have used slightly different assessments of the magnetization measured with and without saturation. For example, De Deene et al. (De Deene et al., 2006b) proposed the "true magnetization transfer ratio" which incorporates the direct effect of the saturating irradiation on the free water. This ratio is given by

$$MT = \frac{M_{H_2O} - M_{sat}}{M_0} = MTR - \frac{M_{dir}}{M_0} \qquad \textbf{Eq. 54}$$

where M_{H_2O} is the experimentally measured magnetization of water after a saturation pulse has been applied and M_{dir} is described by the authors of the work to be the "direct effect contribution which is due to the saturation of the water proton pool." Other studies have published values for the specific parameters that contribute to MT for different types of polymer gel dosimeters as a function of dose (Gochberg et al., 2001, Gochberg et al., 2003).

Here we provide a theoretical and experimental basis for using a slightly different ratio of magnetization transfer measurements for gel dosimetry that results in a linear response of this quantity with dose in the range of 0-20Gy. This approach will be compared to the more traditional transverse relaxation rate measurement for dosimetry gels. In particular, the relative sensitivities of the magnetization transfer and transverse relaxation dose responses to the effects of imperfections in imaging, including errors in the amplitudes of the radiofrequency pulses used, are evaluated.

2. Theory

2.1 Dose response

Traditional transverse relaxation rate measurements of polymer gel dosimeters are performed using spin-echo imaging. Assuming the system is not saturated (i.e., TR>>T1), the signal at echo time TE is given by

$$S = M_0 e^{-R_2 TE} \quad \textbf{Eq. 55}$$

In a region of linear dose response,

$$R_2 = R_{2,0} + \alpha D \quad \textbf{Eq. 56}$$

where α and $R2_{,0}$ are the slope and intercept, respectively. The signal difference generated by any small dose increment ΔD is then

$$\Delta S = -\alpha \cdot TE \cdot S \cdot \Delta D \quad \textbf{Eq. 57}$$

This has a maximum value when TE = $\frac{1}{R_2}$, when the signal change is

$$\Delta S = -0.37 \frac{\alpha}{R_{2,0} + \alpha D} \Delta D.M_0 \quad \textbf{Eq. 58}$$

and decreases with dose *D*. For the most sensitive PAG and MAGIC gels, α is 0.19 and 0.503 and $R2_{,0}$ is 0.9 and 7.653, respectively (De Deene et al., 2006a, Luci et al., 2007). Thus, compared to the signal of an unirradiated dosimeter, a dose of 1 Gy will decrease the gel MRI signal by $0.064M_0$ and $0.151M_0$ initially for PAG and MAGIC gels, respectively, but this decreases to only $0.011M_0$ and

$0.015M_0$ respectively when comparing doses at 20 Gy, even at the optimal echo spacing for that dose. The situation is further compromised because R2 may vary throughout the gel so no single choice of TE is then optimal for all regions. Thus, even without considering errors inherent in calculating values of R2 from multiple echo data, the signal changes available for discriminating regions of similar doses are small. A further complication occurs in multi-echo sequences, which can produce maps of R2 from a single acquisition, but are sensitive to RF and static field inhomogeneities (Majumdar et al., 1986b, Majumdar et al., 1986a), and the precise value of T2 may depend on the echo spacing (Baldock et al., 2001).

A simple method using only two images, and from which a quantity that varies approximately linearly with dose can be easily extracted, would be attractive. A simple MT-sensitive imaging sequence is one that incorporates an off-resonance saturating pulse immediately prior to imaging. The off-resonance pulse can be designed to saturate the immobile or chemically shifted protons and to not affect the free water resonance directly. MT effects alone then cause the signal from the mobile protons to decrease. This approach is the conventional MT imaging option available on commercial MRI systems.

The effect of the off-resonance saturating irradiation is to reduce the signal of the mobile water from M_0 to M_{sat}. The residual MRI signal is given by (Henkelman et al., 1993)

$$\frac{M_{sat}}{M_0} = \frac{R_{1,m}k_{fm} + R_{1,f}R_{rf,m} + R_{1,f}R_{1,m} + R_{1,f}k_{mf}}{\left(R_{1,f} + R_{rf,f} + k_{fm}\right)\left(R_{1,m} + R_{rf,m} + k_{mf}\right) - k_{mf}k_{fm}}. \qquad \textbf{Eq. 59}$$

In this model, suppose the subscript “f” stands for the free water pool, and “m” for a second proton pool which has more efficient relaxation and a broader resonance or is chemically shifted. This pool represents the polymerized product of irradiation and increases in direct proportion to the degree of polymerization and dose, a linear approximation to an exponential change (Lepage et al., 2001b). R_1 is the longitudinal magnetization rate constant, k_{mf} and k_{fm} are the rates of magnetization transfer from the polymer pool to the free pool and vice versa, respectively, and $R_{rf,i}$ is the rate of loss of longitudinal magnetization in either the free or other pool. If we take $R_{rf,f}$ to be zero and $R_{rf,m}$ to be much greater than all other rates, as is the case in an ideal magnetization transfer experiment, Eq. 59 becomes

$$\frac{M_{sat}}{M_0} = \frac{R_{1,f}}{R_{1,f} + k_{fm}} \qquad \textbf{Eq. 60}$$

For the rest of the discussion, $R_{1,f}$ and k_{fm} will be referred to as R_1 and k, respectively, to simplify notation. M_{sat} and M_0 can be rearranged to give

$$\frac{M_0 - M_{sat}}{M_{sat}} = \frac{k}{R_1}. \qquad \textbf{Eq. 61}$$

We will call the ratio $\frac{M_0 - M_{sat}}{M_{sat}}$ the magnetization transfer proportion (MTP). The MTR is related to the MTP:

$$MTR = \frac{M_0 - M_{sat}}{M_0} = \frac{k}{R_1 + k} \;\; ; \;\; MTP = \frac{MTR}{1 - MTR}. \qquad \textbf{Eq. 62}$$

The rate constant *k* will increase with dose in proportion to the amount of polymer produced, as has been shown to be the case for methacrylic-based dosimeter gels in the dose range of 0-20Gy (Gochberg et al., 2003). We therefore may write

$$k = k_0 + \beta D. \qquad \textbf{Eq. 63}$$

We then have

$$MTP = k_0 T_1 + \beta T_1 D. \qquad \textbf{Eq. 64}$$

To calculate the MTP, two images (M_0, M_{sat}) must be measured, which then can be combined to produce a quantity that should vary linearly with dose. The slope of this dose-response is

$$\beta T_1 = \frac{\beta}{R_1}. \qquad \textbf{Eq. 65}$$

The ratio of the slope to the intercept of the dose-response is a useful indicator of sensitivity when considering the detectibility of small changes in dose (Fong et al., 2001); for the magnetization transfer measure this is $\frac{\beta}{k_0}$, compared with $\frac{\alpha}{R_{2,0}}$ for methods measuring transverse relaxation.

Eq. 61 may also be derived by considering the relationship of M_{sat} to M_0 as given by (Wolff and Balaban, 1989)

$$M_{sat} = M_0 \left(1 - kT_{1sat}\right) \qquad \textbf{Eq. 66}$$

where T_{1sat} is the spin lattice relaxation time of the mobile water in the presence of the RF irradiation and is given by

$$\frac{1}{T_{1sat}} = \frac{1}{T_1} + k. \qquad \textbf{Eq. 67}$$

A manipulation of the quantities M_{sat} and M_0 results in the same relationship found in Eq. 61.

Eq. 61 and Eq. 62 illustrate an advantage in calculating the effect of magnetization transfer in terms of the MTP: if k is linear in dose (as given in Eq. 63), so is MTP, but not MTR, even though fundamentally it contains the same information.

The interpretation of the MT-dose relationship can be further understood by considering a two-pool model of MT in more detail, such as that suggested by the results of measurements by Gochberg *et al*. (Gochberg et al., 2003). We can then write the second population as

$$p_m = p_m^0 + \gamma D \qquad \textbf{Eq. 68}$$

where p_m is the size of the relevant polymer proton pool after irradiation, p_m^0 is the size of this second pool in the unirradiated dosimeter, D is the absorbed dose, and γ is the slope of the pool size versus dose relationship. The MT rate constant, in the nomenclature introduced by Gochberg et al. (2003), is then

$$k = k_{mf}\frac{p_m}{p_f} = k_{mf}\frac{p_m^0 + \gamma D}{p_f} \qquad \textbf{Eq. 69}$$

ignoring the (insignificant) changes in p_f. Thus the slope of MTP versus D, as given in Eq. 61 and incorporating Eq. 69, is $\frac{k_{mf}\gamma}{p_f R_1}$. We may also note that for a two pool exchange model of transverse relaxation

$$R_2 = R_{2f} + k_{mf}\frac{p_m}{p_f}. \qquad \textbf{Eq. 70}$$

Thus for this model α, the slope of the R2 versus dose line, is $\frac{k_{mf}\gamma}{p_f}$: thus the ratio $\frac{\alpha}{R_{2,0}} = \frac{k_{mf}\gamma}{p_f R_{2,0}}$.We see that mapping R2 and the MTP are fundamentally related, both reflecting increases in the contribution of the fraction of polymer gel. However, the fractional increase in R2 per dose is smaller than the increase in MTP by the ratio $\frac{R_2}{R_1}$, which can be as large as 10. Moreover, the slope to intercept ratio for the MT-based approach is $\frac{\gamma}{p_m^0}$ whereas for the conventional R2 method it is $\frac{\gamma}{p_m^0 + \frac{p_f R_{2f}}{k_{mf}}}$ which is clearly smaller.

2.2 Effects of B_1 inhomogeneities

Both quantitative R2 imaging and MTP imaging are vulnerable to variations and inaccuracies in the RF (B_1) field. Significant variations of the B_1 amplitude occur within large samples, especially at higher fields, so the flip angle experienced by any part of the sample may be in error from the ideal intended value. The

sensitivity of multi-echo measurements of R2 to such errors has been well documented (Majumdar et al., 1986b, Sled and Pike, 2000a). When the refocusing pulses in a CPMG sequence are not precisely 180 degrees, the percent deviation in estimating T2 is a function of T2 itself; i.e., samples with higher T2 value (and lower R2) experience higher fractional deviations in T2 (and thus, dose extracted from a calibration curve) for a given error in B_1 than samples of lower T2. These inaccuracies in transverse relaxation time estimates can result in an apparent non-linearity of R2 versus dose and miscalibration of the dose response curve.

The susceptibility of magnetization transfer measurements to variations in B_1 has not been as thoroughly explored. In practice the RF pre-pulse may produce incomplete saturation of the broad component and/or partial saturation of the narrow water resonance. An apparent linear dependence of the MTR on variations in B_1 has previously been reported (Samson et al., 2006). We therefore have evaluated the effects of B_1 errors on estimates of dose in polymer gels for both the MTP and R2 approaches.

3. Methods

3.1 Gel preparation and irradiation

MAGIC (9% methacrylic acid) and MAGIC-2 gel dosimeters were produced as previously described (Fong et al., 2001, Luci et al., 2007). The components of the two formulations are the same but in different proportions, as the MAGIC-2

formulation has been optimized for measurement of the transverse relaxation rate in the 0-20Gy dose range. The manufacturing process is as follows: a Pyrex beaker containing the water for the desired volume of gel was placed in a water bath, along with a magnetic stirrer, on a hot plate. The desired quantity of gelatin was added and allowed to bloom. The temperature of the system was brought to 45 degrees C, at which point the water-gelatin solution was in liquid form. The monomer, ascorbic acid, and cupric sulfate were added and the system stirred for approximately 3 minutes. The solution was poured into 14mL Pyrex screw-top text tubes and placed in a refrigerator until irradiation. Samples were brought to room temperature, immersed in a water bath, and irradiated with 6MV photons with a dose rate of 2.84 Gy/min. Total dose increments of 2Gy were applied parallel-opposed fashion in sub-increments of 1 Gy each, in a range of 0 to 20Gy. A single gel dosimeter from each formulation was removed after each application of 2Gy of irradiation to create the set of gels in the desired range and dose separation. Samples were returned to refrigeration after irradiation. The MAGIC gels were manufactured 48 hours before irradiation, and the MAGIC-2 gels were manufactured 24 hours before irradiation.

3.2 Imaging measurements

After a refrigeration period of nine days following irradiation, samples were allowed to come to room temperature and imaged at 4.7T using a 31-cm bore Varian Inova (Varian Inc., Palo Alto, CA, USA) spectrometer using a 63mm quadrature coil. The imaging matrix was 64x64, the field of view 70x70mm, and

slice thickness 4mm. All samples from a given formulation were imaged together. Magnetization transfer imaging was performed with a MT-prepared spoiled gradient echo sequence (Sled and Pike, 2000b), as this method is relatively fast and does not have the potential disadvantage of heating of the samples. To prevent stimulated echoes, spoiler gradients and rf spoiling were used to disperse transverse magnetization, and complete spoiling was assumed. A 10ms Gaussian MT pulse was applied at 30 offset frequencies logarithmically distributed between 100 and 200,000 Hz for three different nominal MT pulse angles (283, 566, and 849 degrees), as well as at power levels of +/- 5 and 10% from each of these three powers. These powers are equivalent to 4.44, 8.88, and 13.32 μT, respectively (Tozer et al., 2003, Tofts et al., 2005). These powers were chosen to be representative of the strength of MT pulses available on clinical scanners. The signal was acquired via a 7 degree excitation sinc pulse. The TR was 25 ms and TE was 4ms, and the data from two acquisitions were averaged together for each measurement.

Transverse relaxation measurements were made with a 32 echo CPMG-type pulse sequence with TR of 15s and TE of 10ms. The transverse relaxation time was estimated using a pixel-by-pixel fit (using Matlab's "robustfit" function) of the log of the data to a linear model (see Eq. 55). Transverse relaxation rate maps were measured as negative slope of the linear fit to the data for each pixel. One acquisition was taken for each measurement.

Reported values for MTP and R2 were taken as the average value of pixels from a circular region (radius of 3 pixels) of interest for each sample.

4. Results

4.1 Magnetization transfer proportion measurements

Figure 21 displays an example MTP image of the data acquired from the MT experiment for the MAGIC-2 dosimeter. The image was created by applying Eq. 10 to images acquired for power of 8.88 μT at 200,000 Hz off resonance (M_{sat}) and 1375 Hz off resonance (M_0).

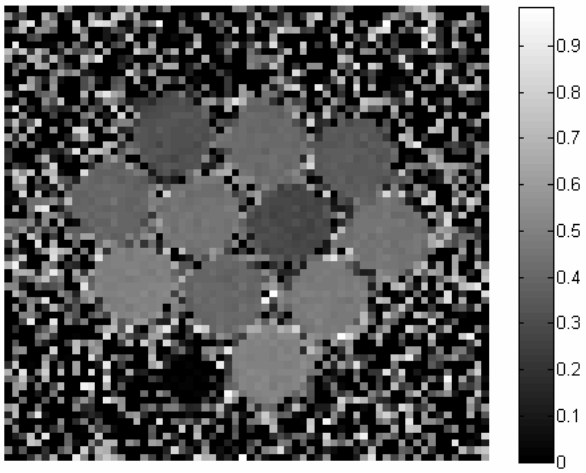

Figure 21: Example MTP image for the MAGIC-2 dosimeter, acquired at 8.88 μT calculated from images acquired at 200,000 and 1375 Hz off resonance. The dose values are, beginning at the top left and reading left to right, (row 1) 2, 10, 4 Gy; (row 2) 6, 12, 9, 14 Gy; (row 3) 18, 8, 16 Gy;(row 4) 20Gy. The dark space to the left of the 20 Gy dosimeter is a small vial of water used for location reference purposes.

Figure 22 and Figure 23 plot the measurement of the MTP for both types of MAGIC gel over a range of dose values, at four different offset frequencies and

different MT powers. Each data point is the mean of a region of interest for each dosimeter, and the standard deviation is the standard deviation of those pixels in the region of interest.

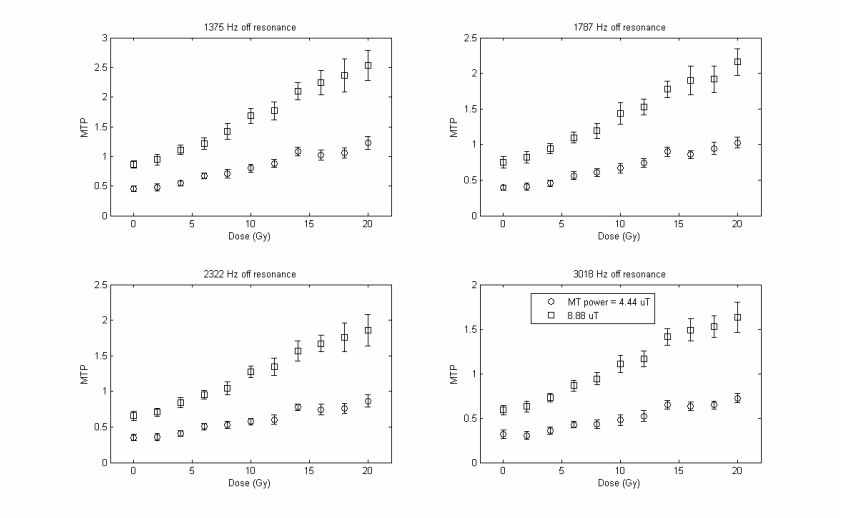

Figure 22: MTP versus dose for the MAGIC dosimeter.

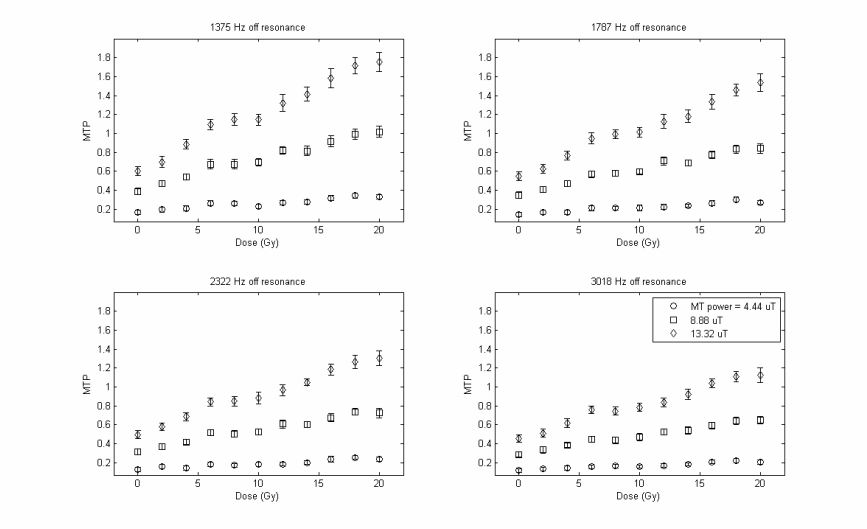

Figure 23: MTP versus dose for the MAGIC-2 dosimeter.

There are a few important features to note from Figure 22 and Figure 23. Sensitivity, defined as the slope of the MTP versus dose, varies with the offset

frequency and power of the MT pulse. At low powers and larger offsets the polymer pool is not fully saturated so the effects of MT are reduced. Additionally, there is a strong dependence of the intercept on the offset frequency and power chosen due to the direct effect of saturation on water, since it increases at small offsets, where the direct effect is strongest. This issue is addressed more fully in the Discussion session. Given this lack of full saturation of the immobilized pool, we do not expect Eq. 61 or Eq. 66 to be valid at all offsets and powers. Indeed, in the Discussion we consider how the theoretical expression for MTP should be modified under these circumstances. Nonetheless, our experimental data do in fact show linear responses, though with a slope and offset that depends upon the offset and power (in disagreement with Eq. 64, but as predicted below). In order to maximize dose sensitivity for MT measurements, the appropriate offset frequency and MT power should be chosen, as will be elaborated in the Discussion section.

Table 15: R^2 for the measurement of the linearity of MTP versus dose, for the MAGIC gel dosimeter.

Offset frequency	MT power = 4.44 μT	MT power = 8.88 μT
1375	0.969	0.989
1787	0.979	0.988
2322	0.961	0.990
3018	0.962	0.985

Table 16: R^2 for the measurement of the linearity of MTP versus dose, for the MAGIC-2 gel dosimeter.

Offset frequency	MT power = 4.44 μT	MT power = 8.88 μT	MT power = 13.32 μT
1375	0.894	0.976	0.982
1787	0.925	0.975	0.983
2322	0.896	0.966	0.982
3018	0.923	0.981	0.976

Table 15 and Table 16 show values of the linear correlation coefficients R^2, a measure of how well these data are represented by a linear relationship, as a function of both offset frequency and power of the B_1 pulse, for the least squares fit of MTP versus dose for MAGIC and MAGIC-2 dosimeters.

The slope and intercept of the dose response relationships can be combined to provide an assessment of dose response sensitivity (Fong et al., 2001). Experimental values for these parameters for MTP are reported below. To aid in assessment of the performance of the MTP in the face of B_1 errors, the results acquired with known B_1 error are also reported.

Table 17: Measured slope of the MTP versus dose line for a variety of MT powers and offset frequencies for the MAGIC-2 dosimeter.

MT power = 4.44 μ T	Error in B_1 pulse angle				
Offset frequency	-10%	-5%	No error	+5%	+10%
1375	0.0070	0.0071	0.0081	0.0089	0.0116
1787	0.0056	0.0054	0.0069	0.0070	0.0093
2322	0.0043	0.0044	0.0058	0.0055	0.0072
3018	0.0032	0.0034	0.0047	0.0042	0.0061

MT power = 8.88 μ T	Error in B_1 pulse angle				
Offset frequency	-10%	-5%	No error	+5%	+10%
1375	0.0254	0.0291	0.0308	0.0335	0.0361
1787	0.0205	0.0228	0.0247	0.0279	0.0299
2322	0.0170	0.0186	0.0209	0.0237	0.0248
3018	0.0140	0.0153	0.0178	0.0185	0.0207

MT power = 13.32 μ T	Error in B_1 pulse angle				
Offset frequency	-10%	-5%	No error	+5%	+10%
1375	0.0521	0.0537	0.0580	0.0621	0.0677
1787	0.0425	0.0461	0.0480	0.0520	0.0578
2322	0.0341	0.0382	0.0399	0.0443	0.0467
3018	0.0294	0.0314	0.0338	0.0377	0.0409

Table 18: Measured intercept of the MTP versus dose line for a variety of MT powers and offset frequencies for the MAGIC-2 dosimeter.

MT power = 4.44 μ T	Error in B_1 pulse angle				
Offset frequency	-10%	-5%	No error	+5%	+10%
1375	0.1467	0.1639	0.1790	0.1944	0.1776
1787	0.1273	0.1448	0.1505	0.1704	0.1635
2322	0.1233	0.1270	0.1323	0.1549	0.1408
3018	0.1086	0.1130	0.1221	0.1427	0.1273

MT power = 8.88 μ T	Error in B_1 pulse angle				
Offset frequency	-10%	-5%	No error	+5%	+10%
1375	0.3656	0.3825	0.4207	0.4388	0.4621
1787	0.3252	0.3530	0.3730	0.3904	0.4173
2322	0.2875	0.3254	0.3367	0.3546	0.3825
3018	0.2668	0.2986	0.3051	0.3285	0.3428

MT power = 13.32 μ T	Error in B_1 pulse angle				
Offset frequency	-10%	-5%	No error	+5%	+10%
1375	0.5549	0.6145	0.6343	0.6519	0.6899
1787	0.5121	0.5400	0.5681	0.5757	0.6068
2322	0.4718	0.4948	0.5196	0.5256	0.5704
3018	0.4247	0.4572	0.4718	0.4783	0.5083

Table 17 and Table 18 display the slope and intercept values calculated from a linear fit of the data acquired at the different powers and a range of +/-10% from the nominal powers, for the MAGIC-2 dosimeter. Values for the MAGIC dosimeter vary similarly.

Table 19: Measured percent change in slope-to-intercept ratio of the MTP versus dose line for a variety of MT powers and offset frequencies for the MAGIC dosimeter. For most powers and offset frequencies, the slope-to-intercept ratio does not vary more than 10% for even a 10% error in B_1 pulse angle.

MT power = 4.44 μ T	Error in B_1 pulse angle				
Offset frequency	-10%	-5%	No Error	+5%	+10%
1375	-0.61%	-1.73%	0.0941	-1.39%	10.05%
1787	-12.68%	-11.43%	0.0941	-0.92%	5.96%
2322	-3.80%	0.87%	0.0815	6.87%	18.92%
3018	-11.07%	-6.75%	0.0766	12.06%	13.41%

MT power = 8.88 μ T	Error in B_1 pulse angle				
Offset frequency	-10%	-5%	No Error	+5%	+10%
1375	-6.17%	0.42%	0.1151	5.51%	3.11%
1787	6.16%	5.15%	0.1058	10.53%	14.42%
2322	-5.31%	4.14%	0.1087	0.45%	12.76%
3018	-3.03%	-4.00%	0.1051	8.16%	8.78%

Table 20: Measured percent change in slope-to-intercept ratio of the MTP versus dose line for a variety of MT powers and offset frequencies for the MAGIC-2 dosimeter. With the exception of the values acquired at the lowest power, the slope-to-intercept ratio does not vary more than 10% for even a 10% error in B_1 pulse angle.

MT power = 4.44 μ T	Error in B_1 pulse angle				
Offset frequency	-10%	-5%	No Error	+5%	+10%
1375	5.93%	-4.48%	0.0452	1.38%	44.15%
1787	-3.49%	-19.47%	0.0459	-10.51%	23.44%
2322	-19.66%	-20.44%	0.0436	-18.69%	17.91%
3018	-24.73%	-22.81%	0.0386	-23.05%	24.66%

MT power = 8.88 μ T	Error in B_1 pulse angle				
Offset frequency	-10%	-5%	No Error	+5%	+10%
1375	-5.16%	4.06%	0.0732	4.20%	6.86%
1787	-5.21%	-2.57%	0.0663	7.60%	7.87%
2322	-4.26%	-7.91%	0.0619	7.88%	4.58%
3018	-9.82%	-12.34%	0.0584	-3.33%	3.40%

MT power = 13.32 μ T	Error in B_1 pulse angle				
Offset frequency	-10%	-5%	No Error	+5%	+10%
1375	2.64%	-4.54%	0.0915	4.04%	7.18%
1787	-1.66%	0.97%	0.0845	6.83%	12.74%
2322	-5.67%	0.57%	0.0767	10.00%	6.81%
3018	-3.25%	-3.92%	0.0715	10.06%	12.34%

Table 19 and Table 20 display the calculated change in slope-to-intercept ratio for the measured MTP of the MAGIC and MAGIC-2 dosimeter. With the exception of the MTP acquired for the MAGIC-2 dosimeter at the lowest power, the slope-to-intercept ratio of the MTP has a range of approximately +/-15% for a range of -10 to +10% error in B_1 power.

4.2 Transverse relaxation simulation and measurement

The effect of B_1 errors on measurements of transverse relaxation has been well characterized in the literature. The observed value of R2 due to a given error in B_1 power can be related as (Sled and Pike, 2000a)

$$R_{2,obs} = R_2 - \frac{\ln f}{\tau} \qquad \textbf{Eq. 71}$$

where *f* is an attenuation factor and τ is the echo spacing of the CPMG-type experiment. The attenuation factor *f* incorporates the effect of errors due to imperfect B_1 pulses, and for a hard pulse sequence, assuming no error in B_0, is given by

$$f = \frac{\cos(\delta)}{2} - \cos(\delta) + \frac{1}{2} \qquad \textbf{Eq. 72}$$

where δ is the degree of the refocusing B_1 pulse. Note that this derivation assumes complete spoiling occurs of any transverse magnetization produced by incomplete nutations and stimulated echoes. Using experimental values for R2 for the MAGIC and MAGIC-2 gel dosimeters and the above relationship, the expected deviation in R2 due to a given error in B_1 can be calculated and the effect on the dose response can be estimated. The values used for the dosimeter

from the experiment described above were 5.00 and 14.40 s^{-1} for the MAGIC dosimeter at 0 and 20Gy, respectively, and 6.29 and 17.69 s^{-1} for the MAGIC-2 dosimeter. These values were calculated from a linear fit of the R2 data acquired in the above experiment to simulate the kind of values that would be taken from a calibration curve. Figure 24 displays the expected variation in $R2_{,obs}$ for a given error in B_1 power for the MAGIC dosimeter as measured via a CPMG-type experiment using hard pulses.

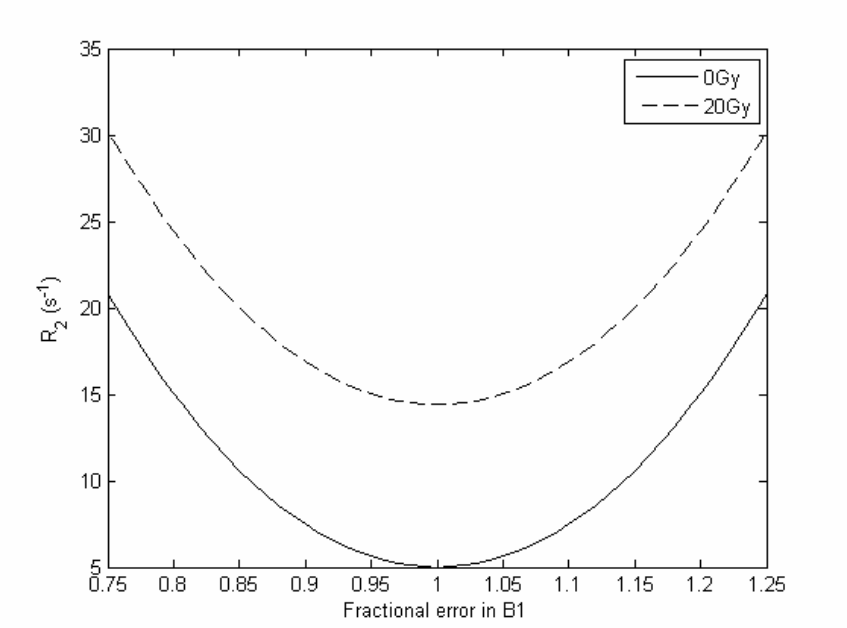

Figure 24: Expected variation in R2 for a given error in B_1 angle for the MAGIC dosimeter.

The simulation shows that while the slope of the R2 versus dose line remains the same (as indicated by the B_1-independent difference in R2 between 20 and 0 Gy), the intercept (the value of R2 at 0 Gy) will change significantly over a range of errors in B_1. Table 21 lists the expected percent change in the slope, intercept, and slope-intercept ratio of R2 versus dose for hypothetical errors in B_1 power.

Table 21: Expected change in the slope, intercept, and slope-intercept ratio of R2 versus dose for inclusion of B_1 angle error. Negative percent error in B_1 angle is not included as the result is symmetrical about zero percent error in B_1.

MAGIC	Percent error in B_1 angle		
	0%	5%	10%
Slope ($s^{-1}Gy^{-1}$)	0.470	0.470	0.470
Intercept (s^{-1})	5.000	5.618	7.4778
Slope-intercept Ratio	0.094	0.0834	0.063
Percent change in slope-intercept ratio	--	-10.99%	-33.13%

MAGIC-2	Percent error in B_1 angle		
	0%	5%	10%
Slope ($s^{-1}Gy^{-1}$)	0.570	0.570	0.570
Intercept (s^{-1})	6.290	6.908	8.768
Slope-intercept Ratio	0.091	0.083	0.066
Percent change in slope-intercept ratio	--	-8.94%	-28.26%

4.3 Comparison of effect of B_1 errors on dose estimates

Finally, a useful measure of the effect an error in B_1 power has on a measurement is to consider the apparent dose that would be calculated in the event of a specific B_1 variation. When polymer gel dosimeters are used for radiation field assessment, a calibration curve is created from dosimeters to which known doses are applied. The form of this line is

$$X = aD + b \qquad \textbf{Eq. 73}$$

where *X* is the measured value, such as R2 or MTP, *a* is the slope of the line, and *b* is the intercept. Once the desired measurement is made of the dosimeter to be assessed for dose, the following equation is used to back-calculate to the apparent dose D_{app}:

$$D_{app} = \frac{X - b}{a}. \qquad \textbf{Eq. 74}$$

If the parameter, be it MTP or R2, has been mis-measured due to B_1 errors, the apparent dose will be different than its true dose. This effect was investigated for the MTP and R2 measurements in the MAGIC and MAGIC-2 dosimeters. The slope and intercept of the calibration curves for MTP data acquired with no B_1 error (the nominal B1 powers referenced above) were applied to MTP values measured with a manually-adjusted power with known error (+/- 5 and 10% of the nominal B1 power) using Eq. 74. Additionally, the slope and intercept calculated for the R2 values were applied to simulated R2 values acquired with a 5 and 10% B_1 error. The percent error in apparent dose was calculated as

$$\frac{D_{app} - D}{D} \times 100. \qquad \textbf{Eq. 75}$$

Figure 25 displays representative data of the percent error in apparent dose acquired in both MTP and R2 measurements, as a function of applied dose. The data show that at lower dose levels, on the order of that which most radiation therapy dose fractionations deliver, measurements of MTP with 10% error in B_1 show much less error in apparent dose than measurements of R2.

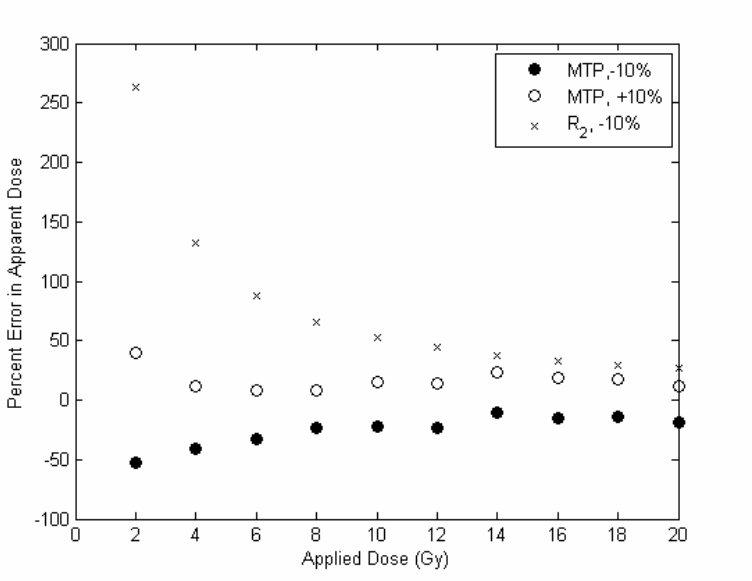

Figure 25: Percent error in the apparent dose for MTP measurements at +/-10% B_1 error, and R2 measurements at 10% error, in the MAGIC gel dosimeter. The MTP data were acquired at MT power 7.92 (-10% error) and 9.68 (+10% error) μT and offset frequency 1375Hz. The R2 data were calculated by simulation using data from Figure 24. Corresponding data for the MAGIC-2 dosimeter show an expected percent error in apparent dose for R2 at 2Gy to be approximately 217%, while the percent error for the MTP was an average of 96% At 4Gy, the percent error in R2 was approximately 109%, while the percent error for the MTP was an average of 54%. With a few exceptions, the data followed this trend for all offset frequencies investigated (1375, 1787, 2322, and 3018 Hz off resonance).

5. Discussion

5.1 Saturation of the two pools

Magnetization transfer measurements of the dose response of gel dosimeters are potentially less dependent upon errors in B_1 power than traditional multi-echo measurements of the transverse relaxation rate. In principle, once sufficient B_1 power is applied off resonance, complete saturation of the broad resonance can be achieved, and using larger powers will have little effect as long as direct saturation of the narrow water line is avoided.

At the powers and offsets shown in this work, complete saturation of the bound pool was not achieved, which may be more typical of conditions when using clinical scanners. The effect of incomplete saturation of the bound pool in the experiment can be estimated by adding a correction factor to Eq. 60 and Eq. 61, which were derived by taking $R_{rf,m}$ to be much greater than k, k_{mf}, R_1, and $R_{1,m}$. A first order correction for incomplete macromolecular saturation can be derived by instead assuming that $R_{rf,m}$ and k_{mf} are much greater than k, R_1, and $R_{1,m}$. This gives

$$\frac{M_{sat}}{M_o} = \frac{R_1}{R_1 + k\left(1 - \frac{k_{mf}}{R_{rf,b} + k_{mf}}\right)}. \qquad \textbf{Eq. 76}$$

The quantity $1 - \frac{k_{mf}}{R_{rf,b} + k_{mf}}$ can be interpreted as a measure of the effect incomplete saturation has on measurements of magnetization transfer. For the MTP, the inclusion of this error results in

$$MTP = \frac{k}{R_1}\left(1 - \frac{k_{mf}}{R_{rf,b} + k_{mf}}\right). \qquad \textbf{Eq. 77}$$

Eq. 77 is strictly linear in dose only if k_{mf} is independent of dose, which is true for BANG gels (Gochberg et al., 2001), but not MAGIC gels (Gochberg et al., 2003). Hence, achieving complete saturation of the macromolecular pool would be ideal. Using published values for R_1, k, and k_{mf} for the MAGIC gel dosimeter, the level of saturation (M_{sat}/M_0) achieved in our experiments can be estimated via Eq. 76. These estimated values for dosimeters irradiated to 0 Gy are on the

order of 84%, 65%, and 53% saturation for the three powers (4.44, 8.88, and 13.32 μT, respectively) of the MT pulse in the experiment, while values for 20Gy dosimeters are on the order of 76%, 49%, and 33% for the three powers. The experiment was designed to perform the magnetization transfer experiment at power levels similar to those available on clinical scanners, but the significant dependence of M_{sat}/M_0 on the rf power is due to incomplete saturation of the macromolecular pool.

It would be ideal to use known values for R_1, k, and k_{mf} to estimate the appropriate MT power strength and offset frequency to use in MTP experiments. Such prior knowledge could aid in ensuring that the assumptions behind Eq. 61 and Eq. 63 are fully met. For example, prior work (Gochberg et al., 2003) has estimated that for the MAGIC gel dosimeter, R_1, k, and k_{mf} for dosimeters at 20 Gy are approximately 1 Hz, 7.2 Hz, and 122 Hz, respectively. To estimate the range of powers and offsets for which $R_{rf,f}$ is much less than and $R_{rf,m}$ is much greater than any other rate, these values can be calculated using lineshape assumptions for the system in question and compared for the regime in which Eq. 61 and Eq. 63 is valid. Figure 26 displays calculations of the saturation of the free and bound pools and an assessment for whether or not the assumptions behind Eq. 61 and Eq. 63 were met. Values for $R_{rf,f}$ were calculated by assuming a Lorentzian lineshape for the free pool and using the relationship

$$R_{rf,f} = \frac{\omega_1^2 T_{2,f}}{1 + \left(2\pi\Delta T_{2,f}\right)^2} \qquad \textbf{Eq. 78}$$

where $T2_{,f}$ is the transverse relaxation time of the water pool, Δ is the offset frequency of the saturation, and ω_1 is the strength of the MT pulse in rad/sec. Values for $R_{rf,m}$ were calculated assuming the bound pool could be characterized by a Gaussian lineshape and the using the relationship

$$R_{rf,m} = \omega_1^2 T_{2,m} \sqrt{\frac{\pi}{2}} T_{2,m} e^{-\frac{(2\pi\Delta T_{2,m})^2}{2}} \qquad \textbf{Eq. 79}$$

where $T2_{,m}$ is the transverse relaxation time of the bound pool. For this value, an estimated value of 10 μs was used.

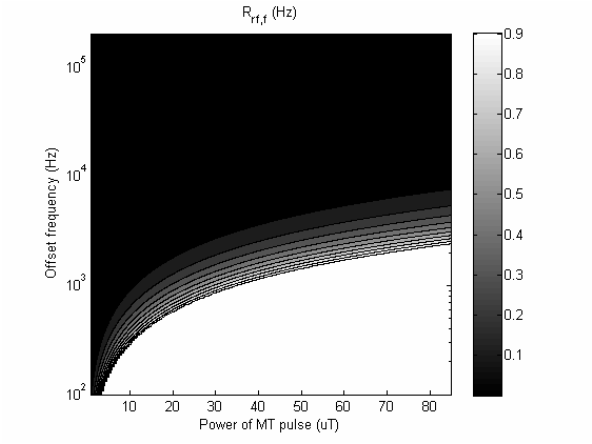

(a)

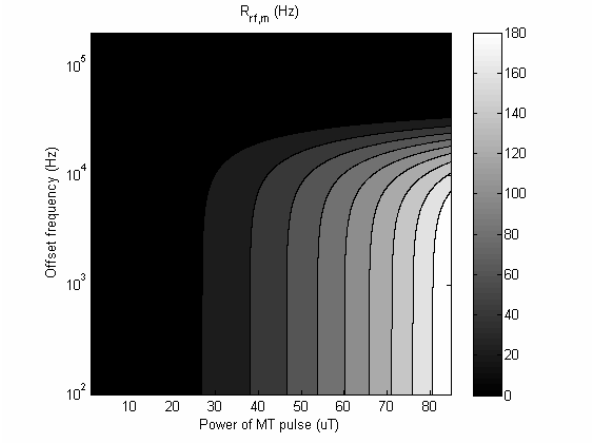

(b)

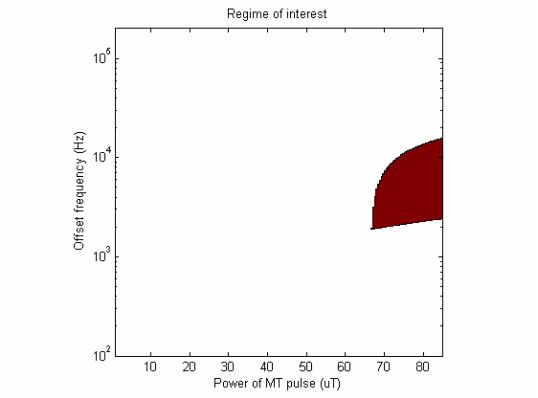

(c)

Figure 26: (a) $R_{rf,f}$ for a 20Gy MAGIC gel dosimeter, (b) $R_{rf,m}$, and (c) region for which the two criteria ($R_{rf,f}$ much less than all other rates, $R_{rf,m}$ much more than all other rates) overlap.

In Figure 26a, $R_{rf,,f}$ is displayed as a function of both MT pulse power and frequency. Values greater than 1, approximately R_1 (the lowest rate of concern), are not plotted to preserve the scale of interest. Figure 26b displays $R_{rf,m}$. Figure 26c is displayed by evaluating at each offset frequency and MT power whether or not the criteria of $R_{rf,f}$ << all other rates and $R_{rf,m}$ >> all other rates are valid, and the shaded area indicates the values for which the criteria are met.

A similar analysis can be used to appreciate the direct effect on the free water line. Assuming steady state conditions, the solution for the uncoupled Bloch equations for the transverse magnetization of the water is given by

$$\frac{M_{sat}}{M_0} = \frac{1+\left(\Delta T_{2,f}\right)^2}{1+\left(\Delta T_{2,f}\right)^2+\left(\frac{\omega_1}{2\pi}\right)^2 T_{1,f}T_{2,f}}. \qquad \textbf{Eq. 80}$$

Using values of $T2_{,f}$ of 1/14.4 Hz and assuming that R_1 is on the order of 1 Hz for polymer gel dosimeters at 4.7T, the direct effect on the free water line can be estimated. Results for a range of frequency offsets and MT powers are displayed in Figure 27.

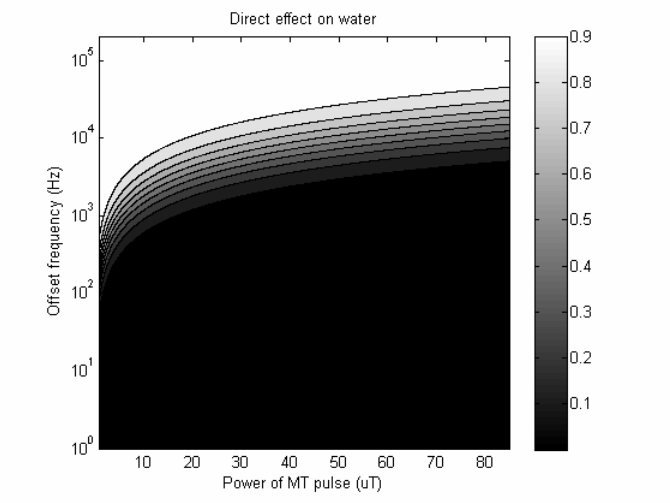

Figure 27: Simulation of the direct effect on water for a range of offset frequencies and MT powers.

It can be estimated from Figure 27 that at the offset frequencies and powers in this work, there was some level of direct effect on the water (M_{sat}/M_0 having a range of approximately 40-70%), and this is likely another reason our measurements of the MTP dose response intercept vary at the different offset frequencies.

These simulations suggest that while an appropriate range of offset frequencies was used for the measurement of MTP as displayed in Figure 22 and Figure 23, the MT power strength was less than ideal for a dosimeter with these specific relaxation properties. However, our results show that for clinically-feasible implementation of magnetization transfer experiments, where the power of the MT pulse may not be able to be increased by much or the user may only be able to set a nominal maximum power level, a linear dose response can still be attained. These results suggest that complete saturation of the

macromolecular pool and *a priori* knowledge of the sample parameters are not necessary to achieve linearity in dose.

5.2 Comparison of dose measurement in the presence of B_1 errors

The change in the slope-to-intercept ratio for the measurement of the MTP in MAGIC-type gel dosimeters was approximately +/-15%, while the value of the slope-to-intercept ratio for R2 could be expected to deviate by as much as 33% for 10% error in B_1 power.

The estimated (apparent) dose at dose levels used in most fractionation schemes varies with B_1 but for the range of changes considered here the MTP appears less susceptible to errors in apparent dose than are measurements of R2.

While the measurement of the MTP is linear in dose for a wide range of MT pulse powers and offset frequencies, it is important to note that the sensitivity can be maximized by the appropriate choice of these two variables. *A priori* knowledge of the magnetization transfer rates for a particular type of dosimeter can be used to estimate the appropriate values for MT power and offset frequency, but as has been shown is not necessary to achieve a linear dose response of MTP.

The MTP approach has not been tested in polyacrylamide-type (PAG) polymer gel dosimeters. Some studies (Gochberg et al., 2001, Gochberg et al., 2003) have suggested that magnetization transfer may behave differently in PAG versus methacrylic acid-based dosimeters, which may affect the measurement of

the MTP versus dose in PAG. Note also that the MTP is proportional to k (Eq. 61) and inversely proportional to p_f, the size of the free pool (Eq. 69), so efforts to change these may result in greater sensitivity. Sensitivity should also differ between dosimeters with different amounts of magnetization transfer present due to formulation, as k_{mf} is dependent upon the amount of monomer. We have assumed, based on expectations and some experimental data, that k_{mf} is not dose dependent. In some conditions this may no longer be valid (Gochberg et al., 2003), such that $k_{mf} = k_{mf,0} + \text{mD}$. Then the MTP has both a linear and a quadratic term in terms of D. However, it will still appear linear until $\text{mD} \geq k_{mf,0}$.

The MTP has been described before in the imaging literature, using the name “equivalent cross-relaxation rate (ECR)” (Sogami et al., 2001), for imaging studies for breast cancer. However, the term “cross-relaxation” has usually been reserved in nuclear magnetic resonance to denote dipolar cross-relaxation, whereas magnetization transfer includes chemical exchange and other effects. We therefore feel it is not appropriate to use the ECR name and propose MTP for this quantity.

5.3 Other concerns

Image resolution should not significantly affect these types of measurements unless regions of interest are drawn such that partial volume effects are present in the measurement of the MTP. Creating regions of interest that are well within the boundaries of the samples will ensure this error is avoided.

6. Conclusion

This work has shown that the measurement of the MTP in methacrylic-acid type gel dosimeters is linear with dose and shows promise as a measure of dose response in polymer gel dosimeters. The method has been validated at powers and offset frequencies similar to those used in clinical applications, and prior knowledge of magnetization transfer quantities, while desirable to maximize contrast, is not necessary to acquire useful dose response data. The method is less susceptible to calibration errors than transverse relaxation rate measurements in the presence of B1 inhomogeneities.

References

Baldock, C., Lepage, M., Back, S.A.J., Murry, P.J., Jayasekera, P.M., Porter, D. & Kron, T. (2001) Dose resolution in radiotherapy polymer gel dosimetry: effect of echo spacing in MRI pulse sequence. *Phys. Med. Biol.,* 46**,** 449-460.

De Deene, Y., Vergote, K., Claeys, C. & De Wagter, C. (2006a) The fundamental radiation properties of normoxic polymer gel dosimeters: a comparison between a methacrylic acid based gel and acrylamide based gels. *Phys. Med. Biol.,* 51**,** 653-673.

De Deene, Y., Vergote, K., Claeys, C. & De Wagter, C. (2006b) Three dimensional radiation dosimetry in lung-equivalent regions by use of a radiation sensitive gel foam: Proof of principle. *Med. Phys.,* 33**,** 2586-2597.

Fong, P.M., Keil, D.C., Does, M.D. & Gore, J.C. (2001) Polymer gels for magnetic resonance imaging of radiation dose distributions at normal room atmosphere. *Phys. Med. Biol.,* 46**,** 3105-3113.

Gochberg, D.F., Fong, P.M. & Gore, J.C. (2001) Studies of magnetization transfer and relaxation in irradiated polymer gels - interpretation of MRI-based dosimetry. *Phys. Med. Biol.,* 46**,** 799-811.

Gochberg, D.F., Fong, P.M. & Gore, J.C. (2003) A quantitative study of magnetization transfer in MAGIC gels. *Phys. Med. Biol.,* 48**,** N277-N282.

Henkelman, R.M., Huang, X.M., Xiang, Q.S., Stanisz, G.J., Swanson, S.D. & Bronskill, M.J. (1993) Quantitative interpretation of magnetization-transfer. *Magn. Reson. Med.,* 29**,** 759-766.

Lepage, M., Mcmahon, K., Galloway, G.J., De Deene, Y., Back, S.A.J. & Baldock, C. (2002) Magnetization transfer imaging for polymer gel dosimetry. *Phys. Med. Biol.,* 47**,** 1881-1890.

Lepage, M., Whittaker, A.K., Rintoul, L. & Baldock, C. (2001) C-13-NMR, H-1-NMR, and FT-Raman study of radiation-induced modifications in radiation dosimetry polymer gels. *Journal of Applied Polymer Science,* 79**,** 1572-1581.

Luci, J.J., Whitney, H.M. & Gore, J.C. (2007) Optimization of MAGIC gel formulation for three-dimensional radiation therapy dosimetry. *Phys. Med. Biol.,* 52**,** N241.

Majumdar, S., Orphanoudakis, S.C., Gmitro, A., Odonnell, M. & Gore, J.C. (1986a) Errors in the measurements of T2 using multiple-echo MRI techniques. 1. Effects of radiofrequency pulse imperfections. *Magn. Reson. Med.,* 3**,** 397-417.

Majumdar, S., Orphanoudakis, S.C., Gmitro, A., Odonnell, M. & Gore, J.C. (1986b) Errors in the measurements of T2 using multiple-echo MRI techniques. 2. Effects of static-field inhomogeneity. *Magn. Reson. Med.,* 3**,** 562-574.

Samson, R.S., Wheeler-Kingshott, C.A.M., Symms, M.R., Tozer, D.J. & Tofts, P.S. (2006) A simple correction for B-1 field errors in magnetization transfer ratio measurements. *Magn. Reson. Imaging,* 24**,** 255-263.

Sled, J.G. & Pike, G.B. (2000a) Correction for B-1 and B-0 variations in quantitative T-2 measurements using MRI. *Magn. Reson. Med.,* 43**,** 589-593.

Sled, J.G. & Pike, G.B. (2000b) Quantitative interpretation of magnetization transfer in spoiled gradient echo MRI sequences. *J. Magn. Reson.,* 145**,** 24-36.

Sogami, M., Era, S., Kinosada, Y., Matsushima, S., Kato, K., Tomida, M. & Hirabayashi, T. (2001) Basic studies on the equivalent cross-relaxation rate imaging (equivalent CRI) - phantom studies. *NMR in Biomed.,* 14**,** 367-375.

Tofts, P.S., Cercignani, M., Tozer, D.J., Ramani, A. & Barker, G.J. (2005) Quantitative magnetization transfer mapping of bound protons in multiple sclerosis (vol 50, pg 83, 2003). *Magn. Reson. Med.,* 53**,** 492-493.

Tozer, D., Ramani, A., Barker, G.J., Davies, G.R., Miller, D.H. & Tofts, P.S. (2003) Quantitative magnetization transfer mapping of bound protons in multiple sclerosis. *Magn. Reson. Med.,* 50**,** 83-91.

Wolff, S.D. & Balaban, R.S. (1989) Magnetization transfer contrast (MTC) and tissue water proton relaxation in vivo. *Magn. Reson. Med.,* 10**,** 135-144.

CHAPTER V

MODEL OF DOSE RESPONSE BASED ON T2

1. Introduction

The purpose of this work is to understand in more detail the molecular basis of the strong dose response of the MAGIC-type gel dosimeter. From previous work it is clear that several MR parameters change upon irradiation, including R2 and MT properties of the water in the gel. These are measured as indirect indicators of specific physicochemical features of the constituents. Here we seek to better understand the precise basis of the dose response in terms of molecular changes within the gel, particularly for the R2 dose response. These studies hope to better describe the relaxation mechanisms and possibly point the way towards better design and understanding of the factors that affect dose response.

2. Theory

2.1 Known relaxation mechanisms in methacrylic acid

The monomer used in the MAGIC-type gel dosimeter is methacrylic acid. This material is a carboxylic acid with formula $C_4H_6O_2$ and molecular weight (in monomer form) of 86.08 g/mol. It is slightly denser than water. Its molecular structure is displayed in Figure 28.

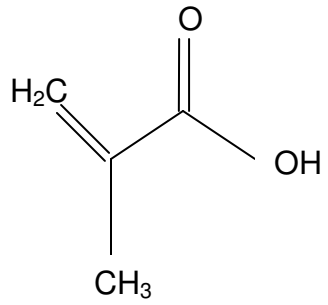

Figure 28: Chemical structure of methacrylic acid

For the monomer, peak assignments of the main resonances in an NMR spectrum are given in Table 22 (Sasaki, 1985), from spectra of the monomer in solution with $CDCl_3$.

Table 22: Peak assignments for methacrylic acid (Δ ppm with respect to water).

Peak of interest	ppm
CH_3	2.72
CH_2 (1)	1.00
CH_2 (2)	1.57
OH^-	-6.69

In its monomer form, the methylene group appears as a doublet, indicated by the (1) and (2) in Table 22.

Spectra of methacrylic acid and poly(methacrylic) acid (Mw = 7750), measured at 400MHz, are shown in

Figure 29. Note that the OH resonance is not seen in this spectrum because the proton is in very rapid exchange with the large water signal, and collapses to a small shift effect on the water peak.

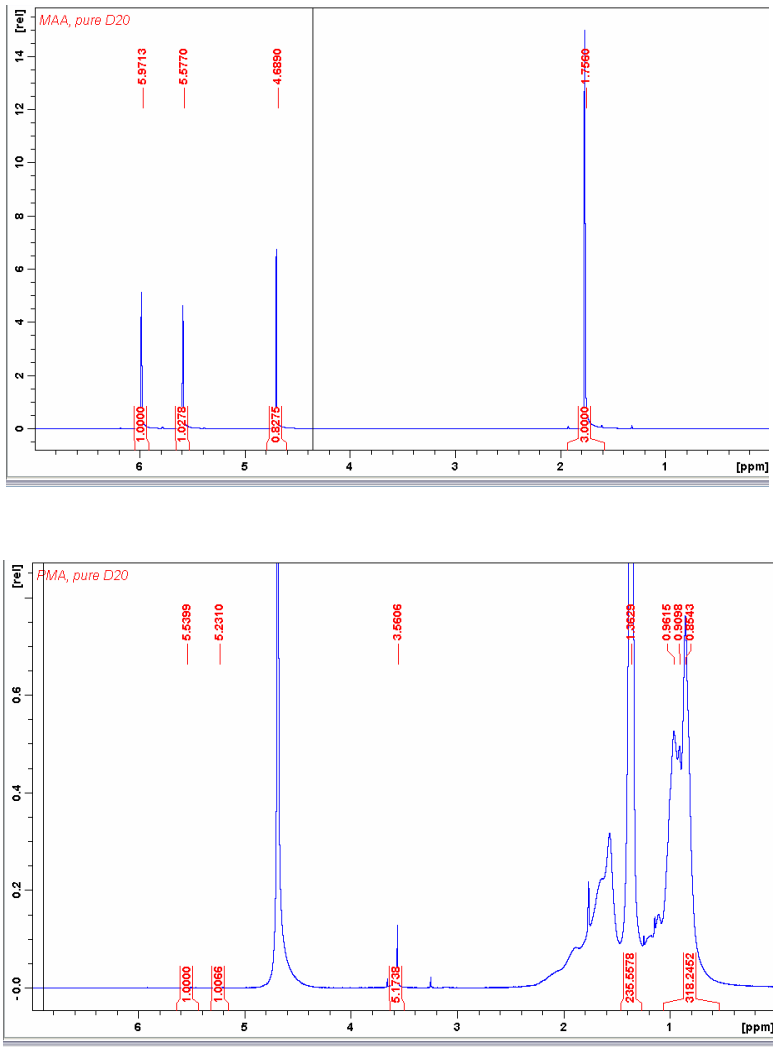

Figure 29: NMR spectra of methacrylic acid (top) and poly(methacrylic acid) (bottom) at 400MHz in deuterated water.

Evidence in the literature points to chemical exchange mediated by the COOH carboxyl proton as the main influence on solvent relaxation in solutions of water and poly(methacrylic acid) (Mulder et al., 1983). This particular study performed CPMG-spacing experiments and selective inversion recovery experiments on pH-neutral solutions of poly(methacrylic acid) (molecular weight of approximately 400,000) and concluded that if cross-relaxation to the non-exchanging protons was present at all, its effects were negligible. Conceivably

cross-relaxation to these other protons might still be important in polymer gels because the polymer particle molecular weights are thought to be much greater, but efforts to demonstrate such effects e.g. by looking for a transient NOE following selective inversion of the water, suggest this is not the case. The earlier studies of magnetization transfer show that magnetization transfer takes place, so we have looked to see whether a simple model of chemical exchange can explain the dose response of polymer gels based on methacrylic acid.

2.2 Chemical Exchange

In addition to intrinsic relaxation rates, NMR signals can be affected by chemical exchange. The physical exchange of protons between different environments can cause an averaging of their relaxation properties. For example, a small number of efficiently relaxing sites can affect a much larger number of less efficiently relaxing protons if the exchange rate is fast. In addition, exchange between protons that inherently have different resonance frequencies (chemical shifts) can introduce an additional contribution to the overall transverse relaxation rate. In methacrylic acid, we may consider a two-pool model involving proton exchange between the free water and the COOH site, in both the monomer and the polymer. The monomer does not relax very efficiently, whereas the polymer does reduce T2 by much more. Given that the exchange rate and number of exchangeable protons are not expected to change, the dose response may be accounted for if the chemical shift and intrinsic relaxation rate of the COOH proton changes with polymerization. If the contribution of the chemical shift

difference is significant, we would then predict there would be a variation of dose sensitivity with magnetic field.

In order to model chemical exchange contributions to overall relaxation, the traditional Bloch equations need to be amended. Several such models have been proposed previously, each with certain assumptions. The McConnell model (McConnell, 1958) considers a two-spin system (a and b) with unequal chemical shifts ($\delta\omega_a \neq \delta\omega_b$), equal spin-spin relaxation rates ($T_{2a} = T_{2b} = T_2$), and exchange site lifetimes of τ_a and τ_b. Exchange rates are the inverse of the exchange site lifetimes and are called k_a and k_b. The Luz and Meiboom model limits the species of interest to have $T_{2a} = T_{2b}$ and assumes fast exchange (Luz and Meiboom, 1963). Neither of these simpler models seems appropriate for polymer gels. These restrictions were removed by the work of Carver and Richards (Carver and Richards, 1972), who used the measurement of R2 versus inverse CPMG spacing ($1/\tau_{CPMG}$) to determine the rate of chemical exchange and other parameters in a sample for the general case. Hills and co-workers found a slight error in the equations of Carver and Richards and published corrections (Hills et al., 1989). The equations are

$$\frac{1}{T_2} = \frac{1}{\tau_{CPMG}} \ln \lambda_1 \qquad \textbf{Eq. 81}$$

where

$$\lambda_1 = -\tau_{CPMG} \frac{\alpha_+}{2} + \ln\left[\left(D_+ \cosh^2 \xi - D_- \cos^2 \eta \right)^{\frac{1}{2}} + \left(D_+ \sinh^2 \xi - D_- \sin^2 \eta \right)^{\frac{1}{2}} \right] \qquad \textbf{Eq. 82}$$

$$2D_\pm = \pm 1 + \frac{\left(\psi + 2\Delta\omega^2 \right)}{\sqrt{\psi^2 + \zeta^2}} \qquad \textbf{Eq. 83}$$

$$\xi = \frac{\tau_{CPMG}}{2\sqrt{2}} \left\{ \pm \left[+\psi + \left(\psi^2 + \zeta^2 \right)^{\frac{1}{2}} \right]^{\frac{1}{2}} \right\} \quad \textbf{Eq. 84}$$

$$\eta = \frac{\tau_{CPMG}}{2\sqrt{2}} \left\{ \pm \left[-\psi + \left(\psi^2 + \zeta^2 \right)^{\frac{1}{2}} \right]^{\frac{1}{2}} \right\} \quad \textbf{Eq. 85}$$

$$\psi = \alpha_-^2 - \Delta\omega^2 + 4k_a k_b \quad \textbf{Eq. 86}$$

$$\zeta = 2\Delta\omega^2 \alpha_- \quad \textbf{Eq. 87}$$

$$\alpha_\pm = \frac{1}{T_{2a}} \pm \frac{1}{T_{2b}} + k_a \pm k_b \quad \textbf{Eq. 88}$$

Additionally,

$$P_a k_a = P_b k_b \quad \textbf{Eq. 89}$$

and

$$P_a + P_b = 1 \quad \textbf{Eq. 90}$$

where P_a and P_b are the molar fractions of the total population of the nuclei in the a and b sites, respectively. In this work, the subscript *a* will refer to the solvent water, and *b* to the macromolecule pool in exchange with the water. For the polymer gel dosimeters, it is assumed that the protons in water and the carboxyl group of methacrylic acid/poly(methacrylic acid) are in fast exchange, as evidenced by the high resolution spectra mentioned earlier. Note that here “fast” exchange implies the exchange rate is >> the difference in frequencies, which are believed to be of the order of 6 – 7 ppm.

2.3 Model of dose response

As discussed in the Introduction to this thesis, the monomers in the gel dosimeter polymerize upon exposure to irradiation. In the simplest case, this implies that radiation causes the production of a number of polymer "particles". We assume that for a given dose rate, this leads to a narrow distribution of particle sizes, and that the larger changes in relaxation (or MT) seen at higher doses are the result of increased numbers of particles only. Each particle is assumed to contain then a fixed number of monomer units, each with one exchanging COOH proton, and the increase in relaxation rate in the gel arises because the COOH proton itself is relaxing more efficiently by being part of the larger polymer particle, and possibly has a different chemical shift to the monomer. The increased intrinsic relaxation rate of the COOH proton is expected because its motional properties are quite different to the monomer.

Assume that an unirradiated gel initially contains J_0 grams of monomer per liter. After dose ΔD is applied, there are ΔJ grams of monomer lost and the amount remaining is *J*

$$J - \Delta J = J - \lambda \Delta D \qquad \textbf{Eq. 91}$$

where λ is the probability of initiating polymerization per gram of monomer per dose to the volume, which is assumed to be a constant. Thus *J* reduces exponentially as

$$J = J_0 e^{-\lambda D}. \qquad \textbf{Eq. 92}$$

The amount of polymer formed per volume of gel dosimeter, for a dose *D*, is given by

$$J_0 - J = J_0\left(1 - e^{-\lambda D}\right). \qquad \textbf{Eq. 93}$$

Note that this shows a quasi-linear growth at low doses, followed by saturation of the response as the monomer is used up, similar to the actual dose response of polymer gels. As each polymer particle is formed, its molecular weight, M, is the product of the number of monomers linked together (N) and the molecular weight of the monomer (m). Therefore, the number of relaxing polymer particles per volume is related to dose by $\frac{J_0 N_0}{Nm}\left(1 - e^{-\lambda D}\right)$, where N_0 is Avogadro's number.

In this model, each particle has N exchanging $-COOH^-$ protons, and each of these protons has intrinsic relaxation rate R sec^{-1} M^{-1}. Therefore, the change in R2 with dose is

$$\Delta R_2 = \frac{J_0 R}{m}\left(1 - e^{-\lambda D}\right). \qquad \textbf{Eq. 94}$$

For 2-site fast exchange, if we ignore for now the chemical shift between the species, the overall relaxation rate of the water in the gel is given by

$$R = p_a R_a + (1 - p_a) R_b. \qquad \textbf{Eq. 95}$$

If the number of water molecules is much greater than the number of polymer molecules, as is true for the polymer gel dosimeters, then

$$R = R_{water} + p_b R_b. \qquad \textbf{Eq. 96}$$

In 1 liter of polymer gel there are approximately 111 moles of water protons, and the number of exchangeable protons can be estimated as

$\frac{J_0 N_0}{Nm}\left(1-e^{-\lambda D}\right)N$ carboxyl sites. Therefore, $p_b \cong \frac{J_0}{111m}\left(1-e^{-\lambda D}\right)$. The transverse relaxation rate as a function of dose can be given by

$$R_2 = R_{2,0} + \frac{J_0}{111m}\left(1-e^{-\lambda D}\right)R. \qquad \textbf{Eq. 97}$$

3. Methods

To investigate chemical exchange in the monomer and polymer component of the gel dosimeters, samples of methacrylic acid and poly(methacrylic) acid sodium salt standards of various molecular weights were mixed in solution with water and placed in 5mm NMR tubes. The monomer sample was 20% w/w. Molecular weights and concentrations of the polymer samples are given in Table 23. P_b, the calculated fractions of the exchangeable protons that are in the macromolecular pool, are also given.

Table 23: Molecular weights and concentration of polymer samples

Sample	Molecular weight	Concentration (% w/w)	P_b
1	7,750	20	0.028
2	31,100	21	0.028
3	790,000	21.8	0.029

Additionally, selected polymer gel samples irradiated to 0, 6, 14, and 20Gy were studied in their test tube containers, as well as a sample of pure gelatin in water (9% w/w). A CPMG-type NMR experiment, with varied tau spacing (Carver and Richards, 1972, Hills et al., 1991) was performed at 0.5T using a benchtop Maran imaging system. The length of the 90 degree pulse was approximately 14

us for the polymer samples and 16 us for the gel samples. The minimum length of tau was limited by the length of the 90 degree pulse; tau ranged from 45us to 2ms. The log of the decay data were fitted to an linear model and the R2 value measured as the negative of the slope of the least squares fit. The experiment was repeated 3 times for each sample and the values of R2 averaged for each tau spacing point.

These data points were fitted to the model given in Eq. 81 through Eq. 88 using a non-linear least squares fitting method in MATLAB. Free parameters were k_b, T_{2b}, and $\Delta\omega$, while T_{2a} was set to 2.259 seconds, the T_2 of water found through a separate CPMG experiment with τ_{CPMG} = 1ms.

4. Results

R2 versus 1/tau for the monomer and polymer samples are shown in Figure 30.

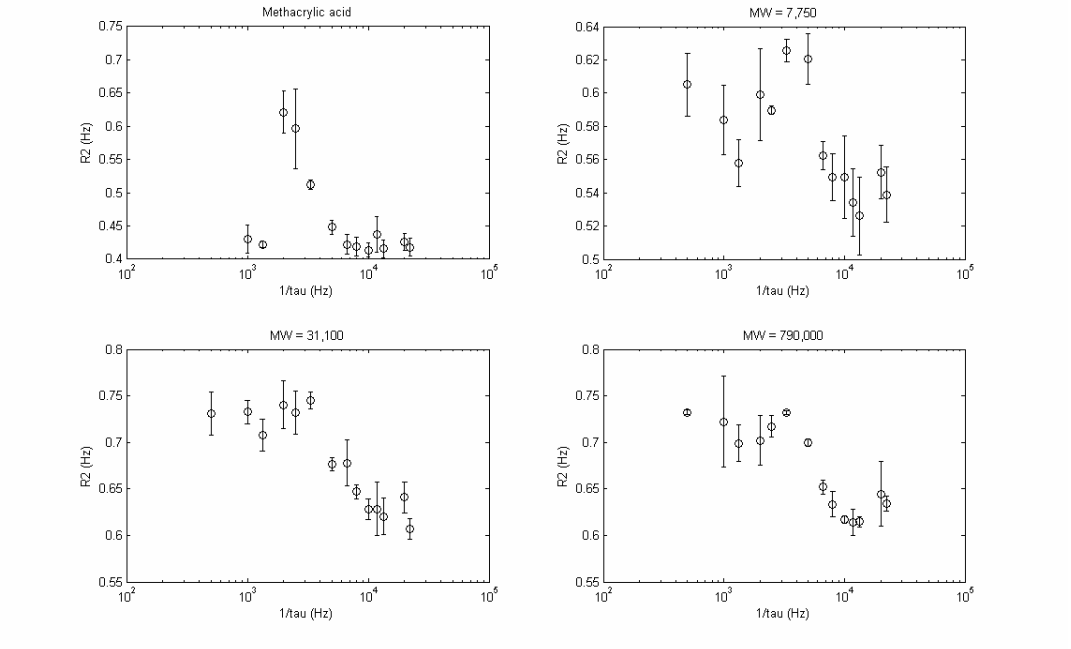

Figure 30: R2 versus 1/ τ_{CPMG} for the monomer and polymer samples.

The samples qualitatively show evidence of chemical exchange, as seen in the sigmoidal shape in a logarithmic plot of the data. Note however that the polymer relaxivity is not much greater than the monomer, suggesting that at the molecular weights studied the intrinsic relaxation rate of the exchangeable protons was not much different.

Figure 31 shows results for the CPMG experiment performed upon gelatin and polymer samples. The polymer relaxation rate changes by much more as tau is varied, and the pulse frequency at which the relaxation rate changes most dramatically is very similar to the polymers, of the order of 5kHz.

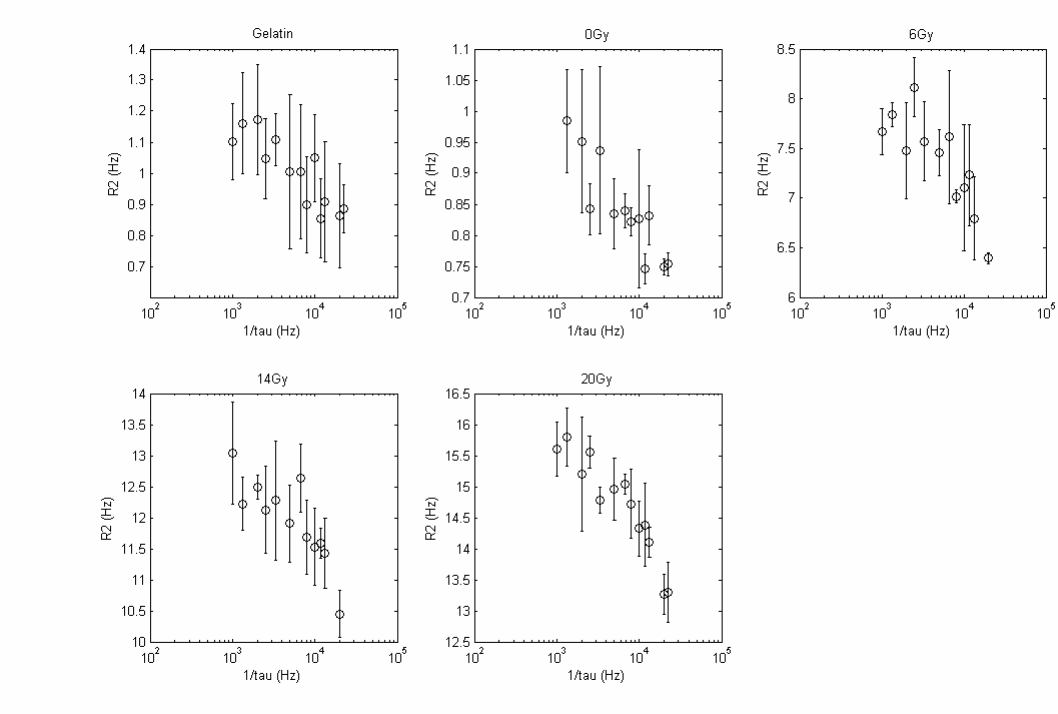

Figure 31: R2 versus 1/tau for the polymer gel samples.

Figure 32 displays the polymer data in Figure 30 with an overlay of the best fit of the polymer data to the model, while Table 24 gives the quantitative results from the fit.

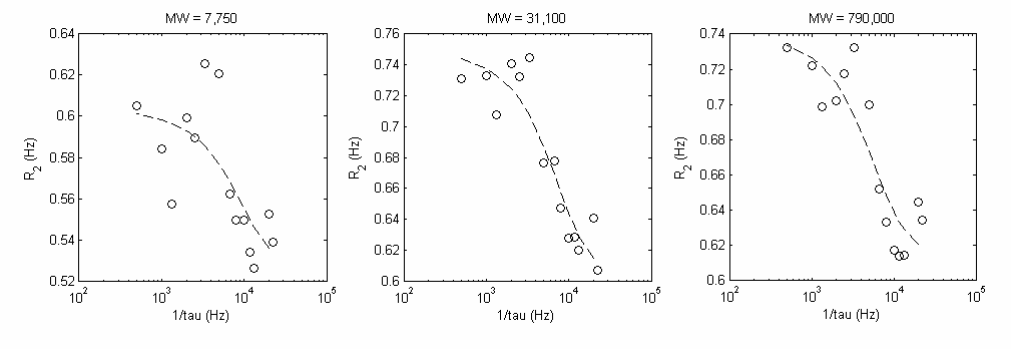

Figure 32: Best fits of the chemical exchange model to the measurement of R2 versus inverse CPMG spacing for the monomer and polymers

Table 24: Results from the fit of the model to the data.

Sample	k_b (s^{-1})	$\Delta\omega/(2\pi)$ (Hz)	T_{2b} (s)
MW 7,750	2.8838×10^4	287.8243	0.2982
MW 31,100	2.2708×10^4	359.7303	0.1637
MW 790,000	1.7584×10^4	286.8669	0.1586

The data in Table 24 suggest that the chemical exchange rate decreases with polymer weight, while the transverse relaxation time of the polymer pool decreases with polymer weight as well. However, the values for the chemical shift difference are larger than expected at this field strength.

5. Discussion

The data strongly suggest that chemical exchange plays an important role in relaxation in the polymer gel system, as seen in Figure 31, similar to the simple

polymers. Because the polymer gels are likely to have a variety of polymer molecular weights present at each dose level, each with a range of properties, the single dispersion curve behavior seen for the more homogeneous polymers is not as obvious, though many features are preserved. As polymerization progresses in the gel dosimeter, the average molecular weight of the polymer pool may increase with dose, or there may be dose rate effects if the rate of initiation (but not termination) of polymerization is itself dose rate dependent. As the average polymer molecular weight increases, the exchange rate k_b seems to decrease and T_{2b} decreases; the latter are expected, and the former may reflect local changes in lifetime caused by polyelectrolyte behavior or restrictions on exchange.

In light of results found in Chapter III, which showed that T_2 decreased with dose applied to the polymer gels (and, presumably, increased average molecular weight of the polymers formed in the gels), these results suggest that the increase in the R2 dose response with increasing field is primarily facilitated through increasing contributions of chemical exchange with some contribution from the increased chemical shifts of the exchanging species.

The model introduced above can be used to better understand the R2 dose response in polymer gel dosimeters. At 0.5T, the change in R2 from 0 to 20Gy was approximately 14 Hz. For a linear dose response in the range of 0-20Gy, this corresponds roughly to $\lambda = 0.05$. Using Eq. 97 and values of $J_0 = 4$ (the percent weight of methacrylic acid in the MAGIC-2 dosimeter) and m = 86.06, the expected transverse relaxation time of the macromolecular pool is

approximately 18.6 us. At 4.7T, the change in R2 was shown in Chapter III to be approximately 22Hz. Applying the same model gives an expected transverse relaxation time of 12 us, which is of the same order of magnitude as the transverse relaxation time of the macromolecular pool estimated in Chapter III via the CWPE model.

Recall that in Chapter III the pool size ratio of the MAGIC-2 dosimeter did not show significant change over the range of doses. If these two techniques measure the same phenomena, then this contradicts the predictions of the chemical exchange model, unless the fitting implies that the COOH pool is a mixture of monomer and polymer protons (in which case the total pool does not change, but they become less mobile on average). These results suggest that it is the change in the transverse relaxation rate of the macromolecular pool with increasing dose that increases the overall transverse relaxation rate of the polymer gel dosimeter. Similarly, it expected that for magnetization transfer it is not the change of the macromolecular pool that produces the changes in MT parameters as a function of dose, but a change in the MT rates.

Previous studies have shown the diameter of polymer particles formed in the MAGIC-2 dosimeter at approximately 20 Gy to be around 300 nm (Whitney and Gore, 2006) for the dose rate used to produce these gels. To estimate the molecular weight present in the polymer gel dosimeters at 20Gy, we assume the particles to be spherical. With a carbon-carbon bond length of 1.1 Å in methacrylic acid (Ukaji, 1959), we can assume that the volume of a particle contains approximately 10,000 units of methacrylic acid. This would imply a

molecular weight of about 860,000, not much different from the highest molecular weight polymer considered. However, in the gel the polymer particles may graft to the gelatin, thereby further reducing the mobility and decreasing the frequency of segmental motions, and making the relaxation more efficient.

There is perhaps some additional contribution to the transverse relaxation rate of the macromolecule. In the polymer gels, hydrogen peroxide is formed in a secondary reaction in the hydrolysis process as a product of the oxidation of ascorbic acid (Fong, 2003), and it can facilitate grafting of the acrylic monomers to gelatin. This could act as an additional mechanism for chemical exchange-mediated transverse relaxation, and the validation of this is left for future work.

6. Conclusions

By studying the monomer, polymer, and gel using CPMG methods, it can be seen that chemical exchange is strongly present and the effects increase with polymer molecular weight. The model for R2 dose response is shown to agree with measurements for the transverse relaxation rate of the macromolecular pool, as found in previous chapters.

References

Carver, J.P. & Richards, R.E. (1972) General 2-site solution for chemical exchange produced dependence of T2 upon Carr-Purcell pulse separation. *J. Magn. Reson.,* 6**,** 89-&.

Fong, P.M. (2003) Development and characterization of normoxic polymer gels for ionizing radiation dosimetry. New Haven, CT, Yale University.

Hills, B.P., Cano, C. & Belton, P.S. (1991) Proton NMR relaxation studies of aqueous polysaccharide systems. *Macromolecules,* 24**,** 2944-2950.

Hills, B.P., Wright, K.M. & Belton, P.S. (1989) Proton NMR studies of chemical and diffusive exchange in carbohydrate systems. *Mol. Phys.,* 67**,** 1309-1326.

Luz, Z. & Meiboom, S. (1963) Nuclear magnetic mesonance study of the protolysis of trimethylammonium ion in aqueous solution---order of the reaction with respect to solvent. *J. Chem. Phys.,* 39**,** 366-370.

Mcconnell, H.M. (1958) Reaction rates by nuclear magnetic resonance. *J. Chem. Phys.,* 28**,** 430-431.

Mulder, C.W.R., Schriever, J., Jesse, W.J. & Leyte, J.C. (1983) Nuclear magnetic-relaxation of solvent nuclei in concentrated aqueous poly(methacrylic acid) solutions. *J. Phys. Chem.,* 87**,** 2342-2348.

Sasaki, S.-I. (1985) *Handbook of Proton-NMR Spectra and Data,* New York, Academic Press, Inc.

Ukaji, T. (1959) The molecular structure of the monomer and the dimer of methacrylic acid. *Bulletin of the Chemical Society of Japan,* 32**,** 1270-1275.

Whitney, H.M. & Gore, J.C. (2006) Measurement of particle size in polymer gel dosimeters using spectrophotometry. *J. of Phys.: Conf. Ser.,* 56**,** 160-163.

CHAPTER VI

CONCLUSION AND FINAL DISCUSSION

This work has focused on studies on the design, use, and characteristics of the methacrylic acid-based polymer gel dosimeter. Three primary issues continue to confront the field of polymer gel dosimetry. First, what is the best gel for practical use for mapping radiation dose distributions accurately in three dimensions? This requires studies of the composition and dose responses of different formulations in order to optimize characteristics such as sensitivity, uniformity and stability. Several other investigators have undertaken some such studies but there was no prior study optimizing the sensitivity of the MAGIC formulation. The MAGIC dosimeter was optimized for greatest dose response sensitivity for the measurement of the transverse relaxation rate, the measurement most typically used in practice for measuring dose effects. The primary change in formulation was a reduction in the amount of methacrylic acid, and this new formulation was called MAGIC-2.

A second recurring issue is to identify the optimal method for measuring the dose (which is not unrelated to the first issue of design). In practice transverse relaxation times are used most commonly, but there are other contrast effects that can be exploited. In particular magnetization transfer is one option that was hypothesized to be less dependent on the uniformity of the RF pulses used for imaging. A more complete study of relaxometry and

magnetization transfer measurements of the MAGIC-2 dosimeter was therefore pursued. A complete measurement of the magnetization transfer parameters was attempted, and for the first time two different methods to measure MT, selective inversion recovery and pulsed magnetization transfer, were compared side-by-side on the same samples. The MAGIC-2 formulation exhibits less sensitive dose response in terms of magnetization transfer than does the original MAGIC gel formulation. Magnetization transfer was also investigated for its robustness in the face of B_1 inhomogeneities and compared to that of relaxation rate measurements. A new magnetization transfer parameter, the magnetization transfer proportion (MTP), was introduced. It was shown that the MTP was less susceptible to errors in B_1 than R2 for measuring doses accurately. Future work could focus on optimizing MRI sequences for measuring R2 dose response.

A third recurrent issue is our poor understanding of the basic relaxation mechanisms that account for the dose response, which could guide the development of alternative improved dosimeters. To improve our understanding, the dosimeter was deconstructed into its components and investigations into the contributions of chemical exchange to transverse relaxation and magnetization transfer were performed. A model was developed that estimated the change in R2 for a given dose, percent weight of monomer, and relaxation rate of the exchangeable protons on the macromolecular polymer. The results suggest that the rates of chemical exchange and transverse relaxation of the polymer pool decrease as polymer weight increases, and lend support to the theory that chemical exchange acts as a primary mechanism of R2 dose response in the

polymer gel dosimeters. It was also shown that the model agrees with the measured T2 of the macromolecular pool as found in Chapter III. The phenomenon of grafting to the gelatin matrix is one possible additional relaxation source that could be included into the apparent bound pool measurement used in the model for dose response introduced in this work.

It was the goal of this work to delve more deeply into better understanding of a particular formulation of polymer gel dosimeters. Many authors have either simply reported calibration measurements for a given formulation, illustrated its use in selective radiation therapy applications, or pursued development of more formulations in the name of "improvement" of formulation, but there has been little work done to better understand and focus on a single formulation.

There are other issues in polymer gel dosimetry that should be addressed, such as ease of use for radiation therapy groups that do not have easy access to imaging and chemistry facilities. Additionally, it would be useful to optimize the methacrylic acid-based dosimeter for magnetization transfer studies, since this work suggested that such studies could be better for mapping dose response in the presence of B_1 inhomogeneities, especially for situations when radiation therapy physicists might not have full control or understanding of their facility's imaging capabilities. These basic studies show that it is possible to quantify the relaxation mechanisms within a complex polymer by an appropriate range of methods, and it is hoped that this work encourages others to pursue more detailed studies as well.